UNIVERSITÉ DE SHERBROOKE
Faculté de génie
Département de génie Mécanique

OPTIMISATION DE TRANSDUCTEURS PIÉZOÉLECTRIQUES POUR LA GÉNÉRATION D'ONDES GUIDÉES

Thèse de doctorat
Spécialité : génie mécanique

Peyman YAZDANPANAH MOGHADAM

Jury : Patrice MASSON (directeur)
Nicolas QUAEGEBEUR
Ahmed MASLOUHI
Pierre BÉLANGER

Sherbrooke (Québec) Canada Octobre 2015

To my father, Ali, my mother, Akram, my brother, Ehsan, all my teachers, family and close friends who have always supported and encouraged me in my life to continue my education in the name of freedom and humanity.

RÉSUMÉ

Les systèmes de surveillance de santé structurale sont proposés pour la détection d'endommagement dans les infrastructures qui dépassent leur durée de vie en utilisant les ondes guidées (GW). Les ondes guidées peuvent parcourir de longues distances et sont sensibles à une variété d'imperfections. Les transducteurs piézoélectriques sont communément utilisés pour générer et mesurer les ondes guidées dans des structures minces. Comme la détection du défaut et sa localisation sont souhaitées, la nature de la génération des ondes guidées sous forme de plusieurs modes implique une complexité supérieure dans le traitement du signal. Pour remédier à cette limitation, une nouvelle méthode est présentée ici pour la génération des ondes guidées par sélection de mode, et un nouveau transducteur piézoélectrique est ensuite conçu, fabriqué et testé.

Tout d'abord, la génération des ondes guidées par optimisation systématique du profil interfacial de la contrainte de cisaillement en mode sélectif est étudiée. En utilisant le principe de superposition, une méthode d'analyse est d'abord développée pour la modélisation de la génération des ondes guidées par un nombre fini de segments de contrainte de cisaillement uniforme, chacun contribuant à un profil élémentaire d'une contrainte constante de cisaillement. Sur cette base, deux fonctions coût sont définies afin de minimiser les modes indésirables et amplifier le mode sélectionné et le problème d'optimisation est résolu avec un cadre d'optimisation d'algorithme génétique parallèle. Les avantages de cette méthode par rapport à d'autres approches de conception de transducteurs classiques sont (1) la contrainte de cisaillement peut être explicitement optimisée à la fois pour exciter un mode et supprimer d'autres modes indésirables, (2) la taille de la zone d'excitation n'est pas limitée et l'excitation en mode sélectif est toujours possible, même si la largeur d'excitation est inférieure à toutes les longueurs d'onde excitées, et (3) la sélectivité est accrue et la largeur de bande est étendue.

La méthode analytique et les fonctions coût sont ensuite développées pour concevoir un transducteur piézoélectrique à éléments multiples (MEPT) simple et performant. Une méthode numérique est tout d'abord mise au point pour extraire la contrainte interfaciale entre un seul élément piézocéramique et une structure d'accueil et ensuite utilisée comme entrée d'un modèle analytique pour prédire la propagation des ondes guidées à travers l'épaisseur d'une plaque isotrope. Deux nouvelles fonctions coût sont proposées pour optimiser la contrainte de cisaillement interfaciale pour supprimer le(s) mode(s) indésirable(s) et maximiser un mode désiré. Simplicité et faible coût de fabrication sont deux principales cibles visées dan la conception du MEPT. Un prototype TPEM est ensuite fabriqué à l'aide de micro-usinage laser. Une procédure expérimentale est présentée afin de valider les performances de la TPEM comme une nouvelle solution pour la génération des ondes guidées en mode sélectif. Des essais expérimentaux illustrent la forte capacité du TPEM pour la génération des ondes guidées en mode sélectif, puisque le mode indésirable est supprimé par un facteur allant jusqu'à 170 fois par rapport aux résultats obtenus avec un seul piézocéramique.

Mots-clés: Surveillance de santé structurale, ondes guidées, transducteur piézoélectrique à éléments multiples, mode-sélectif, optimisation, modélisation piézoélectrique

ASTRACT

Structural Health Monitoring (SHM) systems are being proposed for damage detection of infrastructures that exceed their life using ultrasonic Guided waves (GWs). GWs can travel over long distances and are sensitive to variety of defects. Piezoelectric transducers (PZTs) are commonly used to generate and measure GWs in plate-like structures. As damage detection and localization is sought, the multi-mode nature of GW generation involves higher complexity in signal processing. To overcome this limitation, a new method is presented here for mode-selective GW generation, and a novel mode-selective PZT is then designed, manufactured and tested.

First, mode-selective generation of GWs by systematic optimization of the interfacial shear stress profile is investigated. Using the superposition principle, an analytical method is first developed for modeling GWs generation by a finite number of uniform shear stress segments, each contributing with a constant elementary shear stress profile. Based on this, two cost functions are defined in order to minimize the undesired modes and amplify the selected mode and the optimization problem is solved with a parallel Genetic Algorithm (GA) optimization framework. Advantages of this method over more conventional transducers tuning approaches are that (1) the shear stress can be explicitly optimized to both excite one mode and suppress other undesired modes, (2) the size of the excitation area is not constrained and mode-selective excitation is still possible even if excitation width is smaller than all excited wavelengths, and (3) the selectivity is increased and the bandwidth extended.

The analytical method and objective functions are then developed to design a novel and cost-effective multi-element piezoelectric transducer (MEPT). A numerical method is first developed to extract the interfacial stress between a single piezoceramic element and a host structure and then used as the input of an analytical model to predict the GW propagation through the thickness of an isotropic plate. Two novel objective functions are proposed to optimize the interfacial shear stress for both suppressing unwanted mode(s) and maximizing a desired mode. Simplicity and low manufacturing cost are two main targets driving the design of the MEPT. A prototype MEPT is then manufactured using laser micro-machining. An experimental procedure is presented to validate the performances of the MEPT as a new solution for mode-selective GW generation. Experimental tests illustrate the high capability of the MEPT for mode-selective GW generation, as unwanted mode is suppressed by a factor up to 170 times compared with the results obtained with a single piezoceramic.

Keywords : Structural Health Monitoring, Guided waves, multi-element piezoelectric transducer, mode selective, optimization, piezoelectric modeling

ACKNOWLEDGMENTS

I would like to say thank you to my supervisor Prof. Patrice Masson for all his support and consideration. It has been a great honor for me to be your student. Under your supervision, I learned how to work professionally. Thank you for helping me to become a mature researcher. You never let me down; instead you helped me get things better. Thank you very much.

I would like to say thank you to my colleague, Nicolas Quaegebeur, for all his professional support. Nicolas, thank you for sharing your knowledge and experience in SHM with me. Thank you very much.

I would like to say thank you to all my colleagues in SHM team at the GAUS, Kyle Mulligan and Pierre-Claude Ostiguy, for sharing their knowledge and expertise on simulation and experimental tests to support this project.

I would like to say thank you to my parents and my brother for all their support. I learned from my parents that humanity and honesty should be always first priorities of my life.

From all my friends, I wish to especially thank Mr. Javad Ensmaelpanah and Mr. Ehsan Masouni who instead to remain anonymous for being true friends.

This study has been conducted with the financial support from the Natural Sciences and Engineering Research Council of Canada (NSERC).

TABLE OF CONTENTS

LIST OF FIGURES

LIST OF TABLES

LIST OF SYMBOLS

Symbols	Definition
α_i	Complex correction coefficient corresponding to element *i*
A	Amplitude of input harmonic excitation signal
a	PZT element width
c_p	Phase velocity
c_g	Group velocity
c_L	Longitudinal (pressure) velocity
c_T	Transverse (shear) velocity
ρ	Material density
d	Half thickness of host structure
E	Material Young's Modulus
Γ	Shear-lag coefficient
ε	Strain field
φ^0	Phase of input harmonic excitation signal
f_0	Driving frequency
g	Gap size between PZT elements
∇	Gradient operator
J_{S_0}	Objective function for suppression of A_0-mode
J_{A_0}	Objective function for suppression of S_0-mode
λ_{mode}	Wavelength of excited guided wave mode
v	Poisson's ratio for isotropic elastic material
H	Heaviside step function
τ	Interfacial shear stress
P	Power flow of propagated wave
φ	Potential of longitudinal wave
ψ	Potential of shear wave
Δx	Segment width at excitation area
$\Delta\xi$	Wavenumber band
r	Half of the excitation area
t_{p}	Thickness of PZT
ω	Circular frequency
x	Horizontal distance form center (Cartesian coordinate)
y	Vertical distance form center (Cartesian coordinate)

LIST OF ACRONYMS

Acronym	Definition
Al	Aluminum
ANN	Artificial Neural Network
CLoVER	Composite Long-Range Variable-Direction Emitting Radar
EMAT	Electromagnetic Acoustic Transducers
FEM	Finite Element Method
FSAT	Frequency Steerable Acoustic Transducer
GA	Genetic Algorithm
IDT	Interdigital Transducers
GW	Guided Wave
MFC	Micro-Fiber Piezoelectric Composites
MEPT	Multi-Element Piezoelectric Transducer
NDT	Nondestructive Test
PVDF	Polyvinylidene Fluoride
PZT	Piezoelectric Lead Zirconate Titanate Transducer
SAW	Surface Acoustic Wave
SHM	Structural Health Monitoring
TAPP	Tilted Angle Polarization Type Piezoelectric Transducer
WW	Withdrawal Weighting

CHAPTER 1

INTRODUCTION

The term “Smart Structures” or “Intelligent Material Systems” is a relatively young field of study among the engineering community. Rogers (Rogers, 1993) proposed two definitions for intelligent material systems. The first definition is based a technology paradigm: “the integration of actuators, sensors, and controls with a material or structural component.” The second definition addresses the goal of intelligent material systems: “material systems with intelligence and life features integrated in the microstructure of the material system to reduce mass and energy and produce adaptive functionality.” One application of smart structures is for the inspection, evaluation or damage detection in structures, a field known as Structural Health Monitoring (SHM).

Nowadays, there are many different types of non-destructive evaluation (NDE) techniques and some of them may be adapted SHM systems. The NDE methods that may be adapted for SHM purpose are ultrasonic methods based on Guided Waves (GW) for damage detection in solid structures.

SHM systems have been constantly improved in the past decades. A complete system should consist of two main components: a set of actuator(s) and sensor(s) that are networked on a monitored structure and a system that analyzes data for its processing and interpretation.

Based on Lord Rayleigh’s work, Horace Lamb discovered in 1917 waves that can exist in thin plates with parallel free stress boundaries. These types of waves are now called GWs. Their main advantage is that they may travel over a long distance in different types of materials which allows for examination of large area with only few transducers. GWs are highly sensitive to a variety of structural damages.

The implementation of SHM systems within new structures or to those structures that exceeded their life enhances reliability, safety and maintenance performance as well as economic aspects, but it still needs to be demonstrated. An on-line SHM system consists of a network of smart transducers for data acquisition to excite and receive GW which are permanently attached the structure. By analyzing the sensor signals, different kinds of structural damage can be detected (Giurgiutiu, 2007; J. L. Rose, 2004). Several techniques are used to generate GW, like piezoelectric transducers, so called PZTs in this thesis, electromagnetic acoustic transducers (EMATs), laser generation, etc.

1.1 Problem statement

PZTs have a significant potential to be used in active SHM to generate and sense GWs (Giurgiutiu, 2007; Raghavan & Cesnik, 2005; I. Viktorov, 1967). GWs have a multi-mode nature and two fundamental symmetric mode (S_0-mode) and anti-symmetric mode (A_0-mode) are excited at any given frequency. This involves higher complexity in signal processing and defect detection (Santoni, Yu, Xu, & Giurgiutiu, 2007), because each mode has its own dispersive characteristic and interaction with structural discontinuities that lead to complex wave fields. SHM systems have not been largely implemented yet because of their complexity and inaccuracy, partly explained by multi-mode GW generation, so that single-mode GW generation is required to improve performance of SHM systems.

1.2 Objectives

Maintenance industry is requesting improvements in SHM systems, so that they can installed on structures. To decrease the complexity of using GWs in SHM system, the objectives of this thesis are to optimize, design, manufacture, and test in laboratory scale a novel PZT transducer for mode-selective GW generation to improve the performances of SHM systems. So, four major problems should be investigated:

1. Present an analytical solution for modeling GW propagation though-the-thickness of the plate generated by an arbitrary interfacial shear stress profile.

2. Present the best objective functions for optimization of interfacial shear stress for mode-selective generation.

3. Present an approach for optimization of the interfacial shear stress for mode-selective GW generation.

4. Design, manufacture, and test a mode-selective GW transducer.

1.3 Originality

The mode-selective transducer presented in this thesis is designed for global conditions; in other words, it is not a local design and optimization. The manufactured Multi-Element Piezoelectric Transducer (MEPT) could be installed on structures with any thickness, and then using global optimization approach, input signals sent to the MEPT could be obtained. Originality of this thesis can be divided in categories as follow:

1. The interfacial shear stress at inner area of the transducer is very complicated at higher frequencies. So, a hybrid method is used to consider this complexity.

2. Analytical method is developed for GW modeling through the thickness of the plate.

3. Advantages of this method over more conventional transducers tuning approaches are that (1) the shear stress can be explicitly optimized to both excite one mode and suppress the other undesired modes, (2) the size of the excitation area is not constrained and mode-selective excitation is still possible even if excitation width is smaller than all excited wavelengths, and (3) the selectivity is increased and the bandwidth extended with respect to a single PZT element.

4. Novel systematic approach and objective function for global optimization are presented.

5. The MEPT is designed, fabricated, and successfully tested experimentally. Simplicity and low fabrication cost are two main advantages of the MEPT.

1.4 Thesis outline

The second chapter deals with literature review. The concept of SHM systems and its advantages over traditional NDT/NDE methods are reviewed. GW generation and propagation are presented briefly. The multi-mode nature of the GW is highlighted and requirement for mode-selective GW generation is discussed.

Several well-known analytical methods for modeling GW propagation and induced interfacial shear stress are presented and their advantages and limitations are discussed. A comprehensive literature review is then performed on mode-selective transducers and their advantages and limitations.

In addition, different optimization methods in the field of SHM are studied and their usage for optimization of transducers design is presented. Genetic algorithm (GA), artificial neural network (ANN), and withdrawal weighting are investigated.

The third chapter presents the methodology for mode-selective generation of GW by systematic optimization of the interfacial shear stress profile. Using the superposition principle, an analytical method is first developed for GWs excitation by a finite number of uniform segments, each contributing with a constant elementary shear stress profile. Based on this, cost functions are defined in order to minimize the undesired modes and amplify the selected mode and the optimization problem is solved with a parallel GA optimization framework. This paper has been published in the Journal Smart Materials and Structures (Yazdanpanah Moghadam, Quaegebeur, & Masson, 2015) and presented in the international conference (Yazdanpanah Moghadam, Quaegebeur, & Masson, 2013).

The fourth chapter presents an approach for modeling GW accurately considering the effect of wave propagation on non-excited PZT elements. Two new objective functions are presented for global optimization of interfacial shear stress. A novel idea is presented to design the MEPT. The MEPT is then manufactured using laser-micromachining. An experimental procedure is presented to validate the performances of the MEPT as a new solution for mode-selective GW generation. This paper has been submitted in the Journal Smart Materials and Structures and presented in the international conference (Yazdanpanah Moghadam, Quaegebeur, & Masson, 2015).

The fifth chapter presents a conclusion of this thesis. Advantages and limitations of the presented MEPT are discussed.

CHAPTER 2

Literature review

In this section, SHM systems and their advantages over typical damage detection systems are explained. GWs that are used in SHM technology are described briefly and requirements for mode selective GW generation are then discussed. Several methods for modeling GW are introduced. In the next section, different types of PZTs with their advantages and disadvantages are reviewed. The ability of each type of these transducers in generating a specific mode is investigated by presenting the related literature. The general categorization for GW sensors or actuators is:

1) monolithic piezoelectric transducers,
2) ring and circular shape,
3) interdigital transducer (IDT),
4) phased array transducer,
5) micro-fiber piezoelectric composites (MFC),
6) wedge angle transducer,
7) tilted angle polarization (TAPP),
8) electromagnetic acoustic transducers (EMAT),
9) composite long-range variable-direction emitting radar (CLoVER),
10) frequency steerable acoustic transducer (FSAT).

In spite of unique advantages of these transducers, they have some disadvantages. A comprehensive literature review is presented in the following section.

2.1 Structural Health Monitoring (SHM)

There are many civil, mechanical, and aerospace structures that have exceeded their life and many billion dollars is required annually for maintenance of infrastructure plants, equipments, and facilities. Damage detection of these structures using typical NDE methods is costly and time consuming. Manual inspection often involves techniques such as visual inspection, radiography, and eddy current. Damage detection systems facilitate tracking the location and type of defect and making decision regarding when and where to apply maintenance remedies. A range of different technologies have been developed during the past decades for damage detection in metallic and composite materials.

SHM is a new born technology to overcome limitations of previous damage detection techniques. The SHM systems should be improved significantly because of sensitivity to temperature variation, the amount of data that may be exhaustive, transducer deboning. SHM system may be installed permanently on a structure for continuous monitoring. Automated SHM systems could ensure reduced time and cost of defect inspection, improved performance and higher operator availability, increased public safety and reliability, and extended life of structure. The adoption of SHM allows an optimal use of the structure, and gives an additional advantage for design improvement.

A SHM system is generally composed of an acquisition system, sensor networks, and data analysis systems; in this way, it can be compared with biological neural systems as SHM mimics the synaptic parallel computation networks. For instance, delamination that is a common mode of failure in composite structures could be detected by SHM technique, as shown in Figure 2. 1.

SHM's four-step process includes (Farrar & Worden, 2007):

i. operational evaluation,
ii. data acquisition, normalization and cleansing,
iii. feature selection and information condensation, and
iv. statistical model development for feature discrimination.

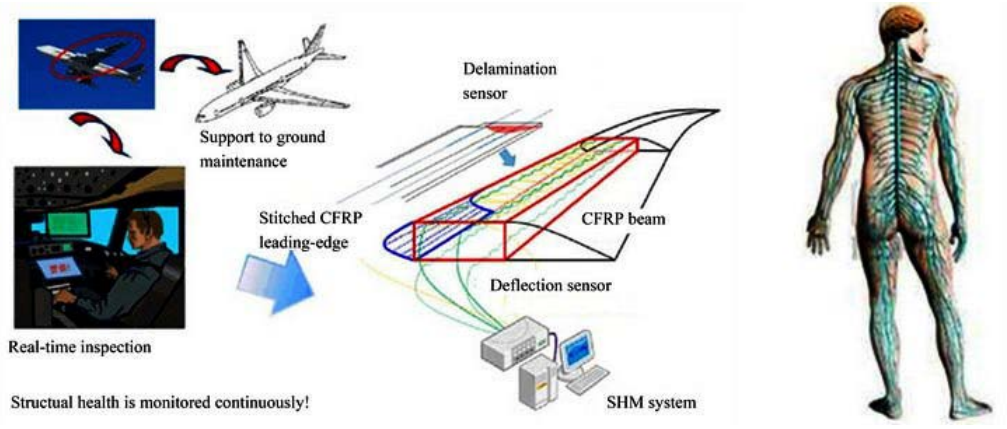

Figure 2. 1 Human neural network concept in structural health monitoring of aircraft structure (Trilaksono et al., 2013).

The purpose of the SHM system (Hayward, Hailu, Farlow, Gachagan, & McNab, 2001) is to provide early enough warning of collapse or catastrophic failure,

i. provide information for planning maintenance activities on-demand, rather than on a usage or post-event basis,
ii. determine if the structure meets predetermined performance criteria.
iii. identify the presence of fault conditions,
iv. provide structural condition assessment information for use in maintenance, operational, and rehabilitation activities,
v. evaluate the condition of the structure upon discovery of a problem, such as cracks,
vi. assess the integrity of the structure following catastrophic events,
vii. provide data to estimate the remaining lifetime of the structure,
viii. provide information that aids in the development of new design codes and procedures,
ix. assist in construction processes by increasing safety and/or productivity,
x. establish the viability and performance of novel sensor or SHM systems,
xi. certify the safety of prototype and production designs, and
xii. provide a maintenance history and state assessment as part of an economic assessment of a structure.

2.2 NDT and SHM systems

Eddy current and ultrasonic equipments used in NDT are expensive and should be used by an operator that makes usage of these systems time-consuming.

Various NDT techniques have been presented and developed for damage detection in infrastructures over past decades. Most common methods described in Table 2. 1 include: Visual inspection and enhanced visual inspection using liquid penetrant and magnetic particle, eddy current, microwave, thermography, optical interferometry, acoustic inspection, ultrasonic inspection, acoustic emission, and vibration/modal analysis.

Table 2. 1 Available techniques for typical SHM systems.

Method	Advantages	Limitations	Data Rate / Power
Strain gages	embeddable simple procedure	expensive limited info	1 kHz / 70mV
Optical fibers	embeddable simple results	expensive no transverse info	1 GHz / 10 W
Eddy current	surface mountable most sensitive	expensive localized	100 MHz / 800 mW
Modal data	surface mountable good coverage	complex results global results	100 kHz / 200 mW
Acoustic emission	good coverage surface mountable	complex results event driven	100 MHz / 100 mW
Guided waves	inexpensive Surface penetrating	complex results linear scans	1 MHz / 300 mW

The advantages of SHM over conventional NDT are (Huston, 2010):

i. no access to the inspection area required,

ii. safe inspection of hazardous areas,

iii. continuous online monitoring of many locations at the same time, and

iv. reduced influence of the human factor on inspection results.

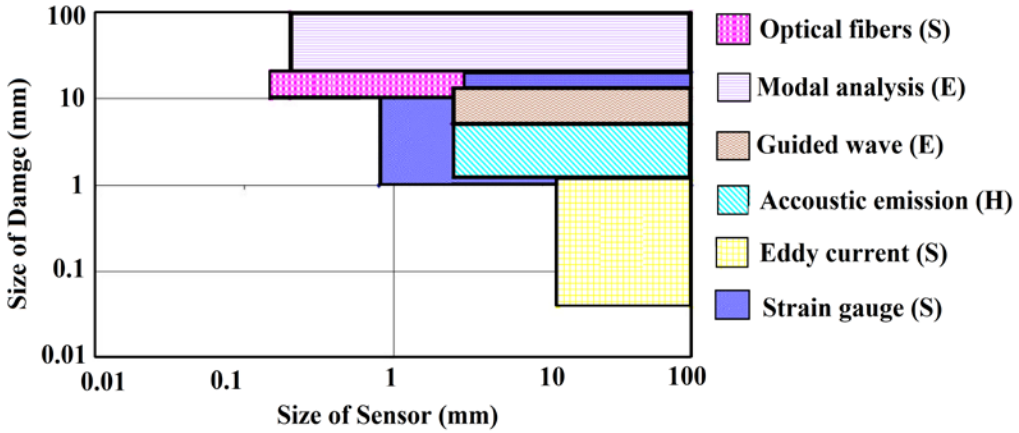

Figure 2. 2 Variation of damage delectability versus sensor size for the common SHM techniques in the case of a composite panel of 1 m × 1 m. For each technique, the detection is effective locally (L), on the half plate (H) or on the entire plate (E). The only reliable techniques on the entire structure are GW and modal analysis (Seth Stovack Kessler, 2002).

The relative efficiency of each technique for crack detection on metallic structures is described in Figure 2. 2. On this figure, it appears that the only techniques that are sensitive to cracks on the entire structure are the modal analysis and the GW technique. Since modal analysis give only global results and no local information, GW generation appears to be the most reliable technique for embedded SHM. Smaller sizes of damage reaching a few millimeters can be detected using GWs in the frequency range from 100 kHz to 1 MHz, as seen in Figure 2. 2 for the case of GWs, this gives GW based damage detection techniques advantage over established NDE techniques. The main reason for the limited damage size sensitivity is that the small wavelength waves could interact with the micro-structural details of the material, such as grain size of rolled sheets, thus contaminating the signal with multiple reflections to the degree that it yields no useful information (Seth Stovack Kessler, 2002).

2.3 Damage detection using GWs

Damage could be defined as change(s) to the material and/or geometrical properties of a structure. For instance, loosened bolts, corrosion, and cracks that form in a mechanical part

produce a change in geometry that alters the stiffness characteristics of that part could be considered as a damage. Damage could be detected when GWs propagate and interact with it in a structure. This interaction is dependent on type, location, and size of the damage.

2.3.1 GWs propagation in plate-like structures

SHM applications tend to monitor large areas of a structure with a minimum number of transducers. Ultrasonic GWs can travel large distances in thin-wall structures, such as pipelines and pressure vessels, with only little loss of energy. GWs are highly sensitive to the interaction with damages, depending on mode and frequency ranges. GWs can be generated by excitation devices, commonly an actuator that is integrated into the structure or bonded on the surface of a structure, to induce normal and shear stress to the host structure. The induced stresses to the plate generate bulk waves known as longitudinal and shear waves, as presented in Figure 2. 3.

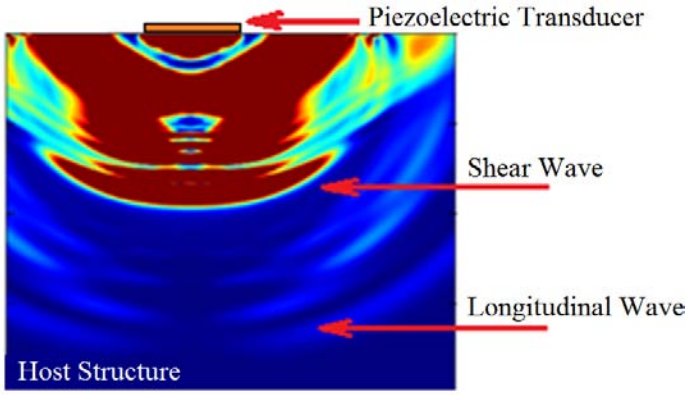

Figure 2. 3 Bulk wave generation with a bonded PZT. Longitudinal and shear waves are generated in the plate.

Reflected longitudinal and shear waves superimpose and propagate along a plate-like structure to generate dispersive symmetric (S_0, S_1, S_2, …) and anti-symmetric (A_0, A_1, A_2, …) modes, as shown in Figure 2. 4. Solving the wave equation of motion of the plate, GW symmetric modes are formulated as:

$$\frac{\tan(qh)}{\tan(ph)} = -\frac{4k^2qp}{\left(k^2-q^2\right)^2} \tag{2.1}$$

and anti-symmetric modes are defined as:

$$\frac{\tan(qh)}{\tan(ph)} = -\frac{\left(k^2-q^2\right)^2}{4k^2qp} \tag{2.2}$$

where $p^2 = \frac{w^2}{c_L^2} - k^2$, $p^2 = \frac{w^2}{c_T^2} - k^2$, $k = w/c_p$. Eq. (2.1), correlates the propagation velocity with its frequency, implying that GWs, regardless of the mode, are dispersive (velocity is dependent on frequency).

At any given frequency, at least two fundamental (A_0 and S_0) GW modes are excited simultaneously, and as the frequency-thickness product increases, larger number of modes appear. Figure 2. 5 illustrates the group and phase velocity dispersion curves of a 2 mm thick Al plate for first three symmetric modes, red curves labeled S_0, S_1, S_2, and first three anti-symmetric modes, blue curves labeled A_0, A_1, A_2.

In addition, Figure 2. 5-a shows also phase velocity dispersion curves of Axial, Rayleigh and Flexural waves. At lower frequencies, the velocity of the first symmetric mode (S_0) is almost non-dispersive and so close to the speed of axial wave, though A_0-mode has very close phase velocity to the flexural wave. However, as the frequency increases, they become separated, and at higher frequency, they differ substantially. At the other end of the spectrum, Rayleigh waves are a high frequency approximation of the S_0 and A_0-modes. As the frequency becomes very high, the S_0 and the A_0 wave speeds coalesce, and both have the same value, corresponding to the Rayleigh wave speed. At high frequency, the particle motion of GWs becomes restricted to the proximity of the free surfaces, and thus resembles that of the Rayleigh waves (Giurgiutiu, 2007).

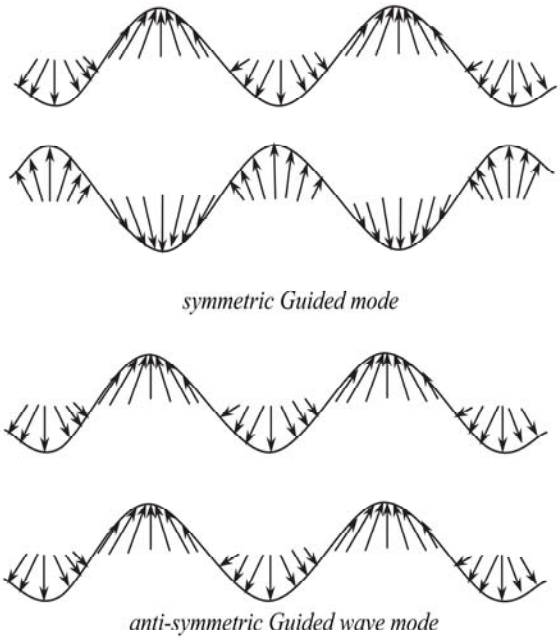

Figure 2. 4 Symmetric and anti-symmetric GW modes (Su, Ye, & Lu, 2006).

(a)

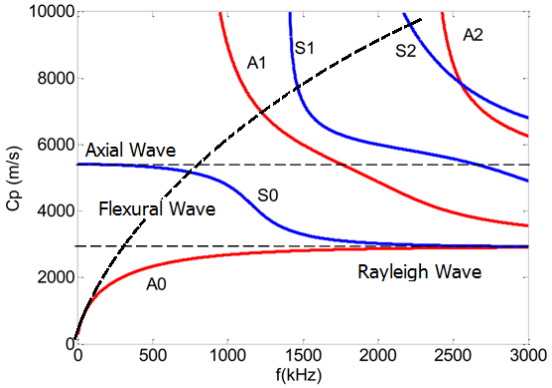

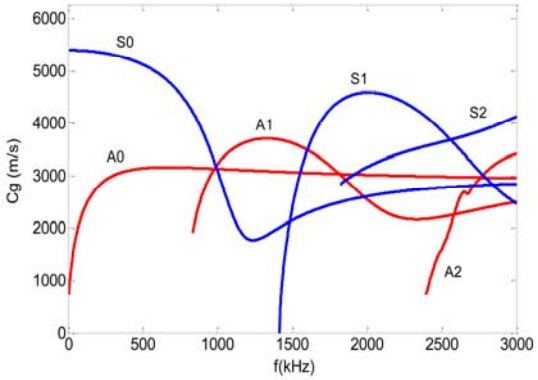

(b)

Figure 2. 5 (a) Phase velocity dispersion curves for a 2 mm thick aluminum plate. (b) Group velocity dispersion curves for a 2 mm thick aluminum plate (Wan, Zhang, Xu, & Tse, 2014).

2.3.2 GW mode selection

A successful damage inspection with SHM and GWs should be performed based on type of the damage under investigation. Shape, size, geometry, and location of the damage affects its interaction with different GW modes (Alleyne & Cawley, 1992). The selected GW mode should

have high sensitivity and detectability to the type of the damage (Wilcox, Lowe, & Cawley, 2001). Furthermore, a proper generated GW mode should be non-dispersive, lightly attenuated and easily excitable (Nicolas Quaegebeur, Micheau, Masson, & Maslouhi, 2011). In addition to proper GW mode selection, frequency of excitation strongly affects damage detection based on the fact that the wavelength of the selected mode must be lower than or equal to the size of the damage (Castaings, Le Clezio, & Hosten, 2002).

Symmetric modes exhibit higher sensitivity to defects anywhere in the thickness such as vertical cracks, loosened bolts (Lemistre & Balageas, 2001). On the other hand, anti-symmetric modes show considerable interaction with surface cracks and corrosion, but it may not be suitable for long-distance propagation because of its high attenuation rate (Pierce, Culshaw, Manson, Worden, & Staszewski, 2000). As anti-symmetric modes have considerable transverse movement, they are very sensitive to defects with horizontal posture such as delamination and transverse ply cracks (Grondel, Delebarre, Assaad, Paget, & Levin, 2001). Thus, this thesis provides a solution for mode-selective GW excitation that improves accuracy of damage detection in SHM systems and decrease, complexity of usage of GWs in these systems since piezoelectric transducers are commonly used in SHM systems to generate GW in plate-like structures, modeling GWs by a PZT considering the coupled piezo-elastodynamic behavior between the actuator and the host medium is one of the fundamental issues for designing a mode-selective actuator.

2.4 Piezoelectric transducers

Waves in elastic structures can be excited using different methods. For NDT purpose the excitation devices that can be used are not necessarily coupled or weakly coupled with the structure, for SHM the wave actuators need to be integrated into the structure or mounted on its surface. A comprehensive review on piezoelectric transducers is performed here for GW excitation. Actually, piezoelectric materials can generate an electric charge an electric charge in response to applied mechanical stress, so called direct piezoelectric effect, as they are used as

sensors. On the other hand, the applied electric potential to a piezoelectric materials lead to stress and when they are used as actuators it induces interfacial shear stress to the substructure.

Using coordinate transformation, for linear piezoelectric medium, the stress, strain, electric field, and temperature rise are related by

$$\begin{Bmatrix} \{\sigma\} \\ \{D\} \end{Bmatrix} = \begin{bmatrix} [\bar{Q}] & -[\bar{Q}^P]^t \\ [\bar{Q}^P] & -[\bar{Q}^e] \end{bmatrix} \begin{Bmatrix} \{\varepsilon\} \\ \{E\} \end{Bmatrix}, \tag{2.3}$$

where stress $\{\sigma\}$ and electrical displacement $\{D\}$ in the plate may be written as

$$\{\sigma\} = \begin{bmatrix} \sigma_x & \sigma_y & \sigma_{xy} & \sigma_{yz} & \sigma_{xz} \end{bmatrix}^t, \ \{D\} = \begin{bmatrix} D_x & D_y & D_z \end{bmatrix}^t. \tag{2.4}$$

Also, $\{E\} = \begin{bmatrix} E_x & E_y & E_z \end{bmatrix}^t$ is the electrical field vector; $[\bar{Q}]$, $[\bar{Q}^P]$, and $[\bar{Q}^e]$ are the transformed plane stress reduced stiffness matrix, the matrix of transformed piezoelectric stress module, and the transformed permittivity matrix. The electric field at any point within the plate is expressed as

$$E_i = -\Phi_{,i}, \quad i = 1,2,3. \tag{2.5}$$

where Φ is the applied potential to the piezoelectric actuator (Yazdanpanah Moghadam, Tahani, & Naserian-Nik, 2013). In this thesis, surface boded PZTs are selected because of their perfect coupling with the host structure. They have a negligible added mass, are easy of integration, excellent mechanical strength, wide frequency responses, low power consumption and acoustic impedance, as well as low cost.

2.4.1 Monolithic piezoelectric transducers

Many investigations have been done to selectively measure and generate GW using PZT. Selecting the desired GW mode depends on the nature of the damage, host-structure, properties and geometries of the type and location of the used transducers, etc. As noted, at any given

frequency at least two fundamental GW modes, symmetric mode (S_0, S_1, S_2, …) and anti-symmetric mode (A_0, A_1, A_2, …) can be generated.

(Shelke, Kundu, Amjad, Hahn, & Grill, 2011) used two adjusted and co-localized PZT transducers on the opposite sides of a plate. Therefore, both symmetric and anti-symmetric GW modes could be generated. They investigated the best given frequency and mode type for delamination detection in a laminated plate. A_0-mode was selected as the proper mode for delamination detection as its conversion to S_0 and A_1-modes indicate presence of delamination. It was investigated that A_0-mode converts to symmetric mode in interaction as delamination processes, but S_0 and S_2-modes are not converted to anti-symmetric modes by the delamination.
(Santoni et al., 2007) investigated analytically and experimentally the GW-mode tuning with PZT. They found those frequencies in which the amplitude of one of the generated modes completely dominates the other ones. In addition, they tried to find the effective PZT dimension. They concluded that in addition to the given frequency, the shape and geometry of a sensor affect the sensed signal(s).

(Grondel et al., 2001) used dual-element transducers for damage detection in composite plates. They expanded the investigation of (Moulin, Assaad, Delebarre, & Osmont, 2000) about the development of hybrid modeling technique. Based on this method, they tried to select the best GW mode and given frequency for SHM of a composite laminated plate. (Grondel, Paget, Delebarre, Assaad, & Levin, 2002) the found S_0 and A_0-modes are not significantly dispersive and selected a frequency before appearance of A_1-mode to have least dispersion and wavelength. Their investigation concentrated on the A_0-mode generation, because of its smaller wavelength than the S_0-mode, and its higher detectability consequently. Overall, it is possible to excite a PZT to generate one dominant GW mode. The dimension and geometry of PZT strongly affects mode generation. By selecting the proper frequency, the amplitude of a selected GW-mode can be maximized or minimized. The resonance frequency of the transducer has to be considered in design process to have the required mechanical to electrical conversion (Clarke, Simonetti, & Cawley, 2009).

One of the important parameters in optimization of transducers is the material properties. Piezoelectric materials, like polyvinylidene fluoride (PVDF), or piezoceramic (PZT) are commonly used for GW based SHM. Piezopolymers are flexible and can be applied on curved structures. They are lightweight as well as cheaper and easier to manufacture than piezoelectrics (Monkhouse, Wilcox, Lowe, Dalton, & Cawley, 2000). PVDF has higher internal damping than PZT, and they possess a much lower modulus of elasticity and actuation force in comparison to PZT. Thus, piezopolymers are less suitable for actuator applications. Due to the limited temperature range of -40°C to +110°C piezopolymers are inappropriate for aerospace applications. The piezopolymers, with weak piezoelectric properties, high internal losses, low mechanical quality factor and very low acoustic impedance, yield maximum bandwidth when left untuned (Brown, 2000).

2.4.2 Ring and circular piezoelectric transducer

Fundamental symmetric (S_0) and antisymmetric (A_0) GW-modes are coupled in excitation. If the distance between two edges of a transducer ($2a$) is equal to the half-integer number of wavelengths (λ) of excited GW-mode as

$$2a = \lambda\left(n + \frac{1}{2}\right), \quad n = 0, 1, 2, \ldots \tag{2.6}$$

it can carry maximum energy in low frequency range (Evgeny Glushkov, Glushkova, Kvasha, & Seemann, 2007; EV Glushkov, Glushkova, Seemann, & Kvasha, 2006). Similarly, if the size of the transducer is equal to the integer of a number of the wavelengths, minimal values of energy are obtained.

$$2a = \lambda n, \quad n = 0, 1, 2, \ldots \tag{2.6}$$

(Yeum, Sohn, & Ihn, 2011) designed a PZTs to present a mode decomposition technique that is a dual PZT composed of a concentric ring and a circular PZT that can decouple A_0 and S_0-modes

at a given frequency. The approach is based on the changing amplitude rate of S_0 and A_0-modes, as the sizes of the excitation and sensing PZTs vary. They could define a scaling factor as a function of wavenumbers in which the difference between the wavenumbers of the S_0 and A_0-modes rises especially at high frequency. The main investigated parameter here was the inner and outer radius of the ring and circular parts without changing other parameters.

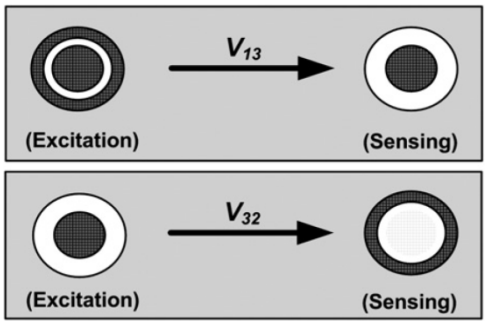

Figure 2. 6 V_{13} denotes a response measured by the inner circular part of the sensing PZT when both the outer ring and the inner circular parts of the excitation PZT are activated. (Here, the subscripts, 1, 2 and 3 denote the entire dual PZT, the outer ring PZT and the inner circular PZT, respectively.) The darker area of the dual PZT represents the PZT component(s) activated either for excitation or sensing (Yeum et al., 2011).

As shown in Figure 2. 6, ring, circular or entire parts of this transducer can be used to generate and sense the desired mode. For instance, A_0-mode can be excited but S_0-mode sensed by the sensor, and the difference between A_0 and S_0 mode is increased at higher frequency, because their formulation is a function of wavenumber and the difference between the wavenumbers of the S_0 and A_0 modes raised at a high frequency. The advantages of this method over the conventional approaches are that (1) PZTs need to be placed only a single surface of a specimen and (2) mode decomposition can be performed at any desired frequency without changing the PZT size and/or spacing configuration. The proposed method is based on the 'pin-force' model (Raghavan & Cesnik, 2005) that considers the interfacial shear stress induces to the host structure mostly around its circumference boundary which is not accurate higher frequencies. In

addition, this technique is limited to S_0 and A_0 modes, therefore, the given frequency was limited below the cutoff frequencies of the S_1 or A_1 modes.

(EV Glushkov, Glushkova, Kvasha, & Lammering, 2010) investigated a special choice of the amplitudes and time delays of the sinusoidal tone burst driving signals for each element of a PZT with several coaxial ring-shaped elements for mode-selective GW excitation, as shown in Figure 2. 7. As the transient solution tends towards the solution of the corresponding time-harmonic problem for an increasing number of cycles, they defined the driving amplitudes and time delays required via the amplitudes and phase shifts obtained from the related time harmonic problem.

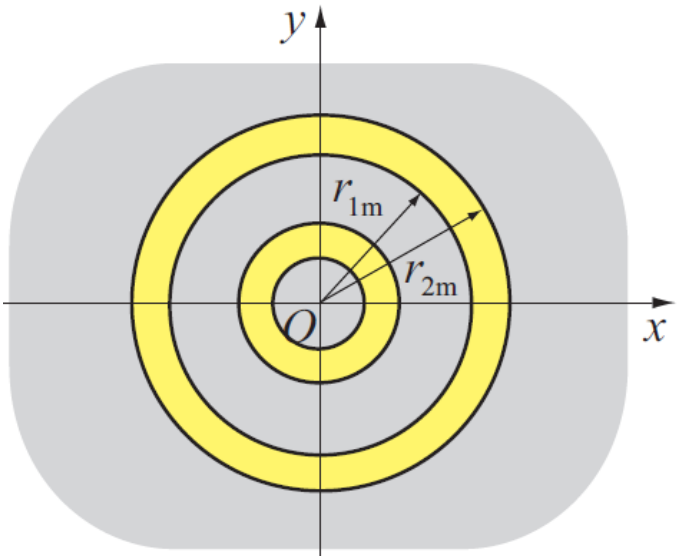

Figure 2. 7 Elastic plate with piezoelectric actuators (EV Glushkov et al., 2010).

2.4.3 Interdigital transducer (IDT)

A popular type of piezoelectric transducers is interdigital transducer (IDT) that are used widely because of their mode selectivity nature, wave directivity, excitation strength, shape flexibility, size and relatively low cost.

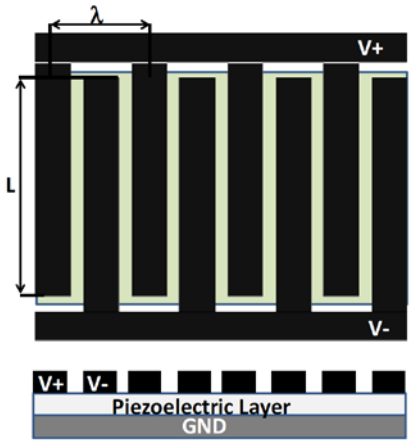

Figure 2. 8 Plane view and cross section of the IDT transducer (Monkhouse et al., 2000).

As shown in Figure 2. 8 , IDT transducer consist of three main layers: bottom (ground) electrode, piezoelectric layer and top (phase) electrodes (Monkhouse, Wilcox, & Cawley, 1997). The second layer, piezoelectric layer, could have different characteristics like the numbers of layers, materials properties, polarization direction, direction of piezoelectric fibers, etc. The material properties of this layer may be of PVDF (Bellan et al., 2005), piezoceramic material (Luginbuhl et al., 1997), piezoceramic composite, or micro fiber composites (MFCs) (Williams, Park, Inman, & Wilkie, 2002).

The most significant part of the IDT is the third layer which consists of top electrode patterns. A number of research efforts are presented in the following in which the pattern of the top electrode was studied. Typically on the top surface, there are two sets of comb shape electrodes. The distance between electrodes (finger separation) defines the length of the induced wavelength λ (Monkhouse et al., 1997), (Monkhouse et al., 2000).

(Mańka, Rosiek, Martowicz, Uhl, & Stępiński, 2010) designed a simple IDT considering wavelength of excited modes. They studied another aspect of IDTs that is directional generation the GWs. GWs are generated in perpendicular direction to the electrodes fingers and divergence of the wave is dependent on the fingers length that is a significant advantage with respect to the

standard PZT patch. As will be seen in CLoVER and FSAT sections, it is possible to generate GWs in a specified direction using directional bonded electrodes.

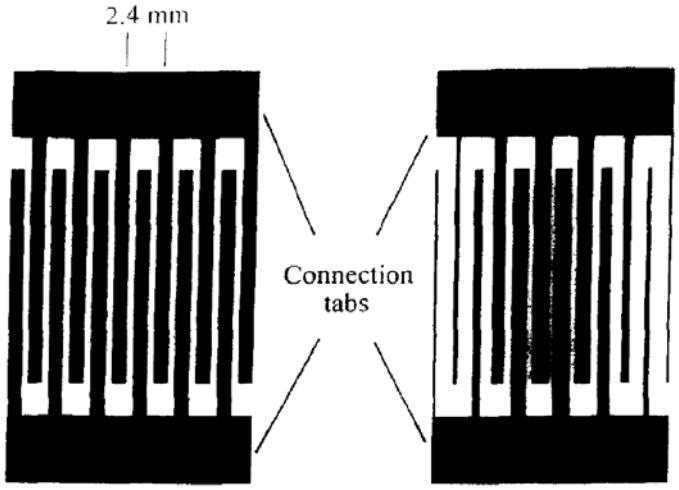

Figure 2. 9 Typical transducer electrode patterns for $\lambda = 2.4$ mm (a) plain; (b) apodised (Monkhouse et al., 1997).

They showed that the bandwidth of wave induced by IDT is narrower which can reduce wave dispersion. Moreover, the energy generated by IDT is focused on desired mode. (Hayward et al., 2001) used FEM and experimental methods to study IDTs and plate transducers to generate uni-modal GW. They selected S_0-mode for propagation because the S_0-mode demonstrates negligible velocity dispersion at lower frequencies. Therefore, the IDT was positioned in the middle of the plate to generate the pure S_0-mode, and they could suppress A_0-mode.

(Monkhouse et al., 1997) developed a cheap PVDF IDTs for SHM systems in order to strengthen the symmetric modes in plates with different thicknesses and materials. They studied the frequencies at which the selected mode with desired wavelength has the fastest group velocity and least dispersion. As shown in Figure 2. 9, they designed an IDT to excite the A_0-mode dominantly by consideration of desired wavelength. By keeping the length of the fingers, they changed the width of the fingers.

The materials of electrical connections are important for GW mode excitation. They used copper material connection on their PVDF film. They showed that as the thickness of copper connections increases, the frequency of maximum response is reduced and the low frequency response is improved.

There is a desire to design an IDT with 360^0 vision inspection ability. (Monkhouse et al., 2000) expanded their previous work to the IDTs with selective area inspection ability. They designed a 60^0 sub-transducer with sector IDT, as shown in Figure 2. 10, to generate a uniformly diverging beam. But results showed that the beam covered uniformly around 40^0 well below the angular aperture (60^0) of the device and this kind of IDT needs more investigation.

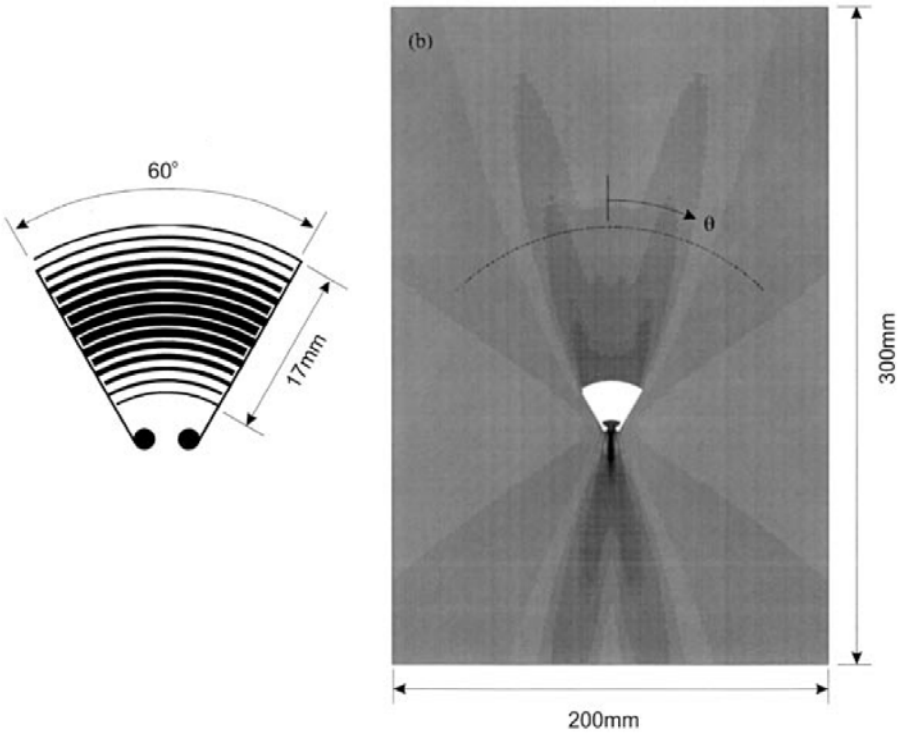

Figure 2. 10 60^0 radial transducer (Monkhouse et al., 2000).

(Liu, Veidt, & Kitipornchai, 2002) investigated the piezoelectric element interaction effects of array of an IDT for low frequency excitation. They used different parameters in their uncoupled formulation to study the influence of effective parameters on GW generation such as the electrical characteristics of the excitation circuit, the material properties of piezoelectric of the

transducer array, the thickness and width of elements, the thickness of the plate and its mechanical properties, the spacing distance between the center of elements, and the number of elements. It was observed that considering the effects of electro-mechanical interaction significantly changes the acoustic wave field generated in all presented cases. This effect was more pronounced for larger number of array elements. They could generate stronger GWs amplitude by increasing the number of the elements in the array, because it increases the transducer's impedance and the transferred energy form its power source to the elements.

(Schmidt, Sinapius, & Wierach, 2013) designed and optimized the mode selective piezocomposite transducer with applied interdigitated electrodes. As can be seen in Figure 2. 11, to increase the effectiveness of their transducer, they used apodisation, but not for the width of the elements, for the overlaps of each electrode pair that was varying along the transducer designed to excite a specific GW-mode. They studied the width variation of electrodes and amplitude of symmetric and anti-symmetric GW-modes. As can be seen in Figure 2. 12, to maximize one mode and minimize another one, an electrode width of 80% of the half-wavelength seems to be obtained.

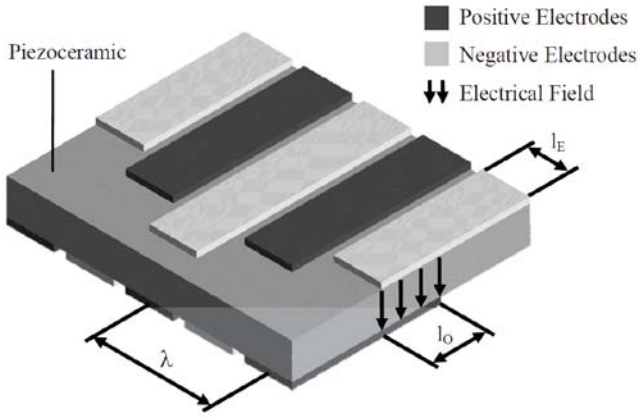

Figure 2. 11 Schematic design of an IDT with apodization (Schmidt et al., 2013).

The complexity of analysis of generated GW by piezoelectric composite IDT increases, when using SAW on composite. (Mahapatra, Singhal, & Gopalakrishnan, 2005) used layerwise theory to develop the equivalent single-layer model based on higher order shear deformation (HSDT) and presented a coupled analysis based in spectral element method (SEM), which overcomes

some of the modeling difficulties. Using this numerical method, they studied the effect of IDT geometrical parameters, the material properties of the each layer, and finite space-time window. It should be noted that (Mohamed & Masson, 2010) presented two-dimensional SEM as modeling tools specifically tailored for rapid computer aided design of SHM applications because of its advantages in comparison with FEM. (Mohamed, Demers, & Masson, 2011) studied the effect of thickness variation on the fundamental GW S_0 and A_0 mode using SEM as a solver.

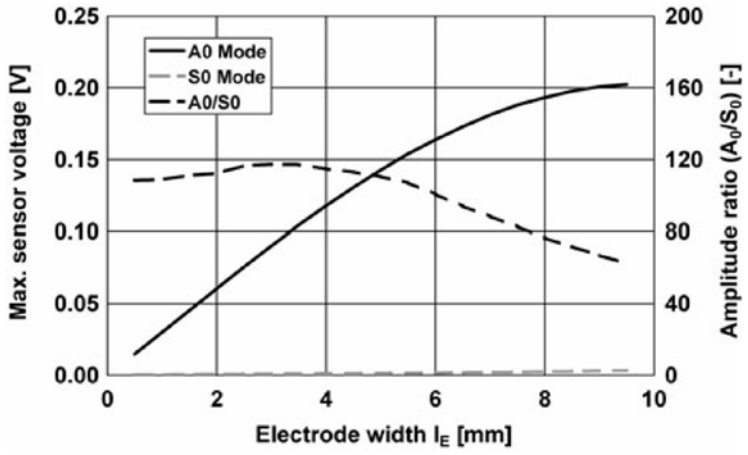

Figure 2. 12 Max. amplitude of A_0 and S_0 mode at different electrode widths, actuator with 7 electrodes, 40 kHz, 2 mm thick CFRP plate (Schmidt et al., 2013).

2.4.4 Phased array transducer

To overcome disadvantages of traditional transducer array, (J. Li & Rose, 2001) built a multi-channel time-delay system to improve the array technology for GW excitation. As shown in Figure 2. 13, for each of these channels an individual output power control, physical time delay, receiver amplifier, and software time-delay were considered. In fact, the resolution and time domain delays can be determined by sending high energy controllable tone-burst signals from each channel. Based on element spacing and dispersion curves of a thin-wall carbon steel hollow cylinder, they determined time delays.

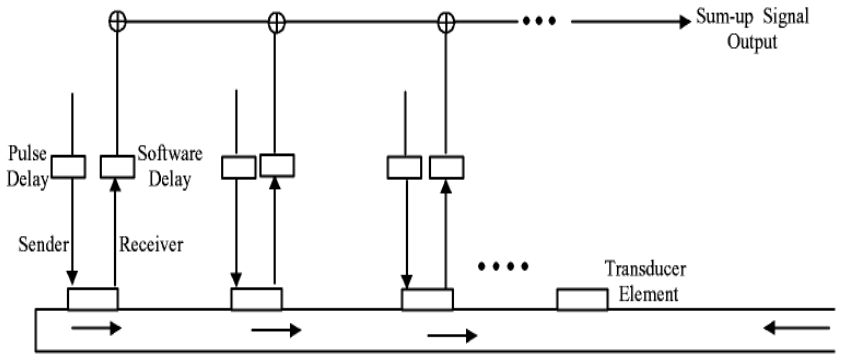

Figure 2. 13 A time-delay system with pulse (physical) delays and software delays for a transducer arrays (J. Li & Rose, 2001).

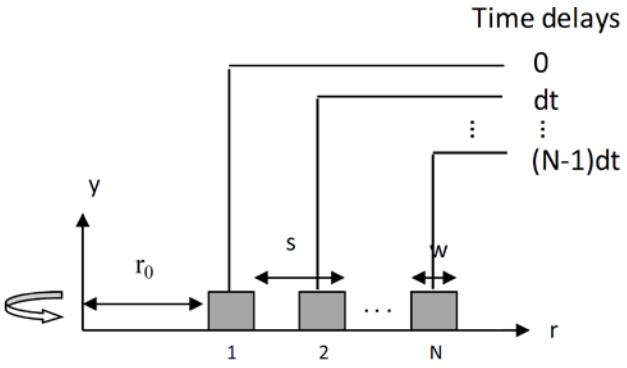

Figure 2. 14 Illustration of a phased annular array with a time delay dt applied between each adjacent array elements (Yan, Borigo, Liang, Koduru, & Rose, 2011).

(Yan et al., 2011) used electronically tuning the GW modes and frequencies to apply different loading function in ultrasonic modal analysis technique. Appropriate time delays were applied to a multiple elements annular array transducer to generate A_0 and S_0-modes selectively, as it is shown in Figure 2. 14. So, they calculated the Hankel transform of the axial source loading profile. They achieved wave mode and frequency tuning by applying proper time delays to each element.

2.4.5 Micro-Fiber-Composite (MFC)

MFCs are made of micro piezoelectric fibers that are localized in the matrix construction of a composite that increases directivity of the transducers. The MFC layer can be aligned or sandwiched between two sets of electrode patterns, as shown in Figure 2. 15.

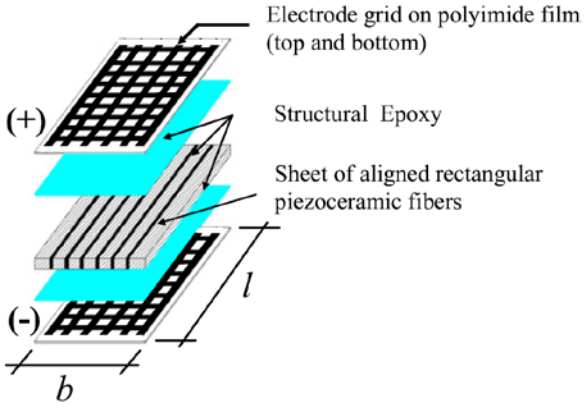

Figure 2. 15 Macro-fiber composite transducer (type P2) with geometrical reference (Matt & di Scalea, 2007).

(Matt & di Scalea, 2007) used Pb(Zr-Ti)O_3 (PZT) fibers to study rectangular MFCs or rosettes as sensors. They investigated the effect of angle between fibers and wave propagation directions in MFC sensors and their location. They used four important parameters in their investigation: length, width, thickness and density of arrays of rosettes for covering large areas. Their sensor sensed the propagated A_0-mode at higher frequencies where the wavelength is comparable to the sensor's dimensions due to tuning effects. It was assumed that the wave fields were not affected by the presence of the sensor. The response of the sensor increased as its length increased. Their experimental tests on both composite and sandwich panels showed that the material property of the host structure is an important factor that has to be considered in MFC transducers design.

Piezoelectric fiber composites (PFCs) are used as actuators in some fields, such as vibration control, energy harvesting devices, and SHM (Bent, Hagood, & Rodgers, 1995; Schulz,

Sundaresan, Ghoshal, & Pai, 2000; Wilkie, High, & Bockman, 2002). Sensitive factors on GW generation by PFCs are polymeric matrix, fiber volume fraction, fiber orientation and poling direction (Sheng Li & Lissenden, 2010; Lissenden, Li, & Rose, 2010).

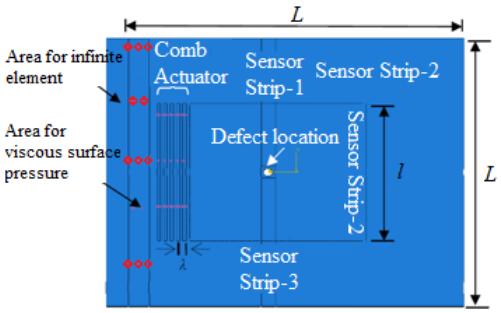

Figure 2. 16 Geometry of the finite element model in ABAQUS (S Li & Cliff, 2011).

(Pasco & Masson, 2009) presented an analytical model in order to simulate PFCs with inter-digital electrodes in the plate-like structure in order to allow ultrasonic wave generation at high frequency. They showed that the length of the sensor and wavelength of the desired GW-mode has to be considered in directivity patterns. Like what was seen in (Matt & di Scalea, 2007), they concluded that the angle between the wave propagation and fibers direction affects on sensibility of this sensor. In addition, they fixed PFC actuator and used it for GW generator in particular direction.

(S Li & Cliff, 2011) simulated PFC transducers using ABAQUS software, as shown in Figure 2. 16, to study the sensitivity of this type of transducer for the detection of different kinds of defects. Selected GW-mode can be excited by adjusting fiber spacing to be equal to the wavelength of the desired mode.

2.4.6 Wedge angle transducer

The angle beam method uses wedges to better control mode generation with higher sensitivity (I. Viktorov, 1967). The desired mode can be excited by changing the wedge angle manually or by using a stepper motor. Water immersion or Plexiglas wedges have to be used to couple the

ultrasonic angle beam transmission into the host structure. The problem is that the involvement of a mechanical system makes the inspection much longer than an electronic scanning system. (I. Viktorov, 1967) analyzed both theoretically and experimentally the wedge method of generating GWs in isotropic layers. He computed the optimal angle wedge on the neighberhood of the Snell's law angle of a given wavenumber. Regarding the incidednt beam only insonifies the layer over a finite portion of its surface, he also concluded that there was actually a continuous dependence of the excitation amplitude of any mode on the angle of incidence that is other than being a single angle at which a particular mode could be generated.

(Ditri & Rajana, 1995) developed wedge technique considering the displacement of the excitation amplitude of the desired GW-mode on the angle of incidence of the wedge. They presented the amplitude of the given mode as a function of the Snell's law phase, and shown its width is dependent only upon the ratio of loading length to wavelength of the mode being generated.

Using two wedge transducers, (Pruell, Kim, Qu, & Jacobs, 2009) presented a technique to identify the plasticity-driven damage by the generated S_2-mode. They improved the wedge design and increased the fundamental amplitude five times more that the similar one in (Bermes, Kim, Qu, & Jacobs, 2007), by using a separate screw-tightened piece to apply a constant pressure on the transducer. At one angle, the wedge transducer generates the S_1 and S_2–mode simultaneously in which their phase velocities are equal. They governed the amplitude of the second harmonic GW by synchronous velocity in which the energy of the fundamental mode transfers to the second harmonic mode. In the measured results, the acoustic nonlinearity increases monotonically with the level of the plasticity. The resonant behavior of the wedge transducer /receiver makes it more sensitive to the S_2-mode which is normally weak thus improving the signal-to-noise ratio.

(Rosalie, Vaughan, Bremner, & Chiu, 2004) used both embedded PZT and wedge transducers to detect the delamination in an aluminum plate by considering the group velocity of the GWs.

As an application of wedges, (Joo, Park, Lee, Kim, & Lim, 2011) designed and used a wedge transducer for an under-sodium visual inspection of the in-vessel structures. They attached a wedge transducer on a 10 m long ultrasonic waveguide sensor module which consists of a plate waveguide. Then, A_0-mode was generated because of its effective radiation capability and its perpendicular displacement to the plate due to the flexural mode and high radiation in the fluid. Because of the contact of the plate and the liquid, the propagated GW become leaky GWs from the solid plate to the longitudinal waves in liquid. They controlled the radiation beam angle ultrasonically by a frequency tuning method of the excitation pulse in the dispersive low frequency range of the A_0-mode.

Modes with a small amount of out-of-plane surface displacement have low leakage attenuation and are also hard to excite with an out-of-plane surface force. For this reason alone it would be expected that the angle incidence technique is not a good transduction method to use with low attenuation GW-modes, and this will shortly be demonstrated quantitatively. Alternative transduction schemes must then be investigated. In spite of the capability of the wedge angle transducers for mode-selective GW generation, PZTs are still more attractive to be used in SHM system because the adhesive layer between the PZT and the host structure leads to maximum transmission level of energy to the host structure.

2.4.7 Tilted angle polarization type piezoelectric transducer (TAPP)

Polarization direction can be considered as another parameter in optimization of PZTs transducers. This polarization is usually perpendicular or parallel to the surfaces of the transducer. As shown in Figure 2. 15, (Imano, 2007) used Snell's law to design a titled angle polarization type piezoelectric transducer (TAPP) with title angle 50^0 for S_0-mode generation. The TAPP was then manufactured by Fuij Ceramics Co. Ltd.:C-13.

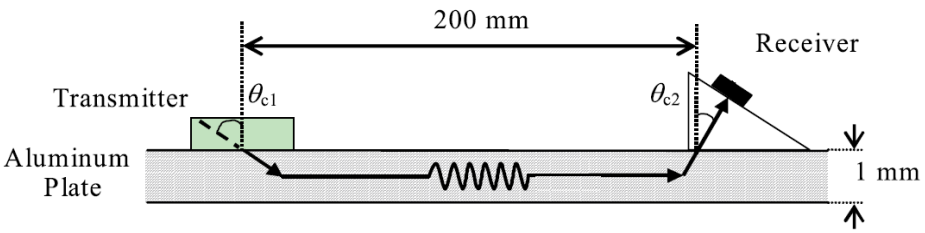

Figure 2. 17 Experimental System (Imano, 2007).

It should be noted that the resonance frequency of both normal type and TAPP transducers were the same. Their experimental results show the amplitude of generated GWs by TAPPs are 10 dB more compared to those obtained by a normal PZT, and they have less dispersion.

(Qin, Chen, Cheng, & Wang, 2010) studied analytically thin film bulk acoustic wave resonators (FBARs) using ZnO and AIN. The tilt angle films in both in-plane and normal plan polarization direction affects strongly on coexistence of the longitudinal and shear mode in resonator. They used ZnO and AIN film and concluded that for ZnO FBARs, pure thickness longitudinal modes occur at 0^0 and 65.4^0, and pure thickness shear mode occur at 43^0 and 90^0. The tilted angles for AIN were investigated similarly and also the shear electromechanical confidents maximized at two specific tilt angles. The dual-mode FBARs can increase sensitivity of sensors because of their large resonance frequency shift.

2.4.8 Electromagnetic acoustic transducer (EMAT)

The EMAT uses the magnetostrictive effect. An EMAT shares a similar design with the interdigital transducer technique although the mechanism of an EMAT is based on the Lorentz force in a magnetic field (Frost, 2012). With the latest improvement of efficiency, the EMAT is receiving a lot of attention because of its coupling-free advantage and efficient SH-guided wave generation capability (Fortunko, King, & Tan, 1982).

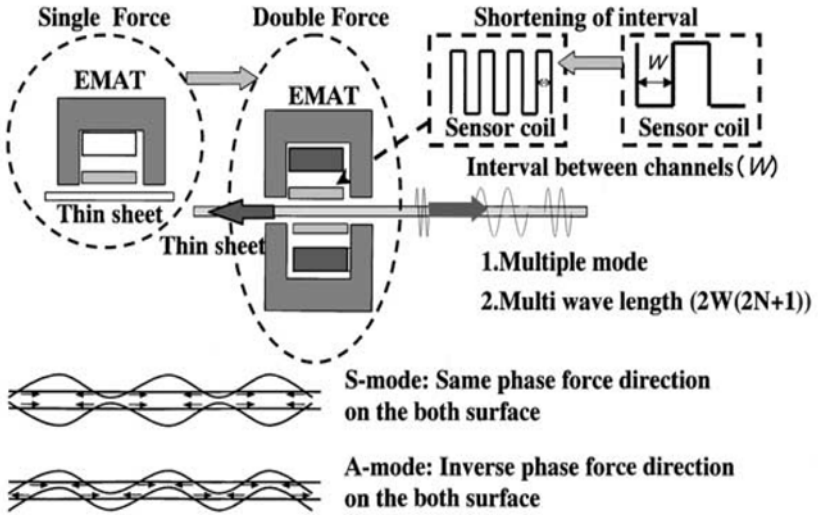

Figure 2. 18 Concept of a trial EMAT (Murayama & Mizutani, 2002).

(Murayama & Mizutani, 2002) presented an EMAT for mode-selective GW generation. They positioned EMATs appropriately and controlled the phase of both transducers at both sides of the metallic plate to generate selective A_0, A_1, S_0, and S_1-modes at special frequencies, as show in Figure 2. 18. As an application of EMATs, the stress distribution evaluation in a tensile metallic plate can be performed based of time of flight of the GWs. Embedded and bonded sensors cannot be used in these systems as they should be in contact with the plate. However, EMATs have found applications in many areas. For example, when tensile stress is applied to the plate, the distance between transducers changes. Thus, (Murayama & Mizutani, 2002) used non-contact EMATs for measurement of GW during tensile testing. They use S_0-mode selectively for the measurement of GW.

Robots are used for non-destructive fault detection in thin-wall structures. Contact transducers cannot be used in these robots because of the need to have a perfect coupling with the host structure. (Murayama & Mizutani, 2002) developed an ultrasonic inspection robot with EMAT that could transmit and receive GW with high sensitivity, such as SH-plate wave. They showed how to generate S_0 and SH_0-modes by using the direction of generated magnetic field to the direction of robot traveling. For instance, when the compound's generation magnetic field is in a parallel direction to the traveling direction, magnetostriction changes that leads to S_0-mode GW generation.

2.4.9 Composite long-rang variable-direction emitting radar (CLoVER)

In addition to mode selectivity, an ideal transducer needs the ability of selective GW propagation direction (directivity). (Salas & Cesnik, 2009) CLoVERs consist of an IDT-shaped anisotropic piezoelectric transducer arranged in circular array to generate GW sequentially in complete 360^0 structural range, as shown in Figure 2. 19.

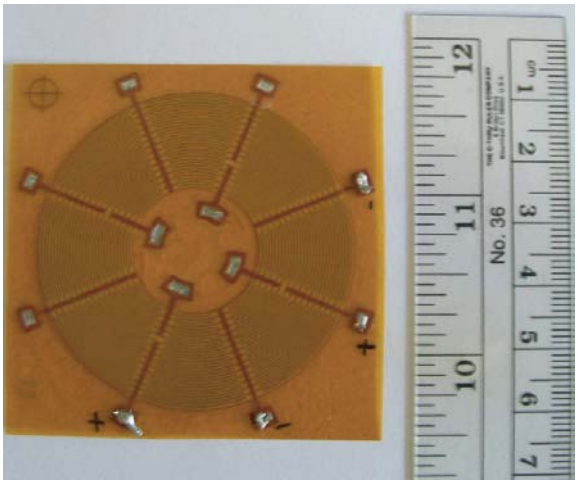

Figure 2. 19 Illustration of the CLoVER transducer (K. Salas & C. Cesnik, 2010).

These transducers conform to curved surfaces due to their composite construction characteristic. As azimuthal span is decreased in CLoVERs, the capacitance decreases that leads to generating GWs with stronger amplitude even than resonant GW-modes in tuning method (Giurgiutiu, 2007). The upper electrode consists of two independent set of radial subdivision fingers that are connected independently to two cables (Figure 2. 20), one as sensor and another one as actuator. Thus, CLoVERs can be used as both sensors and actuators. Its variable-length of electrodes can be used for mode-selective GW excitation by selecting the radial dimension according to the wavelength of the desired mode. (K. I. Salas & C. E. Cesnik, 2010) studied experimentally the use of the CLoVER for SHM of composite materials with different layups. The performance of CLoVERs design at higher frequencies was impaired because (1) the electromechanical coupling between the transducer and the host structure did not considered, (2) the derived 3D equations of electricity of their analysis was based on considering shear tractions along the transducer's radial edges.

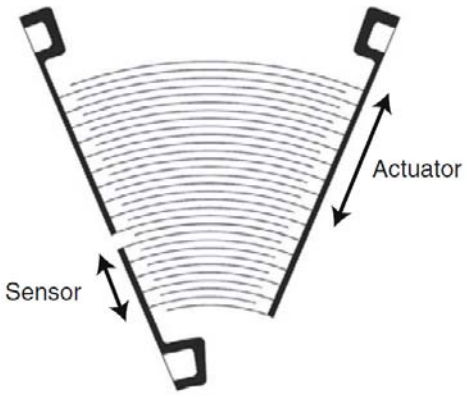

Figure 2. 20 Electrode design used in first generation of CLoVER sectors (Salas & Cesnik, 2009).

2.4.10 Frequency steerable acoustic transducer (FSAT)

(Baravelli, Senesi, Ruzzene, De Marchi, & Speciale, 2011) designed the frequency-steerable acoustic transducer (FSAT) which is a shaped array with a spatial distribution that defines a spiral in the wavenumber domain, as shown in Figure 2. 21. The FSAT controls beam steering on frequency-dependent directional properties using a single two channel device. The direction of the magnified GW-mode beam changes in FSAT as a function of frequency, because the wavelength of generated GW-modes changes as the frequency changes. Thus, GW-modes can be tuned or damped when the wavelength reaches width of spiral elements as justified in Eqs. (1.7) and (2.8), so that spatial shape of the FSAT changes the propagation direction of the beam steering. It should be noted that to fabricate the FSAT, the transducer's elements should be cut completely through the thickness of the piezoelectric material and it is not only electrode patterning.

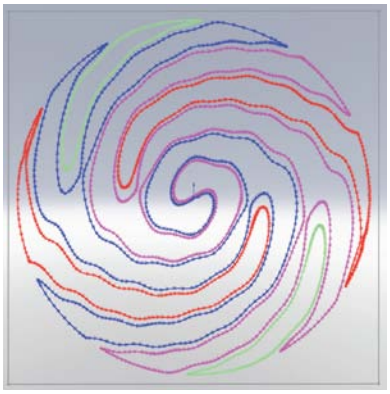

Figure 2. 21 Schematic of electrode patterning of FSAT (Baravelli et al., 2011).

The loss of accuracy they noticed in numerical results could be related to non-uniform spectrum of the excitation, reflectivity properties of the scatterers, and measurement noise. The disadvantages of this transducer are coming from the facts that (1) the fabrication is challenging with piezoelectric ceramics and the prototype sample was fabricated with PVDFs that increases the sensitivity of the transducer to the temperature variation significantly, (2) magnifying the desired mode in preferred direction is not possible at all frequencies. It means they cannot monitor 360^0 area of a structure for SHM application at any given frequency (3) the fabrication process is very expensive. Therefore, an optimization process for this type of transducer can be selected to eliminate the problems noticed.

2.5 Modeling of GW generation

PZTs induce stress to the host structure at their interfacial area. PZTs are commonly bonded on the host structure with an adhesive layer. This discontinuity makes the interfacial shear stress modeling very complicated because it implies the dynamics of PZT, adhesive layer, and the host structure (Ha & Chang, 2010). To overcome those limitations, more refined models have been proposed by (M. Lin & Rogers, 1993) and (Liu et al., 2002) to simulate PZT actuators analytically, based on the Mindlin plate theory. Mindlin plate theory incorporating transverse shear and rotary inertia effects was used and the actuators were modeled as causing bending moments along their edge. The disadvantage of Mindlin plate theory is that it is limited to

relatively low frequencies, below the cut-off frequency at which higher anti-symmetric GW modes other than A_0-mode can appear.

(Lamb, 1917) described first free, time harmonic, plain strain waves propagating in elastic layers. (I. Viktorov, 1967) used Fourier transform to investigate GWs modeling by a specific traction applied to the surface of the plate. (Achenbach & Xu, 1999) modeled GW generation in elastic layers by time harmonic point loads using a membrane carrier wave for the resulting fields which is valid throughout the entire waveguide continuum.

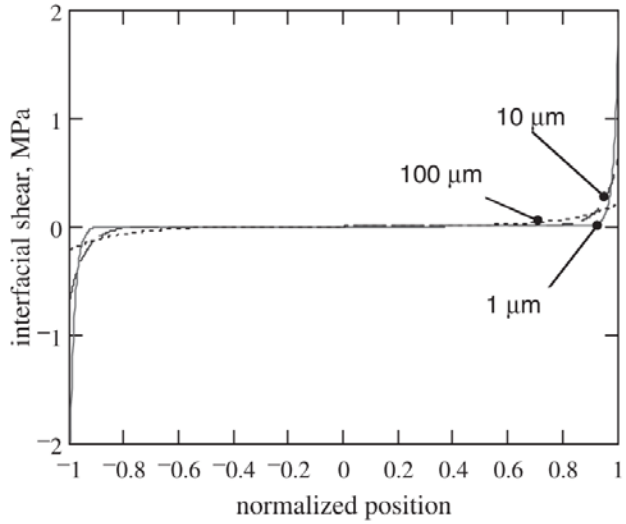

Figure 2. 22 Variation of shear lag transfer mechanism with bond thickness for a APC-850 PZT (E_a = 63 GPa, t_a = 0.2 mm, l = 7 mm, d_{31}= -175 mm/kV) attached to a thin-wall Al structure (E = 70 GPa and t = 1mm) through a bond layer of G_b = 2 GPa (Giurgiutiu & Bottai-Santoni, 2009).

(Crawley & De Luis, 1987) and (Giurgiutiu, 2007) demonstrated that the interfacial shear stress is confined at the edges of the actuator as shown in Figure 2. 22. So, they ideally considered that the PZT is coupled to the host structure and a sharp rise in the shear stress exists at the tips of piezo-actuator, indicating that the strain is transferred between the piezo-actuator and the host structure over an infinitesimal distance near the edge of the actuator (Giurgiutiu & Bottai-Santoni, 2009). This model is known as the pin-force theory. The interfacial shear stress in this theory is expressed using Dirac function $\delta(x)$ as (Giurgiutiu & Bottai-Santoni, 2009):

$$\tau_x(x) = \tau_0\left[\delta(x-a) - \delta(x+a)\right], \tag{2.8}$$

where τ_0 is the pin force magnitude applied at the piezoelectric actuator edges.

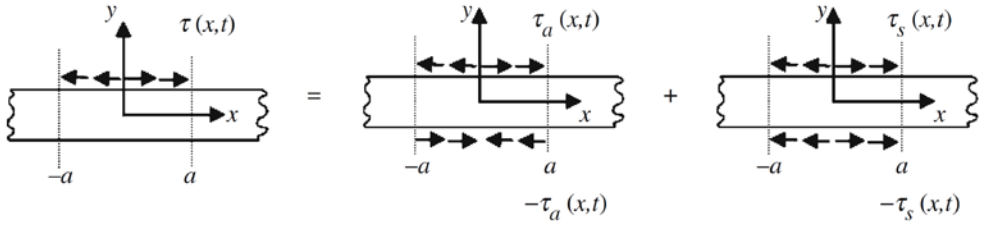

Figure 2. 23 Decomposition of the boundary conditions into symmetric and anti-symmetric parts (Von Ende & Lammering, 2007).

To simulate GW propagation through the thickness of the plate, (Von Ende & Lammering, 2007; Von Ende, Schäfer, & Lammering, 2007) proposed an analytical solution for GW generation by uniform shear stress based on 2D elasticity equations using Fourier transform and residue theorem for inverse transform. Their analytical method was based on decomposition of the interfacial shear stress and considered it as superposition of an applied symmetric shear stress and anti-symmetric shear stress, as illustrated in Figure 2. 23. They considered that the interfacial shear stress has uniform configuration. They were able to obtain the dynamic load transfer between a bonded PZT and an anisotropic elastic medium under in-plane mechanical and electrical loading.

(Crawley & De Luis, 1987) presented the analytical theory for modeling the stress and strain transfer between beams actuated by a PZT wafer though the adhesive layer, known as shear-lag theory. In the model, only non-zero stress within the adhesive layer is the interfacial shear stress, which is assumed as constant through the thickness of the adhesive layer and varies along the longitudinal direction of the adhesive layer (Euler–Bernoulli linear flexural or uniform extension). Basically, the model assumes (*i*) uniform strain in the bonded piezo-actuator, and (*ii*) uniform strain for axial motion and linear strain distribution for flexural motion across the thickness in the beam (Giurgiutiu & Bottai-Santoni, 2009). Considering two bonded PZT at both sides of the plate, the in-plane induced strain in the PZT was calculated as:

$$\varepsilon_{ISA} = d_{31}\frac{v(t)}{h_a}, \tag{2.9}$$

where $v(t)$ is the applied voltage to the PZT, d_{31} the piezoelectric strain coefficient in m/V capturing the coupling between the vertically polarized field and the in-plane induced strain and h_a is the thickness of the actuator. The interfacial shear stress in the adhesive layer is then defined as

$$\tau_{xz} = \frac{h_a\chi}{\alpha(\chi+a)}E_a\varepsilon_{ISA}\left(\Gamma\alpha\frac{\sinh(\Gamma\alpha)}{\cosh(\Gamma\alpha)}\right), \tag{2.10}$$

for $|x| < a$ where

$$\Gamma^2 = \frac{G_b(\chi+\alpha)}{E_a h_a h_b \chi}, \tag{2.11}$$

where $\chi = Eh/(E_a h_a)$, and G_b is the shear modulus of the adhesive material, h_b the thickness of the adhesive layer, E, h, E_a, h_a are Young's modulus and thickness of the plate and the actuator, respectively. The shear-lag parameter Γ is dependent on how the wave modes are excited. Considering two PZT bonded on both sides of the plate, if only axial wave is excited then $\alpha = 1$ (Crawley & De Luis, 1987); if only the flexural wave is excited, then $\alpha = 3$. If single PZT presents $\alpha = 4$.

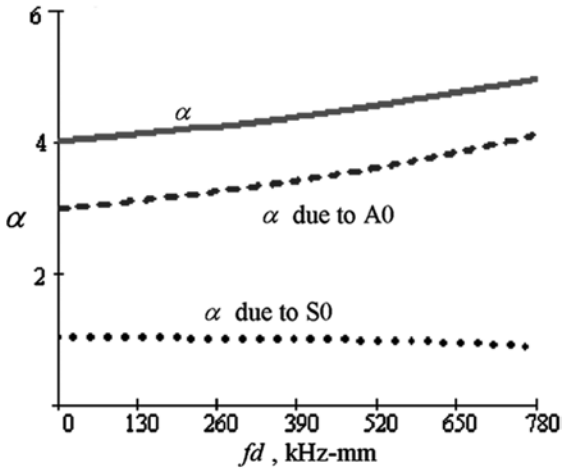

Figure 2. 24 Plots variation of *a* with frequency-thickness products for S_0 and A_0-modes (Giurgiutiu & Bottai-Santoni, 2009).

(Giurgiutiu & Bottai-Santoni, 2009) extended (Crawley & De Luis, 1987) theory to the case of only one piezoelectric element bonded to the thin-wall structure by calculating the total effect as a superposition of symmetric and anti-symmetric contributions and found the value for a single-sided piezoelectric excitation to be $\alpha = 4$. These investigations are valid at lower values of the frequency-thickness product where S_0 and A_0-modes are approximated to axial and flexural waves, respectively. At higher frequencies, the value of α becomes more dependent on frequency. (Giurgiutiu & Bottai-Santoni, 2009) presented an approach to take in to account contribution of A_0 and S_0-modes in final value α as a function of the value of the frequency-thickness value. We used this method and similar results are showed in Figure 2. 24. It illustrates at low frequency, value α is 1 + 3 = 4, but as *fd* increases, α also increases from $\alpha = 4$ to $\alpha = 5$ at high frequencies.

(Huang & Sun, 2006; X. Wang & Huang, 2001, 2003, 2006) simulated GW propagation by surface bonded PZT in an anisotropic plate using the elasticity equation-based model, even at higher frequencies. They divided the interfacial surface between the plate and the PZT into a finite number of points and based on continuity of axial strain at these points, they could determine the unknown constants of their analytical equation. Hence, continuous shear stress profile was obtained, from which propagation waves were simulated. The great advantage of this model is that it includes the coupled dynamic interaction between the actuator and the host

medium, and hence can quantitatively predict the piezoelectrically induced electromechanical behavior.

2.6 Optimization of piezoelectric transducers

Optimization has been used in various area of engineering and economics (Bertsimas & Tsitsiklis, 1997; Nocedal & Wright, 2006; Papadimitriou & Steiglitz, 1998). Many researchers have intended to optimize PZTs' parameters because of their crucial application in SHM. Optimization methods may have single or multi-objective functions. In most practical applications of PZTs, however, multiple design objective function exist and are often contradictory to each other by their very nature. In multi-objective optimization, reaching out global minima for all objectives simultaneously is possible as long as the final result minimizes unwanted status, and this is much dependent on the defined criteria.

In previous section, different types of transducers were categorized. Advantages and disadvantages of each transducer were discussed. So, all parameters that distinguished them from other transducers could be considered as a variable, but those ones that are the simplest and lead to low-price manufacturing process should be considered in next chapters to design and optimize of the transducer.

There are three common concepts in all optimization algorithms that are (1) objective function, (2) variables, and (3) constraints. It should be noted that an optimization method can be constrained or unconstrained (Dennis Jr & Schnabel, 1996), and there could be a large number of variables that increase the number of degrees of freedom of the optimization process. The inequality constraints may be simple bound constraints on individual variable, or they can be complex nonlinear constraints involving multiple variables. Based generally on the type of considered cost function $f(x)$ and related constraint $c(x)$ optimization problem types can be categorized as can be seen in Table 2. 2 (Bader, 2009).

Table 2. 2 Optimization problem types (Bader, 2009)

	Cost function	Constraint
	$f(x)$	$c(x)$
Unconstrained optimization	Nonlinear	None
Linear programming	Linear	Linear
Quadratic programming	Quadratic	Linear
Linear constrained optimization	Nonlinear	Linear
Constrained optimization or nonlinear programming	Nonlinear	Nonlinear

In this section, methods that have been used for optimization of PZTs are described coherently. In the conclusion section, an optimization method for our considered problem is selected and limitation(s) of each method in the context of current project is investigated. In continuous effort to achieve an ideal type of PZT for SHM applications, this thesis is going to concentrate on the design of a mode-selective transducer and present a global optimization approach that can be developed for more complicated cases. It should be noted that there will be two priorities in our design that are (1) simplicity, and (2) cost-effectiveness of the transducer.

2.6.1 Genetic Algorithm (GA)

GA is used as a popular optimization method (Mitchell, 1998). GAs are best used when the cost function is discontinuous, highly nonlinear, stochastic and has unreliable and undefined derivatives (Vose, 1999). The GA is used specifically in optimization approaches where the objective function(s) are clearly defined. (Yi, Li, & Gu, 2011) used a multi-objective optimization method to investigate placement of sensors on a plate for damage detaction. They developed an optimal sensor placement strategy (OSPS) toolbox based on command-line compiling and GUI-aided graphical interface design. (E. B. Flynn & Todd, 2010) used the GA with time-varying mutation rate for optimal transducers placement based on general formulation of Bayes risk. Their objective function was minimizing the expected total presence of errors during damage detection process. Their method had the capability of optimizing non-uniform damage probability distributions, concave structure geometry, and potential sensor failure.

(Bland & Kapania, 2006) also investigated optimal placement of transducers. They simulated GW propagation in an Al plate using the Local Interaction Simulation Approach (LISA), which is more efficient than the FEM. The sensor performance metric (SPM) is then evaluated using the simulated sensor data. They defined the objective function based on maximizing SPM for the entire transducers array using GA optimization process.

2.6.2 Artificial Neural Network (ANN)

ANN is another optimization method. In fact, ANN in SHM is used when any changes appear in the condition of the host plate. A well-trained ANN can predict outcomes under an unknown stimulus according to pre-accumulated knowledge, while avoiding interrogating intricate constitutive relations. In particular, an ANN operates as a parallel computational model to authentically explore the connection between a series of reasons (inputs) and consequences (outputs) for a given system. (Park, 2000) combined ANN with the impedance method to damage identification. They integrated multiple sets of ANN with the impedance-based SHM technique to avoid the complexity introduced by conventional computational methods in high frequency ranges. As a result, their technique was able to determine the severity of damage without considering the knowledge of its host-plate. (Liang & Hwu, 2001) used static strains measured by strain gauges as detector of the inverse problem, and defined the system with on-line identification using an ANN network. They used two hidden layers in ANN network to relate the measured strains to the holes and cracks' parameters. They could identify the size, location, and orientation of defects.

2.6.3 Other popular optimization methods in SHM

IDT optimization has attracted many researchers. (Bausk, 1999) used withdrawal weighting (WW) technique a optimization algorithms for improving the selectivity of IDTs' bandwith. The algorithm tries to find the best IDT configuration on the basis of how well it meets the specifications in the frequency domain.

(Brown, 2000) considered the transferred power of an untuned piezoelectric polymer at resonance frequency, and maximized it by optimization of capacitive reactance (i.e., active area). They considered that the clamped permittivity and dielectric loss tangent vary greatly with frequency (permittivity decreases; dielectric loss tangent increases) for PVDF, as shown in Figure 2. 12. It should be noted that there are two main criteria in choosing a transducer: (1) maximize the strain in the structure per unit volt, (2) keep the magnitude of the power delivered by the function generator below a determined voltage.

Using wavelet decomposition, (Marantidis, Van Way, & Kudva, 1994) and (Seth Stovack Kessler, 2002) studied various parameters of PZTs which affect GW generation. They tried to find out the optimal material properties, geometry, mechanical and electrical properties connections of GW actuating and sensing for damage detection in composite structures. For actuator, they concentrated on investigating the optimal applied voltage to the actuator. As discussed, in ring and circular part (EV Glushkov et al., 2010; Yeum et al., 2011), they experimented the effect(s) of using circular and ring shape of transducers. They found the ring and circular shapes as the optimal shapes for actuators and sensors, respectively.

2.7 Conclusion

PZT transducers are commonly used in SHM systems to generate and measure GW in plate-like structures that can travel over long distances. In most cases, in order to perform damage detection, advanced signal processing techniques are required, since a minimum of two dispersive modes are propagating in a host structure. A comprehensive literature review was performed to investigate the best approach of simulating GW generation. It is concluded that an accurate modeling of interlaminar shear stress is a requirement for successful design of mode-selective transducer to take into account the interlaminar stress at inner areas of PZT especially at high frequencies. Behavior and sensitivity of modes in interaction with variety of defects was investigated, and necessity of mode-selective excitation was justified.

Various designs of mode-selective PZT were presented, and their capability was studied. Since most of these designs are based on the pin-force model; they could not perform efficiently at high frequencies. A mode-selective PZT will be designed in this thesis based on simplicity, cost-effectiveness, and very high accuracy even at high frequencies.

GA is used in this thesis as the preferred optimization algorithm for mode selection of generated GW since this method is preferable when the cost function is discontinuous, highly nonlinear, and stochastic or has unreliable or undefined derivatives. Moreover, even though there is no guarantee of converging to the global minimum, the final solution of GA is less dependent on the initial guess of parameters. GA is generally the preferred method over other optimization methods like the gradient based method since in the latter case; the final result may depend on the initial guess of the parameters and may converge to a local minimum instead of a global minimum.

CHAPTER 3

MODE SELECTIVE GENERATION OF GUIDED WAVES BY SYSTEMATIC OPTIMIZATION OF THE INTERFACIAL SHEAR STRESS PROFILE

Peyman YAZDANPANAH MOGHADAM
Nicolas QUAEGEBEUR
Patrice MASSON

GAUS, Department of Mechanical Engineering
Université de Sherbrooke
Sherbrooke, Québec, Canada

Smart Materials and Structures (Impact factor : 2.502), Submitted in June 2014, Published in November 2014

3.1 Contribution summary

In first step of this research, an accurate analytical model is required for Guided wave (GW) propagation through the thickness of isotropic plates. This analytical model should simulate the generated GW by an arbitrary interfacial shear stress because surface bonded PZTs generate GW in host structures by applying interfacial shear stress. The arbitrary configuration of stress brings more flexibility to design a mode-selective PZT in the following chapter. In addition, arbitrary configuration of interfacial stress enables the analytical model to simulate high frequency behavior as it is not negligible at inner areas of a bonded PZT and a plate. It is then required to investigate a novel optimization approach and objective functions to optimize the interfacial shear stress for mode-selective GW generation in flat plates.

3.2 Abstract

Piezoelectric transducers are commonly used in Structural Health Monitoring (SHM) systems to generate and measure ultrasonic Guided Waves (GW) by applying interfacial shear and normal stresses to the host structure. In most cases, in order to perform damage detection, advanced signal processing techniques are required, since a minimum of two dispersive modes are propagating in the host structure. In this paper, a systematic approach for mode selection is proposed by optimizing the interfacial shear stress profile applied to the host structure, representing the first step of a global optimization of selective mode actuator design. This approach has the potential of reducing the complexity of signal processing tools as the number of propagating modes could be reduced. Using the superposition principle, an analytical method is first developed for GWs excitation by a finite number of uniform segments, each contributing with a given elementary shear stress profile. Based on this, cost functions are defined in order to minimize the undesired modes and amplify the selected mode and the optimization problem is solved with a parallel Genetic Algorithm (GA) optimization framework. Advantages of this method over more conventional transducers tuning approaches are that (1) the shear stress can be explicitly optimized to both excite one mode and suppress other undesired modes, (2) the size of the excitation area is not constrained and mode-selective excitation is still possible even if

excitation width is smaller than all excited wavelengths, and (3) the selectivity is increased and the bandwidth extended. The complexity of the optimal shear stress profile obtained is shown considering two cost functions with various optimal excitation widths and number of segments. Results illustrate that the desired mode (A_0 or S_0) can be excited dominantly over other modes up to a wave power ratio of 10^{10} using an optimal shear stress profile.

3.3 Introduction

Ultrasonic Guided Waves (GWs) are being used in Structural Health Monitoring (SHM) systems as a rapid and robust method for inspection of pipes, rails, thin-walled structures, multilayered structures, and composite materials (Balageas, Fritzen, & Güemes, 2006). GWs can travel over long distances and are highly sensitive to interaction with damages, depending on propagating GW mode and frequency range (J. L. Rose, 2004; I. Viktorov, 1967; X.-M. Wang & Ying, 2001). As damage detection and localization is sought, the multi-mode nature of GW generation involves higher complexity in signal processing, since a minimum of two fundamental symmetric (S_0) and anti-symmetric (A_0) modes are propagating (Castaings et al., 2002; J. Rose, Pilarski, & Ditri, 1993; Santoni et al., 2007; Shelke et al., 2011).

Piezoelectric elements have been studied accurately because of their widely statically and dynamical applications such as structural vibration, acoustical generated noise, etc (Chee, Tong, & Steven, 2000; Sheikh, Topdar, & Halder, 2001; Sze & Yao, 2000; Yazdanpanah Moghadam, Tahani, & Naserian-Nik, 2013). Piezoceramic transducers, generally constituted of Lead Zirconate Titanate (referred as PZT), are used in most of the GW-based SHM applications to generate and measure GW by inducing shear and normal stresses at their bonding interface with the host structure (Huang & Sun, 2006). Previous studies on design techniques for mode selection using simple piezoceramic transducers rely on the local optimization approach (Bland & Kapania, 2006; E. Flynn & Todd, 2009; Seth S Kessler, Spearing, & Soutis, 2001; Marantidis et al., 1994; Yi et al., 2011). Using wavelet decomposition, (Marantidis et al., 1994) and (Seth S Kessler et al., 2001) studied different parameter of PTZs which affect GW generation. They tried to find the optimal mater ial properties, geometry, mechanical and electrical properties for GW

generation and sensing for SHM of composite structures. (Sohn & Lee, 2010) tuned the size of transducers and the driving frequency for mode-selective generation and sensing of GWs. In all cases, design rules for mode selective generation are based on the accurate modeling of GW generation by piezoceramics (Huang & Sun, 2006; Yazdanpanah Moghadam, Quaegebeur, & Masson, 2013). Classical models are based on the assumption of pin-force excitation, assuming that the shear stress profile corresponds to a delta Dirac function applied on the edges of the transducer. This assumption is valid for low frequency GW generation (Raghavan & Cesnik, 2005) and does not take into account the distributed shear and normal stress profiles induced by the transducer at higher frequency. Moreover, the dynamics of the PZT is usually not considered, such that classical theories are limited for generated wavelengths large compared to the transducer size.

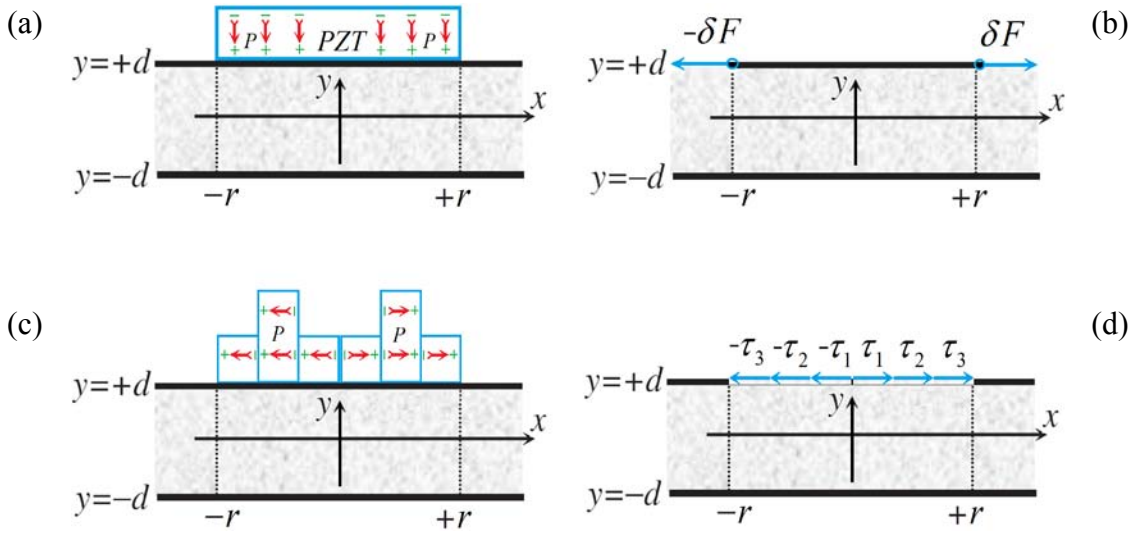

Figure 3. 1 Comparison of classical actuator design models for PZT transducers using the pin-force assumption (a, b) with possible actuator design using parallel polarization directions (c), with the capability of controlling individual elements (d).

To overcome those limitations, more refined models have been proposed. (M. Lin & Rogers, 1993) and (Veidt, Liu, & Kitipornchai, 2001) analytically simulated PZT actuators, based on the Mindlin plate theory. The disadvantage of Mindlin plate theory is that it is limited to relatively low frequencies, below the cut-off frequency at which higher antisymmetric GW modes other

than A_0-mode can appear. (Von Ende & Lammering, 2007; Von Ende et al., 2007) proposed an analytical solution for GW generation by uniform shear stress based on 2D elasticity equations using Fourier transform and residue theorem for inverse transform. They were able to obtain the dynamic load transfer between a bonded PZT and an anisotropic elastic medium under in-plane mechanical and electrical loading. (Huang & Sun, 2006) simulated GW propagation by surface bonded PZT in an anisotropic plate which improved accuracy, even at higher frequencies. They divided the interfacial surface between the plate and the PZT into a finite number of points and based on continuity of axial strain at these points, they could determine the unknown constants of their analytical equation. Hence, continuous shear stress profile was obtained, from which propagation waves were simulated.

In order to obtain a more selective GW generation, multi-element transducers have been proposed in the literature. For instance, (Yeum et al., 2011) proposed a mode decomposition technique by a dual PZT composed of a concentric ring and a circular PZT that can decouple A_0 and S_0-modes at a given frequency. (EV Glushkov et al., 2010) presented an omnidirectional co-axial multi-element transducer for mode-selective generation of GW. Their proposed transducer is composed of several coaxial ring-shaped PZT elements. They optimized the number of PZT element rings, and the number of cycles of the input signal on each ones. Using energy distribution between excited modes, undesired mode was suppressed and the time delay of the excitation signals to the rings was reduced to zero by replacing the actuating contact traction by a pair of concentrated opposite ring tangential forces. To overcome the disadvantages of traditional transducer arrays, (J. Li & Rose, 2001) built a multi-channel time-delay system to improve the array technology for guided wave excitation. They could generate a single GW mode by introducing time delays between the PZT elements into arrays. (Kannajosyula, Lissenden, & Rose, 2013) presented an exact analysis of annular PZTs for mode selective GW generation. In wavenumber spectrum the smallest phase and time delays of each ring were obtained and the corresponding ring width was defined with respect to the wavelength of the desired mode. As external environment factors like water loading can affect the measured signals significantly, (Koduru & Rose, 2013) used circular array configuration of PVDF transducers to excite pure S_1 and A_1 modes for corrosion and water loading detection, respectively. In the literature (EV Glushkov et al., 2010; Yeum et al., 2011) only the induced shear stress of a PZT to the plate has

been considered, while the normal stress contribution has been neglected under the thin actuator assumption (N Quaegebeur, Ostiguy, & Masson, 2015). The validity of this assumption has been assessed through FEM simulation (Yazdanpanah Moghadam, Quaegebeur, et al., 2013), especially when the polarization direction is parallel to surface of the plate. Inter-digital transducers (IDTs) are also used for selective GW mode excitation. (C. M. Lin, Chen, Felmetsger, Senesky, & Pisano, 2012) have used AlN/3C–SiC composite layer that enables the third-order quasi-symmetric (QS_3) GW mode with a high quality factor (Q) characteristic and an ultra-high phase velocity.

The first step of the global optimization process for mode selective actuator is the optimization of the interfacial shear stress. The design of a transducer with the ability of applying such an interfacial shear stress would be second step of the work to be conducted. As an example, one way to control such a shear stress profile would be to use multiple piezoceramic elements with polarization directions parallel to the host structure, as shown in Figure 3. 1-c and Figure 3. 1-d, that could be controlled individually. In order to fabricate the transducer proposed in Figure 3. 1c and Figure 3. 1d, multiple rectangular PZT with opposite polarization directions parallel to their surface (shear plates) could be used. Another option could be to use multiple shear plates with the same polarization direction, or a single PZT wafer with a micro-machined electrode pattern, to drive each element individually and use inverted voltage to simulate opposite polarization directions.

The systematic optimization approach presented in this paper forms the basis for the design of mode-selective PZTs. An analytical model is first developed based on the 2D linear elasticity equations and Fourier transform to obtain the GW displacement field through the thickness of the plate when an arbitrary profile shear stress is applied on a segment of the top surface of the host plate. The excitation area and consequently the shear stress profile are then divided into a finite number of segments with the arbitrary uniform shear stress applied over each segment. Using the superposition principle, the final GW displacement field is obtained by integrating the displacement fields generated by each individual shear stress segments. A parallel Genetic Algorithm (GA) is used for optimization of shear stress profile in order to reject the undesired mode. A cost function is then defined to excite one mode dominantly and suppress the energy of

the other undesired modes. Advantages of this method over more conventional transducers tuning approaches are that (1) the transducer can be explicitly designed to both excite one mode and suppress other undesired modes, (2) the size of the excitation area is not constrained and mode-selective excitation is still possible even if excitation width is smaller than all excited wavelengths, and (3) the selectivity is increased and the bandwidth extended. The complexity of the optimal shear stress profile obtained is shown considering two cost functions with various optimal excitation widths and number of segments. Examples are presented to demonstrate the capability of the presented approach for mode-selective generation of GWs.

3.4 Methodology

3.4.1 Analytical solution of GW excitation by an arbitrary shear stress profile

Considering an isotropic plate with a total thickness of 2*d* as presented in Figure 3. 2, the displacement field $u = \left(u_x, u_y\right)$ is decomposed, under the plane strain assumption, as:

$$\begin{aligned} u &= \nabla\varphi + \nabla\times\psi \text{ , with} \\ \nabla.\psi &= 0 \text{ ,} \end{aligned} \tag{3.1}$$

where φ and ψ denote the potentials associated with longitudinal and shear waves respectively, and ∇ denotes the gradient operator. For a time harmonic process, the potentials φ and ψ satisfy the following wave equations:

$$\frac{\partial^2\varphi}{\partial x^2} + \frac{\partial^2\varphi}{\partial y^2} + p^2\varphi = 0 \text{ ,} \tag{3.a}$$

$$\frac{\partial^2\psi}{\partial x^2} + \frac{\partial^2\psi}{\partial y^2} + q^2\psi = 0 \text{ ,} \tag{3.b}$$

where $p=\sqrt{\omega^2/{c_L}^2-\xi^2}$, $q=\sqrt{\omega^2/c_T-\xi^2}$, c_T and c_T denote the longitudinal (pressure) and transverse (shear) velocities, and ξ the wavenumber of the considered mode (Giurgiutiu, 2003, 2005).

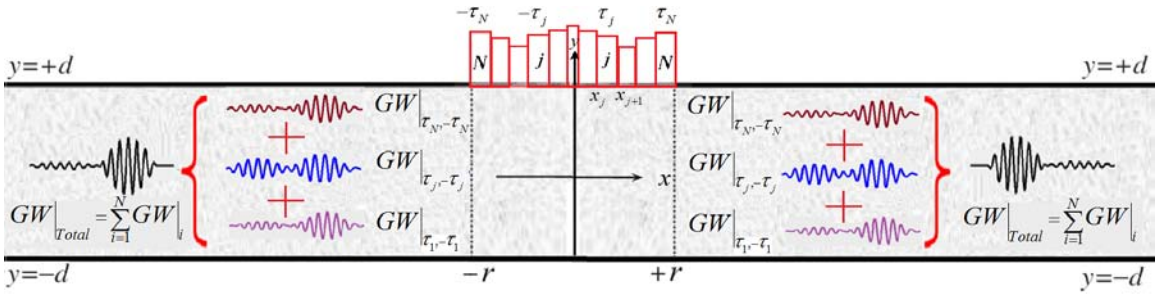

Figure 3. 2 Description of the geometry and arbitrary symmetric shear stress profile used in the study.

Propagating modes in the *x*-direction are considered, such that the solutions for φ and ψ are defined as:

$$\begin{aligned}\varphi &= \bar{\varphi}e^{j\xi x},\\ \psi &= \bar{\psi}e^{j\xi x},\end{aligned} \tag{3.3}$$

leading to a set of ordinary differential equations of second order for which general solution in the $y-$direction can be expressed as:

$$\begin{aligned}\bar{\varphi} &= C_1\sin(py)+C_2\cos(py),\\ \bar{\psi} &= C_3\sin(qy)+C_4\cos(qy),\end{aligned} \tag{3.4}$$

where unknown coefficients C_2 and C_3 are associated with symmetric modes, and unknown coefficients C_1 and C_4 are associated with anti-symmetric modes which can be determined based on the shear stress conditions on the top and bottom surfaces. The determination of these

unknown coefficients is not straightforward analytically when a complex profile shape shear stress is considered at the boundaries.

In this study, the excitation area at the top surface of the plate is divided into N equal segments, each one subjected to unknown constant shear stress τ_j, as it is shown in Figure 3. 2. Hence, there are N sources of uniform shear stresses and all together compose an arbitrary shear stress profile. Based on the superposition principle, the total displacement field U^t is obtained from superposing of all displacement fields coming from each individual segment as

$$U^T(x,y) = \sum_{j=1}^{N} u_j(x,y), \tag{3.5}$$

where $u_j(x,y)$ represents the displacement field induced by the segment j. In this way, Eq. (3.4) can be written for each segment j as a set of $2N$ equations as

$$\begin{aligned} \overline{\varphi}_j &= C_1^j \sin(py) + C_2^j \cos(py), \\ \overline{\psi}_j &= C_3^j \sin(qy) + C_4^j \cos(qy), \end{aligned} \qquad j = 1,2,...,N \tag{3.6}$$

where C_1^j, C_2^j, C_3^j and C_4^j are $4N$ unknown coefficients that can be determined using stress boundary conditions at upper and lower surfaces of the plate at each section which are defined based on Heaviside step function H as

$$\tau(x,y) = \begin{cases} \tau_j\left(H\left[x-x_j\right] - H\left[x-x_{j+1}\right]\right) - \tau_j\left(H\left[x+x_{j+1}\right] - H\left[x+x_j\right]\right), & \text{at } y = +d, \\ 0, \qquad \text{at } y = -d. \end{cases} \tag{3.7}$$

The first term of Eq. (3.7) represents the uniform shear stress for $x \in \left[x_j, x_{j+1}\right]$, while the second term denotes the symmetrical contribution for $x \in \left[-x_{j+1}, -x_j\right]$. The contributions of those segments are chosen symmetrical in order to represent a symmetric generation pattern, such that the guided wave generation is performed identically in both $+x$ and $-x$ directions. After

substituting the coefficients C_1^j, C_2^j, C_3^j and C_4^j into Eq. (3.2.a), the total displacement fields are obtained based on Eq. (3.5):

$$\overline{U}_{x,y}^{T}\left(\xi,y\right)=\sum_{j=1}^{N}\left(\left[\frac{N_{x,y}^{A_0}\left(\xi,y\right)}{D^{A_0}\left(\xi\right)}+\frac{N_{x,y}^{S_0}\left(\xi,y\right)}{D^{S_0}\left(\xi\right)}\right]\times\frac{\overline{\tau}_j\left(\xi\right)}{2}\right), \tag{3.8}$$

where:

$$\begin{aligned}
N_x^{A_0}\left(\xi,y\right)&=q\left(-\left(\xi^2-q^2\right)\sin\left(dp\right)\sin\left(qy\right)+2\xi^2\sin\left(dq\right)\sin\left(py\right)\right),\\
N_x^{S_0}\left(\xi,y\right)&=q\left(\left(\xi^2-q^2\right)\cos\left(dp\right)\cos\left(qy\right)-2\xi^2\cos\left(dq\right)\cos\left(py\right)\right),\\
N_y^{A_0.}\left(\xi,y\right)&=-i\xi\left(2pq\cos\left(py\right)\sin\left(dq\right)+\left(\xi^2-q^2\right)\cos\left(qy\right)\sin\left(dp\right)\right),\\
N_y^{S_0}\left(\xi,y\right)&=-i\xi\left(2pq\cos\left(dq\right)\sin\left(py\right)+\left(\xi^2-q^2\right)\cos\left(dp\right)\sin\left(qy\right)\right),\\
D^{A_0}\left(\xi\right)&=\mu\left(4\xi^2pq\cos\left(dp\right)\sin\left(dq\right)+\left(\xi^2-q^2\right)^2\cos\left(dq\right)\sin\left(dp\right)\right),\\
D^{S_0}\left(\xi\right)&=\mu\left(4\xi^2pq\cos\left(dq\right)\sin\left(dp\right)+\left(\xi^2-q^2\right)^2\cos\left(dp\right)\sin\left(dq\right)\right),
\end{aligned} \tag{3.9}$$

and where $\overline{U}_{x,y}^{T}\left(\xi,y\right)$ stands for $\overline{U}_x^{T}\left(\xi,y\right)$ and $\overline{U}_y^{T}\left(\xi,y\right)$, the total in-plane and out-of-plane displacements, and $\overline{\tau}_j\left(\xi\right)$ represents the Fourier transform of the excitation term τ_j that can be defined analytically as:

$$\overline{\tau}_j\left(\xi\right)=\frac{i\tau_j}{\xi}\left(e^{i\xi x_{j+1}}-e^{i\xi x_j}\right)+\frac{-i\tau_j}{\xi}\left(e^{i\xi(-x_j)}-e^{i\xi(-x_{j+1})}\right)=\frac{i\tau_j}{\xi}\left[e^{-i\xi x_j}\left(e^{-i\xi\Delta x}-1\right)+e^{i\xi x_j}\left(e^{i\xi\Delta x}-1\right)\right] \tag{3.10}$$

where $\Delta x=x_{j+1}-x_j$ represents the segment width.

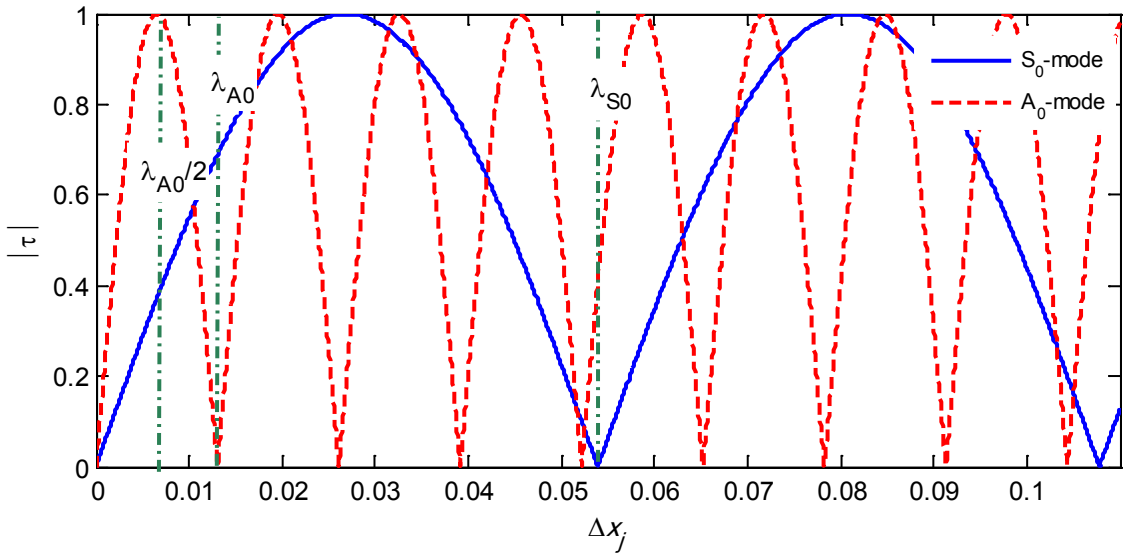

Figure 3. 3 Variation of normalized excitation term $\frac{i\tau_j}{\xi}e^{i\xi x_j}\left(e^{i\xi\Delta x}-1\right)$ for different with respect to segment width Δx_i for both A_0 and S_0-modes.

The size of Δx must be chosen to achieve stability on mode-selectivity of shear stress profile. Stability here refers to the condition for which minor change of Δx do not induce a large deviation on mode-selective excitation. As an example, the evolution of $\bar{\tau}_j$ in the case of a 2 mm thick aluminum plate with material properties $E = 70$ GPa, v= 0.33 and $\rho = 2700$ kg/m^3 is presented in Figure 3. 3 for both S_0 and A_0-modes. In Figure 3. 3, blind points at which $\bar{\tau}_j$ vanishes can be observed when Δx is equal to the wavelength λ of the considered mode. In this case, the well-known result is obtained where the specific mode cannot be generated and natural mode selectivity occurs. Thus, for mode selectivity, the value for Δx must be chosen below the smallest wavelength λ_{A_0} of the A_0 mode.

Upon substituting Eq. (3.10) into Eq. (3.8), and taking inverse Fourier wavenumber transform with respect to the *x* component, the total through-the-thickness displacement field in the space domain is obtained as follows:

$$U_{x,y}^{T}\left(x,y\right)=\int_{-\infty}^{\infty}\overline{U}_{x,y}^{T}\left(\xi,y\right)e^{-i\xi x}d\xi=\sum_{j=1}^{N}\int_{-\infty}^{\infty}\left(\frac{N_{x,y}^{A_0}\left(\xi,y\right)}{D^{A_0}\left(\xi\right)}\frac{\overline{\tau}_j}{2}+\frac{N_{x,y}^{S_0}\left(\xi,y\right)}{D^{S_0}\left(\xi\right)}\frac{\overline{\tau}_j}{2}\right)e^{-i\xi x}d\xi \qquad (3.11)$$

The roots of functions $D^{S_0}\left(\xi\right)$ and $D^{A_0}\left(\xi\right)$ are the symmetric and anti-symmetric wavenumbers respectively, such that Eq. (3.11) can be solved using the residue theorem by choosing the integration path as semi-circles in the upper half of complex ξ plane and the real axis (Giurgiutiu, 2003). Then, the total displacement field of Eq. (3.11) can be summarized using Eq. (3.10) as:

$$U_{x,y}^{T}\left(x,y\right)=\underbrace{\frac{1}{2}\frac{iN_{x,y}^{A_0}\left(\xi_{A_0},y\right)}{\left\{D^{A_0}\left(\xi\right)\right\}'_{\xi=\xi_{A_0}}}e^{-i\xi_{A_0}x}}_{Propagation\ terms}\underbrace{\sum_{j=1}^{N}\overline{\tau}_j\left(\xi_{A_0}\right)}_{Excitation\ term}+\underbrace{\frac{1}{2}\frac{iN_{x,y}^{S_0}\left(\xi_{S_0},y\right)}{\left\{D^{S_0}\left(\xi\right)\right\}'_{\xi=\xi_{S_0}}}e^{-i\xi_{S_0}x}}_{Propagation\ terms}\underbrace{\sum_{j=1}^{N}\overline{\tau}_j\left(\xi_{S_0}\right)}_{Excitation\ term}, \qquad (3.12)$$

where the first terms of the sum refers to A_0-mode and the second term refers to S_0-mode. Each contribution can be separated into propagation and excitation terms respectively. Both wavenumber and distance from excitation zone *x* are considered in propagation terms of Eq. (3.12). Excitation upper the cut-off frequency leads to excitation more GW modes other than A_0 and S_0-modes, like A_1 and S_1-modes that their corresponding displacement terms could be added up similarly to Eq. (3.12) similarly.

3.4.2 Optimal shear stress profile determination

In this section, an objective function based on Eq. (3.12) is defined for determination of the optimal shear stress profile for mode-selective generation using a minimization process. As propagation terms in Eq. (3.12) depend on material and geometrical properties of the host structure, they are independent on the excitation dimension and pattern. On the other side, the excitation terms of each mode in Eq. (3.12) represent the sum of the contribution of all segments *j* on total displacement field for S_0 and A_0-modes. The objective function of this optimization process is chosen as the displacement terms is independent of the excitation terms, only the

excitation terms of Eq. (3.12) are retained for sake of simplicity and efficiency. Thus, the proposed objective function is defined as the ratio of those excitation terms in order to maximize the contribution of a desired mode and minimize the undesired mode. As an example, the following cost function is proposed for maximizing S_0 mode:

$$J_{S_0}(X) = \frac{\sum \overline{\tau}_j\left(\xi_{A_0}\right)}{\sum \overline{\tau}_j\left(\xi_{S_0}\right)}. \tag{3.13}$$

This objective function can be minimized for specific configurations of $\overline{\tau}_j$. The numerator of the objective function defined in Eq. (3.13) may vanish for a specific configuration that totally cancels the undesired mode, such that the optimization process stops inappropriately without trying to maximize the desired mode. In addition, apart from suppressing undesired mode, there is not guarantee that the induced power flow is maximized for the desired mode. Thus, in this analysis, a second term is added to the objective function previously defined in Eq. (3.13) to significantly maximize the induced power flow of the desired mode over whole wavenumber domain as it will be shown in section 3.5.2, such that the final objective function for selective S_0-mode excitation is defined as:

$$J_{S_0}(X) = \frac{\sum \overline{\tau}\left(\xi_{A_0}\right)}{\sum \overline{\tau}\left(\xi_{S_0}\right)} + \frac{2N/\xi_{S_0}\left|e^{i\xi_{S_0}\Delta x} - 1\right|}{\sum \overline{\tau}\left(\xi_{S_0}\right)}, \tag{3.14}$$

where the regulation term $2N/\xi_{S_0}\left|e^{i\xi_{S_0}\Delta x} - 1\right|$ is the maximal value for $\overline{\tau}_j$; therefore, the value of the second term is always constrained between zero and one, such that the lower boundary of the objective function $J_{S_0}(X)$ is one. Similarly, the objective function for pure A_0-mode generation is proposed as:

$$J_{A_0}(X) = \frac{\sum \overline{\tau}\left(\xi_{S_0}\right)}{\sum \overline{\tau}\left(\xi_{A_0}\right)} + \frac{2N/\xi_{A_0}\left|e^{i\xi_{A_0}\Delta x} - 1\right|}{\sum \overline{\tau}\left(\xi_{A_0}\right)}. \tag{3.15}$$

The first terms of Eqs. (3.14) and (3.15) guarantee the minimization of undesired mode, while the second terms are responsible for a maximization of the generation of the desired mode. As it will be shown is section 3.5.2, these objective functions are straightforward, computationally efficient and allow decreasing the computation time for each step of the optimization process. If higher order modes are excited at a given frequency, the objective function should be modified by introducing the excitation terms corresponding to the other undesired modes in the numerator of the first term of the objective function.

3.4.3 Parameters of the optimization process

In this section, the optimization process and effective parameters selection for mode-selective excitation is presented. The Genetic Algorithm (GA) is used in this paper as the preferred optimization algorithm for mode selection of generated GW since this method is preferable when the cost function is discontinuous, highly nonlinear, stochastic or has unreliable or undefined derivatives. Moreover, even though there is no guarantee of converging to the global minimum, the final solution of GA is less dependent on the initial guess of parameters. GA is generally the preferred method over other optimization methods like the gradient based method since in the latter case, the final result may depend on the initial guess of the parameters and may converge to a local minimum instead of a global minimum (M. Lin & Rogers, 1993; Veidt et al., 2001).

In the present case, Parallel Genetic Algorithm (PGA) (Cantú-Paz & Goldberg, 1996; Haupt & Haupt, 2004; G. Wang, Wan, Wang, & Lv, 2008) is used for optimization of shear stress configuration to overcome the slowness of GAs when working with a large number of variables. Table 3. 3 illustrates the options of the GA process for each evolutionary step. The number of segment N is considered constant and the selection of the optimal number of segments N with respect to the minimal wavelength will be studied the following section. The minimization is based on the proper selection of unknown complex uniform shear stresses τ_j with normalized amplitude, such that $|\tau_i| \leq 1$ Pa. Thus, for each segment, a complex value for the shear stress profile is sought, resulting in the existence of $2N$ variables in the optimization process.

Table 3. 1 Parameters and operators of the GA process.

Number of populations	4000
Population function	Linear Feasible
Fitness Scaling	Rank
Selection	Roulette
Crossover	heuristic
Ratio	1.1
Migration	Neighborhood
Interval	10
Direction	Forward
Fraction	0.2
Stopping Criteria	
Generations	450
Stall Generation Limit	300

3.5 Validation of the optimization process

3.5.1 Application

In this section, the proposed optimization approach is used for a 2 mm thick aluminum plate with the following material properties $E = 70$ GPa, ν= 0.33 and $\rho = 2700$ kg/m^3. The driving frequency is chosen at 100 kHz so that only first order A_0 and S_0-modes with corresponding wavelengths $\lambda_{s_0} = 53.9$ mm and $\lambda_{A_0} = 13.0$ mm are generated.

In the following part, four excitation cases of half-width *r* are considered, for which the obtained profiles and conclusions will differ.

Case I: $r \geq \lambda_{s_0}$ which is selected as $r = 100$ mm,

Case II: $\lambda_{A_0} \leq r \leq \lambda_{s_0}$ which is selected as $r =$ 40mm,

Case III: $r \leq \lambda_{A_0}$ which is selected as $r =$ 10 mm,

Case IV: $r = \lambda_{desired}/4$ representative of the classical design approach ($r = \lambda_{S_0}/4 = 13.5$ mm and $r = \lambda_{A_0}/4 = 3.2$ mm for selective S_0 and A_0-mode, respectively).

In cases I to III, the optimization process is used for determination of the optimal shear stress profile. In addition, in order to compare the capability of the presented approach with respect to the classical design approach using the pin-force model, the solution obtained in the case IV is used as a benchmark, considering a unitary delta Dirac stress profile at the edge of the excitation zone, i.e. at $\pm r = \lambda_{desired}/4$.

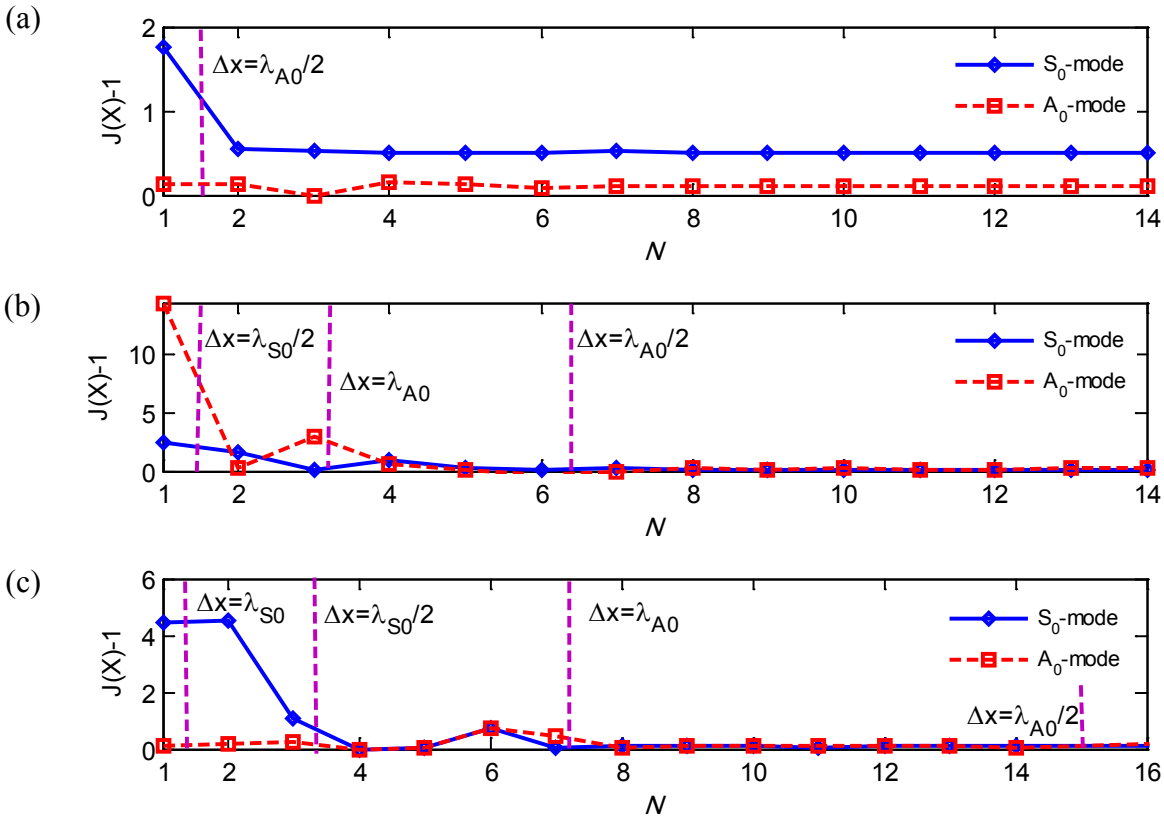

Figure 3. 4 Convergence of objective function based on number of segments N for (a) r = 0.01 m (Case III), (b) r = 0.04 m (Case II), (c) r = 0.1 (Case I) for both A_0 and S_0-modes. The vertical bars indicate the size of one segment in relation to modal wavelength for specific N values.

3.5.2 Results

3.5.2.1 Convergence of the optimization process

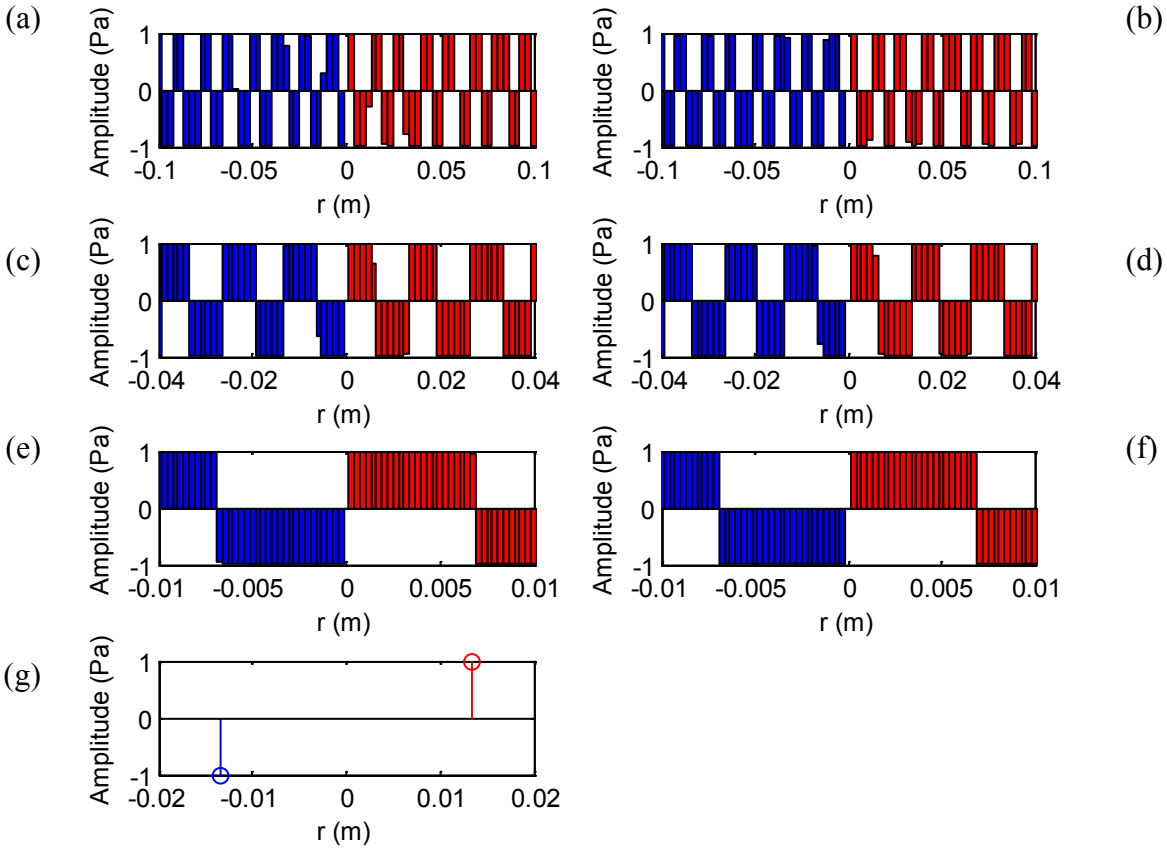

Figure 3. 5 Real (left) and imaginary (right) parts of the optimal shear stress after minimization in the case III r = 0.1 m (a, b), case II r = 0.04 m (c, d), case I r = 0.01 m (e, f), and pin force model case IV r = 13.5 mm (g) for selective S_0-mode excitation at 100 kHz using N =35 segments.

The convergence of the objective functions in Eqs. (3.14) and (3.15) is illustrated in Figure 3. 4 for varying numbers of segments N for cases I to III. For both A_0 and S_0-modes, local minima of the objective functions are obtained when the segment width Δx is a multiple of the unwanted wavelength, i.e. $\Delta x \approx \lambda_{unwanted}, 2\lambda_{unwanted}, \ldots$. This guarantees that the undesired mode is not generated as presented in Figure 3. 3, but does not guarantee a maximum of the desired mode,

such that additional parameters should be considered for optimal selection of the optimal number of segments N.

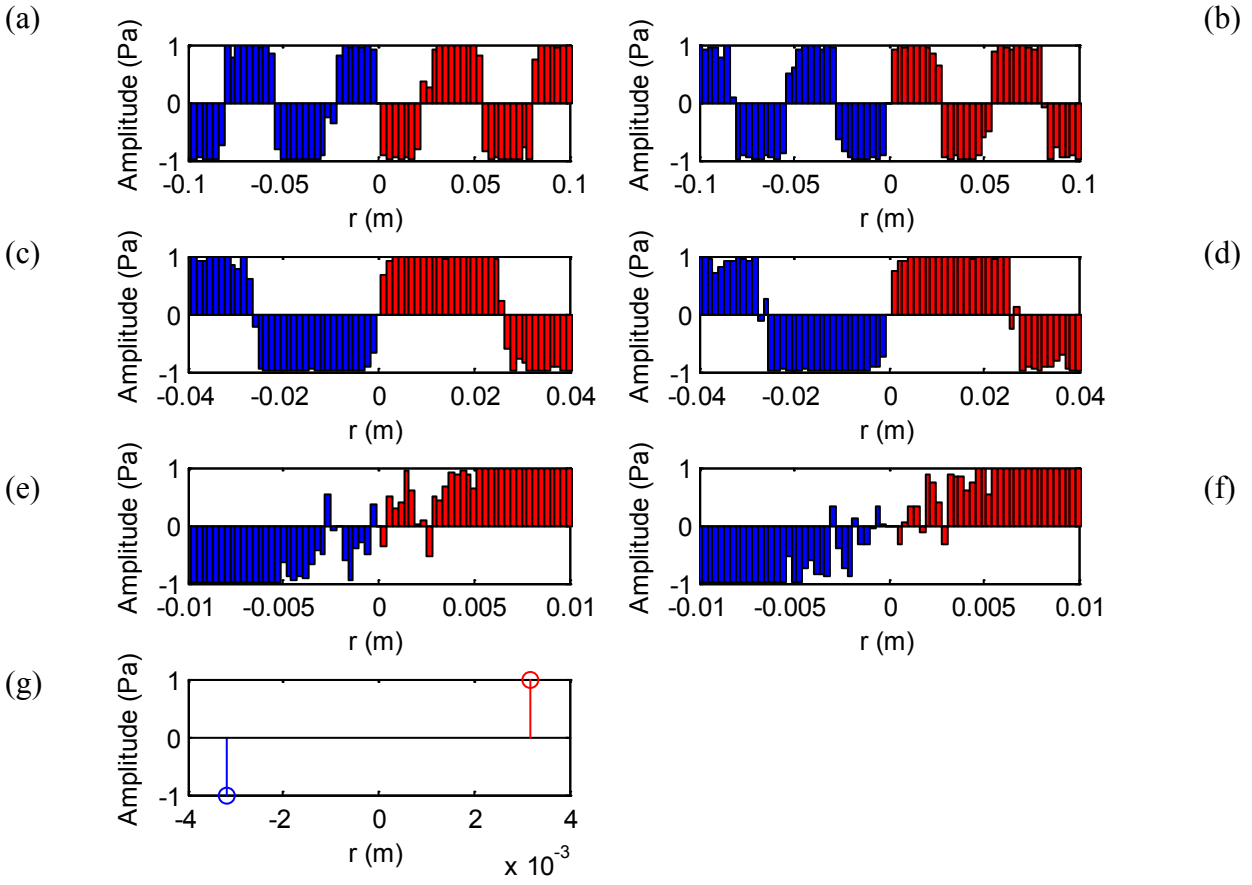

Figure 3. 6 Real (left) and imaginary (right) parts of the optimal shear stress after minimization in the case III r = 0.1 m (a, b), case II r = 0.04 m (c, d), case I r = 0.01 m (e, f), and pin force model case IV r = 3.2 mm mm (g) for selective A_0-mode excitation at 100 kHz using N = 35 segments.

Indeed, due to the high sensitivity of the excitation function $\overline{\tau}_j$ with respect to the segment width Δx, it is preferable to select the number of segments such that the excitation function $\overline{\tau}_j$ is monotonic. Thus, in order to bring stability in mode-selective excitation, the number of segments N should be such that the segments width satisfies $\Delta x \le \lambda_{\min}/2$. This region is referred as the convergence zone that guarantees the mode-selective excitation and convergence of the minimization process. Figure 3. 4 shows that the optimal number of segments are $N = 4$, 7 and

15 for cases I, II and III, respectively. Hence, convergence is obtained with few numbers of segments in cases I-III in which the size of excitation width is $r \leq \lambda_{max}$ so that it is in vain to increase excitation width 2*r* above the maximal wavelength λ_{max} which leads to choosing a large number of segments and increasing complexity of shear stress profile consequently.

3.5.2.2 Optimal shear stress profile

Figure 3. 5 and Figure 3. 6 present the real and imaginary values of the shear stress profile after optimization for selective S_0-mode and A_0-mode excitation respectively and for different sizes of excitation width (cases I-III). The number of segments in half-excitation zone is $N = 35$ for all cases to guarantee that convergence is achieved. Figure 3. 5 shows that as *r* increases, the optimal shear stress profile tends to a periodic rectangular function whose period (or wavelength) corresponds to the one of the desired mode. This allows maximization of the desired mode but is also responsible for generation of higher order harmonics in the wavenumber domain that do not correspond to propagating modes. The small deviations with respect to a rectangular function are attributed to the minimization of the undesired mode.

The comparision of power flow ratios (Kamal, Lin, & Giurgiutiu, 2014) of excited modes using GA optimization are presented in Table 3. 4. Typical results illustrate that the desired mode S_0 and A_0 can be excited dominantly over other mode up to a ratio of 6.6×10^9 and 3.9×10^4, respectively, in power flow using the presented optimization process, guaranteeing the validity of the proposed method for mode selectivity. Moreover, the mode selectivity in terms of power flow reduction is better in the case of large element (case I) than in the case of small elements (case III) for a constant number of elements *N*, suggesting that the mode selectivity is extended when the excitation width is greater than the maximal wavelength. Moreover, in the case of single element actuator (case IV), the mode selectivity is greatly reduced of a factor 10^6 for S_0 mode and a factor 10^4 for A_0 mode, demonstrating the benefit of using multi-element actuators for mode selection.

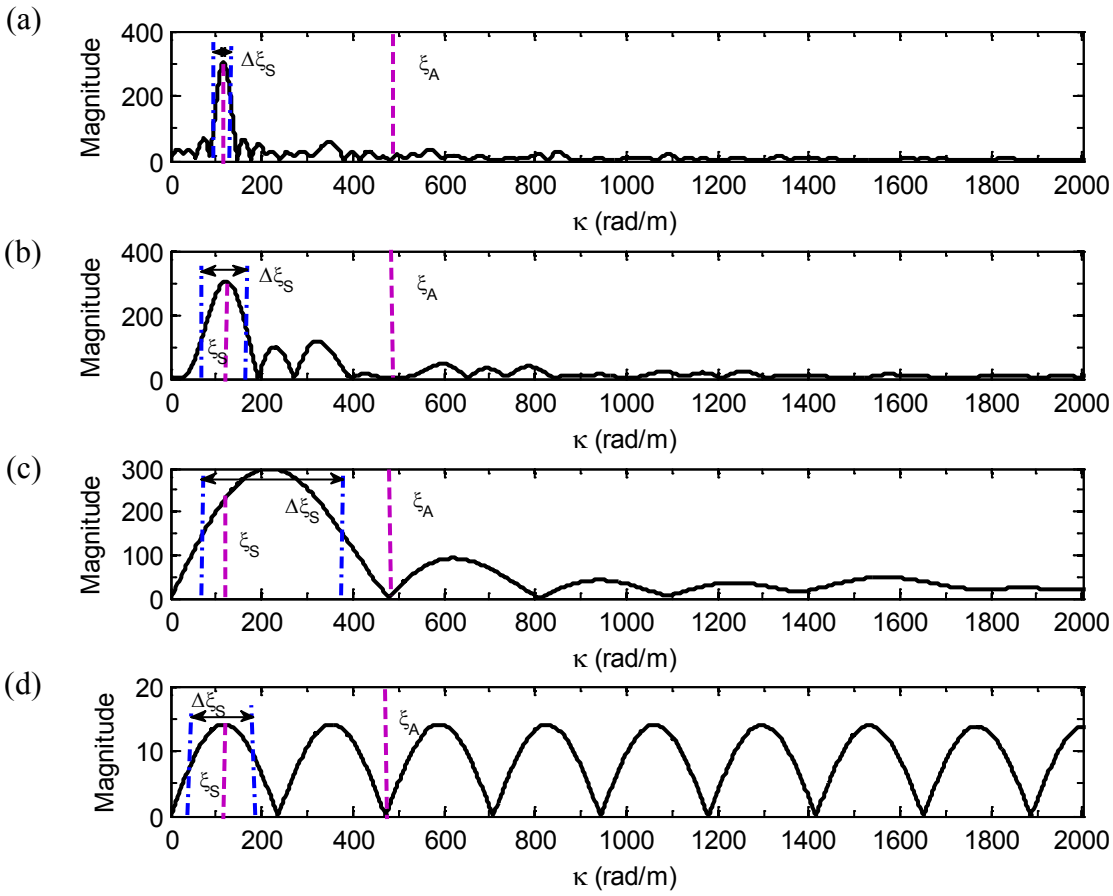

Figure 3. 7 Magnitude of the spatial Fourier transform of the shear-stress profile as a function of wavenumber (k) for selective S_0-mode generation in the cases I (a), II (b), III (c) and IV (d).

In order to properly select the optimal excitation width r that satisfies mode-selectivity and extended bandwidth, wavenumber spectra of obtained stress profiles are computed and presented in Figure 3. 7 and Figure 3. 8. As expected, the spectra peaks in Figure 3. 7 and Figure 3. 8 are assigned to the desired mode occurring for $\xi = \xi_A$ and ξ_S respectively. For all cases I-III both A_0 and S_0-modes are excited dominantly over the wavenumber spectrum, and the regulation term in Eqs. (3.14) and (3.15) allows not only reduction of the undesired mode but also maximization of the desired mode.

A little deviation in maximal peak value is observed as r decreases (case III). This deviation is clearly observable for pure S_0-mode excitation in Figure 3. 7.c in which maximum amplitude of

central lobe occurs at $\xi = 220$ rad/m while ξ_S = 116 rad/m. This is due to the constraint of minimization of A_0-mode that imposes a mode rejection for $\xi = \xi_A$. Therefore, in the case of excitation signal with $r \le \lambda_{\min}$ (case III), a reduced mode-selectivity is observed than in the case of $r \ge \lambda_{\max}$ (case I).

Table 3. 2 Power flow ratios of desired mode to undesired mode using GA optimization procesess.

	Case IV $r = \lambda_{desired}/4$	Case III $r_1 =$ 0.1 m	Case II $r_2 =$ 0.04 m	Case I $r_3 =$ 0.01 m
P_{S_0}/P_{A_0}	1.9e+03	1.9e+09	6.6e+09	5.4e+08
P_{A_0}/P_{S_0}	1.7	1.1e+04	9.9e+03	3.8e+04

Figure 3. 7 and Figure 3. 8 shows that as the excitation width increases, the side lobes amplitude decreases significantly and a reduction of bandwidth in the wavenumber domain is also observed, giving better mode selectivity over the whole wavenumber spectrum. The bandwidth $\Delta\xi$ determined by considering half of maximum amplitude of the central lobe, increases considerably as the excitation width decreases. Figure 3. 8 shows that the bandwidth of central lobe in case I is $\Delta\xi$ = 50 rad/m and increases up to $\Delta\xi$ = 400 rad/m in case III. Figure 3. 8 illustrates a similar increment in bandwidth of central lobe as excitation width decreases for pure S_0-mode excitation. This, however, may give rise to difficulties while selecting GWs at other frequencies around the central frequency (100 kHz) for narrow- or broadband signals generation.

In the case of single element design (case IV presented in Figure 3. 7.d and Figure 3. 8.d), many side lobes are observed and the bandwidth is approximately 150 rad/m and 600 rad/m for A_0 and S_0-modes respectively. Therefore, the amplitude of central lobe is smaller than those obtained by the presented approach because most of its excited energy is split up into undesired side lobes.

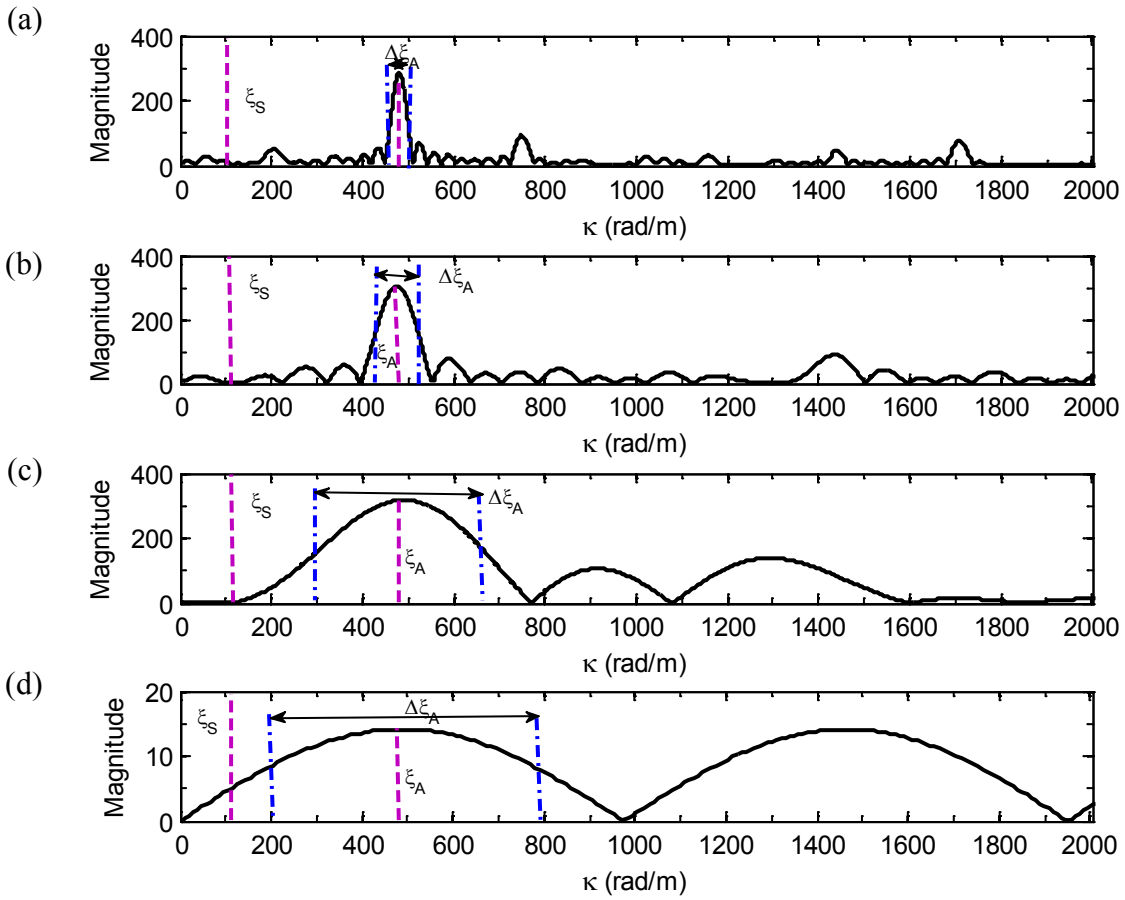

Figure 3. 8 Magnitude of the spatial Fourier transform of the shear-stress profile as a function of wavenumber (k) for selective A_0-mode generation in the cases I (a), II (b), III (c) and IV (d).

(a)

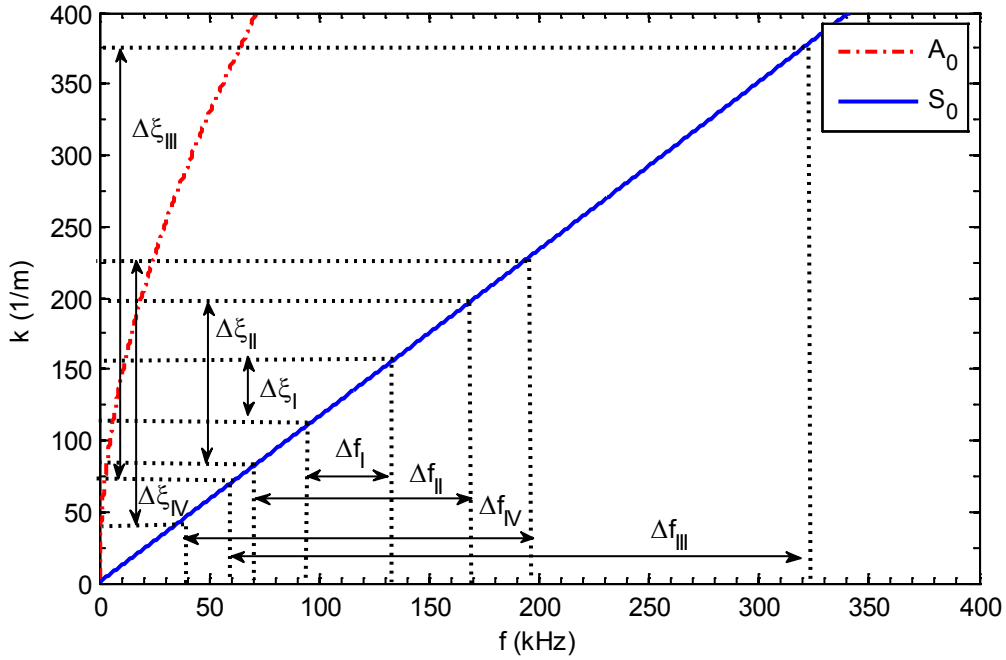

(b)

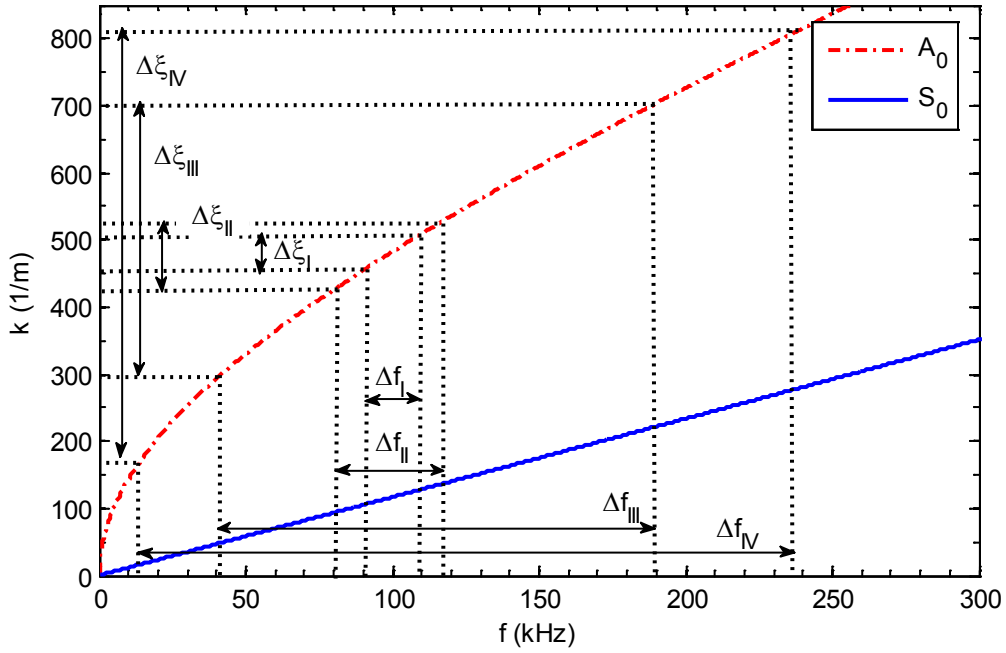

Figure 3. 9 Evolution of the wavenumber versus frequency for A_0 and S_0-modes. The bandwidth of (a) S0-mode and (b) A_0-mode generated by optimal shear stress profiles are indicated using dashed lines.

3.5.3. Discussion

Figure 3. 9 presents the evolution of the wavenumber with respect to frequency and the bandwidth of the mode selection process for all four considered cases I-IV in order to present the potential application to narrow-band signals. In this figure, it appears that the bandwidth of both A_0 and S_0-modes in case I is twice and three times narrower than in cases II and III, respectively. In addition, comparison of Figure 3. 9.a with Figure 3. 9.b shows that the bandwidth for S_0-mode excitation is generally twice larger than for A_0-mode excitation.

This can be explained by the difference in wavelengths for those two modes, while the ratio between bandwidth and wavenumber remains comparable, representing a constant quality (Q-) factor for mode selectivity.

In order to describe the optimal total size r and segment number N, different factors must be considered. First, the objective function value and the ratio of power flows after convergence demonstrate that better mode selectivity is achieved for large excitation widths r. However, this is achieved at the cost of large element number ($N > 16$) as presented in Figure 3. 3. Moreover, the resulting complex shear stress pattern is highly selective in the wavenumber domain, such that it can hardly be used for narrow- or broadband excitations. For instance, using the configuration of case I for A_0-mode selection, the computed profile function is only valid in the frequency range between 90 and 110 kHz corresponding to a 10 cycles burst.

Thus, a compromise in terms of performance, mode selectivity and extended bandwidth can be achieved in the case II for which $\lambda_{\min} \le r \le \lambda_{\max}$, where side lobes in the wavenumber domain are reduced, bandwidth is acceptable and the amplitude is maximized for the desired mode. As an application, using the configuration of case II for A_0-mode selection, the computed profile function is valid in the frequency range between 75 and 125 kHz corresponding to a 4 cycles burst. Thus, the configuration of case II appears as the best candidate for both A_0 and S_0-mode selectivity for the three following reasons: (1) extended power flow maximization than in the case III for which $r \le \lambda_{\min}$ because the amplitude of side lobes decreases significantly; (2) extended validity of the optimized shear-stress profile over a large wavenumber domain, such

that narrowband excitations can be used; (3) reduced number of segments to achieve less complexity in the shear stress profile than those in case I for with $r \geq \lambda_{max}$.

3.6 Conclusion

In this study, an analytical approach is used for determination of the optimal shear stress profile for mode-selective GW excitation. The excitation zone is divided into a number of small elements which are all contributing to the GW generation. Using an objective function based on superposition of contributions from elementary uniform shear stresses and a Genetic Algorithm optimization, the global optimized mode-selective interfacial shear stresses profiles are computed. A regulation term is added up to the objective function to excite one mode dominantly over the whole wavenumber spectrum. The presented approach allows determining the optimal transducer size and element numbers for practical cases and demonstrates that a greater selectivity extended bandwidth, fast convergence and limited complexity can be achieved. The present methodology represents the first step in the optimization of the design of mode selective actuators, while the design of a transducer with the ability of applying such an interfacial shear stress is the second step of the work currently being conducted. In addition, extension in the case of broadband excitation and experimental validation is ongoing.

CHAPTER 4

DESIGN AND OPTIMIZATION OF A MULTI-ELEMENT PIEZOELECTRIC TRANSDUCER FOR MODE-SELECTIVE GENERATION OF GUIDED WAVES

Peyman YAZDANPANAH MOGHADAM
Nicolas QUAEGEBEUR
Patrice MASSON

GAUS, Department of Mechanical Engineering
Université de Sherbrooke
Sherbrooke, Québec, Canada

Smart Materials and Structures (Impact factor : 2.502), Submitted in October 2015, Accepted with revision in December 2015

4.1 Contribution Summary

In this chapter of the thesis, a mode-selective surface bonded PZT is designed, optimized, manufactured, and tested experimentally. The presented analytical method in chapter 3 is used here for modeling GW generation by an arbitrary interfacial shear stress. Applying the optimized interfacial shear stress in chapter 3 to a host strucutre by a PZT is not straightforward. Therefore, presented approach is updated to make manufacturing of the designed PZT possible. The objective functions in chapter 3 is adapted based on performance of the transducer. A novel idea is then required to design the PZT based on two important citeria (1) simplicity and (2) cost. As piezoceramics are fragile, an appropriate laser-machining is used and investigated to manufacture the designed PZT precisely. The performance of the mode-selective PZT is then tested and validated.

4.2 Abstract

A novel Multi-Element Piezoelectric Transducers (MEPT) is designed, optimized, machined and experimentally tested to improve Structural Health Monitoring (SHM) systems for mode-selective generation of guided waves (GW) in an isotropic structure. GW generation using typical piezoceramics makes the signal processing and consequently damage detection very complicated, because at any driving frequency at least two fundamental symmetric (S_0) and antisymmetric (A_0) modes are generated. To prevent this, mode selective transducer design is proposed based on MEPT. A numerical method is first developed to extract the interfacial stress between a single piezoceramic element and a host structure and then used as the input of an analytical model to predict the GW propagation through the thickness of an isotropic plate. Two novel objective functions are proposed to optimize the interfacial shear stress for both suppressing unwanted mode(s) and maximizing a desired mode. Simplicity and low manufacturing cost are two main targets driving the design of the MEPT. A prototype MEPT is then manufactured using laser micro-machining. An experimental procedure is presented to

validate the performances of the MEPT as a new solution for mode-selective GW generation. Experimental tests illustrate the high capability of the MEPT for mode-selective GW generation, as unwanted mode is suppressed by a factor up to 170 times compared with the results obtained with a single piezoceramic.

4.3 Introduction

Inspection of pipes, rails, thin-wall structures, and multi-layer composite structures that have exceeded their life has encouraged different industries to convert their costly, time consuming and manual Non-Destructive Test (NDT) systems (Bates, Smith, Lu, & Hewitt, 2000) into Structural Health Monitoring (SHM) systems for automatic damage inspection (Balageas et al., 2006). Piezoelectric transducers, generally constituted of lead zirconate titanate (referred as PZT) (Huang & Sun, 2006; Yazdanpanah Moghadam, Tahani, et al., 2013), are commonly used in SHM systems to generate and sense ultrasonic guided waves (GWs) (J. Rose et al., 1993; I. Viktorov, 1967). GWs can travel over long distances and are highly sensitive to the interaction with damages, depending on mode and frequency ranges (J. Rose et al., 1993; I. Viktorov, 1967; X.-M. Wang & Ying, 2001). GWs have a multi-mode nature and at least two fundamental symmetric (S_0) and anti-symmetric (A_0) modes are excited at any given frequency, involving a higher complexity in signal processing and damage detection (Castaings et al., 2002; J. Rose et al., 1993; Santoni et al., 2007; Shelke et al., 2011).

Wedges use the angle beam method for better GW mode control and higher sensitivity. Viktorov analyzed both theortically and experimentally the wedge method of generating GWs in isotropic layers (L. A. Viktorov, Zubova, & Kaekina, 1965). He calculated the optimal angle wedge on the neighbourhood of the Snell's law angle of a given wavenumber. Using bonded piezoceramic transducers, mode-selective GW excitation is achieved typically by optimization of the transducers size (Su & Ye, 2004) and tuning of the driving frequency (di Scalea, Matt, & Bartoli, 2007; Santoni et al., 2007). Since the polarization direction of piezoceramic transducers can also be considered as a parameter, (Imano, 2007) used the Snell's law to design and manufacture a

titled angle polarization type piezoelectric transducer (TAPP) with title angle 50^0 for S_0-mode generation but the polarization is highly dependent on the frequency, mode and host structure properties, such that it is of limited application.

To overcome disadvantages of traditional single element transducers, arrays have been proposed (Wooh & Shi, 2001) in the literature. (J. Li & Rose, 2001) built an eight channel time-delay system to improve the array technology for GW excitation. Individual output power control, physical time delay, receiver amplifier, and software time-delay were considered for each element. They determined the resolution and time domain delays for sending high energy controllable tone-burst signals from each channel. (Yan et al., 2011) applied appropriate time delays to the multiple elements of an annular array transducer, and mode-selective GW generation for specific frequencies was achieved. They used the large argument approximation of the Bessel function included in the Hankel transform to show that the excitation spectrum of an inactive annular array with an inner diameter much larger than the element spacing is approximately identical to that of a corresponding comb transducer.

(EV Glushkov et al., 2010) investigated special choice of the amplitudes and time delays of the sinusoidal tone burst driving signals for each element of a PZT with several coaxial ring-shaped elements for mode-selective GW excitation. As the transient solution tends towards the solution of the corresponding time-harmonic problem for an increasing number of cycles, they defined the driving amplitudes and time delays required via the amplitudes and phase shifts obtained from the related time harmonic problem. (Kannajosyula et al., 2013) presented an extended analysis of annular PZTs for mode-selective GW generation. In the wavenumber domain, the smallest phase and time delays of each ring were obtained and the corresponding ring width was defined with respect to the wavelength of the desired mode. (Yeum et al., 2011) designed concentric ring and circular PZTs to present a mode decomposition technique that is based on the varying amplitude rate of S_0 and A_0-modes, as the sizes of the excitation and sensing PZTs vary. They then defined a scaling factor as a function of wavenumbers in which the difference between the wavenumbers of the S_0 and A_0-modes rises especially at high frequency.

Electrode patterning, commonly used for manufacturing of interdigital transducers (IDTs), appears as a promising design solution for NDE and SHM systems, in which the distance between the electrodes (finger separation) defines the length of the induced wavelength (Monkhouse et al., 1997; Monkhouse et al., 2000). In order to extend the directivity of IDTs, Salas and Cesnik presented a Composite Long-rang Variable-direction Emitting Radar (CLoVER) transducer that consists of wedge-shaped anistropic piezoelectric transducers arranged in circular array to be able to generate GW in all 360^0 (K. Salas & C. Cesnik, 2010). They showed that he generated GW by CLoVERs has a stronger amplitude than usual ring shape transducers. (Baravelli et al., 2011) designed the frequency-steerable acoustic transducer (FSAT) which is a shaped array with a spatial distribution that controls the beam steering using frequency-dependent directional properties by a single two channel device. (Yazdanpanah Moghadam et al., 2015) presented a systematic optimization approach for controlling interfacial shear stress to generate GW modes selectively. The influence of the excitation area with respect to the wavelength of excited GW-mode and given frequency has been considered for mode selection or rejection.

In this paper, a novel mode-selective piezoelectric transducer concept is proposed as the result of an optimization process to control the mode selectivity. In section 4.4, an interfacial shear stress approach based on (Yazdanpanah Moghadam et al., 2015) is developed and used in to design an optimized multi-element piezoelectric transducer (MEPT) for mode-selective GW generation. Section 4.5 presents the optimal geometry, number of elements, and size of the MEPT. The designed MEPT is then manufactured using laser micro-machining (http://www.lpkf.com/index.htm) and validated using 3D-Laser Doppler Vibrometer (3D-LDV) measurements. Experimental tests illustrate the high capability of the MEPT for mode-selective GW generation, as unwanted mode is suppressed by a factor up to 170 times compared with the results obtained with a single piezoceramic.

4.4 METHODOLOGY

4.4.1 Modeling GW generation

In this section, a semi-analytical approach is first developed for modeling GW generation and propagation by an array of *N* PZT elements bonded on an isotropic metallic plate. In this hybrid approach, the interfacial shear stress between the PZT and the host structure is extracted numerically using a Finite Element Method (FEM) model in order to integrate the shear stress component in an analytical formulation. This approach avoids the increased complexity of an analytical approach (L. A. Viktorov et al., 1965), while allowing taking into account the complex electromechanical coupling of the PZT (Yazdanpanah Moghadam et al., 2015) and the effect of adhesive layer (Ha & Chang, 2010).

4.4.1.1 FEM modeling and interfacial shear stress extraction

In order to simplify the design of mode-selective transducers, a two dimensional (2D) model in the frequency domain is developed under COMSOL v4.3 for frequencies below 500 kHz as presented in Figure 4. 1. In this model, an array of *N* PZT-5A elements with a thickness of 0.25 mm and length a = 5 mm are bonded on top of a host plate using an epoxy layer of 0.025 mm thickness. The number of elements *N* and the gap between elements g will be investigated in result section based on convergence study and manufacturing limitations. The host plate consists of an aluminum plate with a thickness $2d$ = 1.6 mm, Young's modulus of E = 68.9 GPa, density of ρ = 2700 kg m^{-3}, and Poison ratio of v = 0.33. In the FEM, absorbing layers are modeled at both ends of the host plate to ensure infinite plate conditions by adding an imaginary part to the elastic constant that increases with respect to the propagation distance (Ke, Castaings, & Bacon, 2009).

A minimum of ten nodes per wavelength for minimum wavelength (A_0-mode at upper frequency band, 500 kHz) is ensured by setting the maximal mesh size at 0.22 mm in the targeted area. Quadratic triangular elements are used for a total of approximately 10^7 elements, for all PZT elements, including local strong mesh refinement around the PZT edges. The bottom electrodes

of all PZT elements are all grounded during simulations that are performed in the frequency domain with continuous harmonic wave excitation.

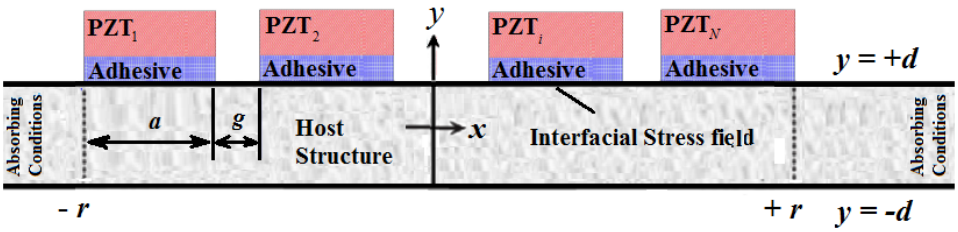

Figure 4. 1 2D schematic of array of *N* PZT elements bonded on a plate used for FEM.

In the following optimization strategy, the element *i* is subjected to a harmonic input voltage of 1V applied on the top electrode of the PZT while all other elements are not excited (free charge condition).

(a)

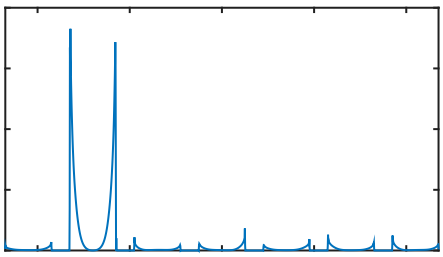

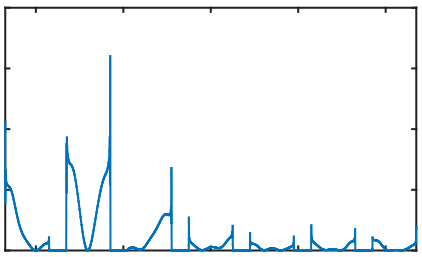

(b)

Figure 4. 2 Absolute value of interfacial shear stress distribution over excitation area $|x| < r$ when only element number two (E2) is excited at frequencies (a) 100 kHz and (b) 500 kHz.

As an example, Figure 4. 2 presents the absolute value of interfacial shear stress field between the PZT element and the host structure at excitation area $|x| < r$ for the case with seven elements, when element number two (E2) is excited at frequencies 100 kHz and 500 kHz.

In both cases, the interfacial shear stress field is not only concentrated at the tip of the actuator and cannot be neglected within the piezoceramic, such that the pin-force (Raghavan & Cesnik, 2005) and shear-lag (Yu, Bottai-Santoni, & Giurgiutiu, 2010) model assumptions are not valid.

Figure 4. 2 illustrates that the interfacial shear stress for non-excited elements also cannot be neglected, especially at higher frequencies (Figure 4. 2b), since the active element induces a GW in the host structure that is responsible for interfacial shear stress between the host structure and surrounding elements. So, for actuator *i*, the total stress field $\tau_i(x)$ can be expressed as the sum of the stress field generated by the actuator itself, and the stress field induced by the surrounding actuators (X. Wang & Huang, 2001). Therefore, the FEM model is applied to each individual element and then used as an input to an analytical method and optimization process.

4.4.1.2 Analytical solution of GW propagated from the MEPT

In this section, the analytical method provided in (Yazdanpanah Moghadam et al., 2015) for decomposing the interfacial shear stress profile extracted for FEM model into many elements is adapted for modeling of non-uniform stress profiles in order to predict the GW field induced by the MEPT. The interfacial shear stress conditions on the top and bottom of the host structure in Figure 4. 1 are expressed as:

$$\tau_j^{tot}(x,y)=\begin{cases}\tau_j\left(H\left[x+r\right]-H\left[x-r\right]\right), j=1,2,...,N & \text{at } y=+d,\\ 0, \qquad \text{at } y=-d.\end{cases} \tag{4.1}$$

where τ_j^{tot} is the interfacial shear stress distribution along the excitation area, $|x|\le r$, when element *j* is the only excited actuator.

The presented analytical method in (Yazdanpanah Moghadam et al., 2015) is then developed to predict the total displacement fields in the host structure using the superposition of displacement fields imposed by each segment:

$$\overline{U}_{x,y}^{T}\left(\xi,y\right)=\left[\frac{N_{x,y}^{A_0}\left(\xi,y\right)}{D^{A_0}\left(\xi\right)}+\frac{N_{x,y}^{S_0}\left(\xi,y\right)}{D^{S_0}\left(\xi\right)}\right]\times\frac{\sum_{j=1}^{N}\overline{\tau}_{j}^{tot}\left(\xi\right)}{2}, \tag{4.2}$$

where $N_x^{A_0}\left(\xi,y\right)$, $N_x^{S_0}\left(\xi,y\right)$, $N_y^{A_0}\left(\xi,y\right)$, $N_y^{S_0}\left(\xi,y\right)$, $D^{A_0}\left(\xi\right)$, and $D^{S_0}\left(\xi\right)$ are functions of wavenumber *k* and can be found in (Yazdanpanah Moghadam et al., 2015) in the case of a 2D plane strain approximation. $\overline{U}_{x,y}^{T}\left(\xi,y\right)$ stands for $\overline{U}_{x}^{T}\left(\xi,y\right)$ or $\overline{U}_{y}^{T}\left(\xi,y\right)$, the total in-plane and out-of-plane displacements, and $\overline{\tau}_j\left(\xi\right)$ represents the spatial Fourier transform of the excitation term τ_j that can be defined analytically as:

$$\overline{\tau}_{j}^{tot}(\xi)=\int_{-r}^{+r}\tau_{j}^{tot}\left(x,d\right)e^{-i\xi x}dx, \tag{4.3}$$

Using inverse Fourier Transform, the total displacement field of Eq. (4.2) can be expressed in the space domain using the residue theorem:

$$U_{x,y}^{T}\left(x,y\right)=\underbrace{\frac{1}{2}\frac{iN_{x,y}^{A_0}\left(\xi_{A_0},y\right)}{\left\{D^{A_0}\left(\xi\right)\right\}'_{\xi=\xi_{A_0}}}e^{-i\xi_{A_0}x}}_{\textit{Propagation terms}}\underbrace{\sum_{j=1}^{N}\overline{\tau}_{j}^{tot}\left(\xi_{A_0}\right)}_{\textit{Excitation term}}+\underbrace{\frac{1}{2}\frac{iN_{x,y}^{S_0}\left(\xi_{S_0},y\right)}{\left\{D^{S_0}\left(\xi\right)\right\}'_{\xi=\xi_{S_0}}}e^{-i\xi_{S_0}x}}_{\textit{Propagation terms}}\underbrace{\sum_{j=1}^{N}\overline{\tau}_{j}^{tot}\left(\xi_{S_0}\right)}_{\textit{Excitation term}}, \tag{4.4}$$

where the first term of the sum refers to the contribution of the A_0-mode and the second term refers to S_0-mode. Each contribution can be separated into propagation and excitation terms respectively. Both wavenumber and distance from excitation zone *x* are considered in the propagation terms of Eq. (4.4).

4.4.2 Optimization approach

4.4.2.1 Parameters

In this section, an approach is presented to optimize the amplitude and phase while the length of elements, *a*, gap between elements, *g*, number of elements, *N*, and thickness of the adhesive layer are kept constant.

First of all, the MEPT is simulated numerically using the FEM as presented in section 2.1.1. At driving frequency, each PZT element is then excited individually with a harmonic input harmonic input voltage of 1V applied on the top electrode of the PZT while all other elements are free of charge and the interfacial shear stresses, $\tau_1^{tot},\tau_2^{tot},...,\tau_j^{tot},...,\tau_N^{tot}$, are extracted, for all elements. Mode-selective GW generation here is based on optimization of the resulting interfacial shear stress when all elements are active at the same time with a dedicated amplitude and phase. Therefore, the optimization strategy is based on the proper selection of a set of complex coefficients which weight the shear stress profile generated by each element:

$$\alpha = \begin{cases} 0 \le |\alpha_i| \le 1, & i = 2,3,...N \\ \alpha_i = 1, & i = 1 \end{cases}, \tag{4.5}$$

where α_i is the complex correction coefficient corresponding to element *i*. Thus, for each element, a complex value for the interfacial shear stress profile is sought, resulting in 2(*N*-1) variables in the optimization process since the first element is used as a reference ($\alpha_1 = 1$).

4.4.2.2 Objective functions

In this section, the displacement of propagated modes in the whole area of the plate is selected as the objective function. Eq. (4.4) shows that the displacement ratio of undesired mode to other excited mode will be a function of excitation term, as the propagation terms are not affected by

the optimization process. Therefore, the objective functions, for instance for suppression of A_0-mode, is expressed as:

$$J_{S_0}\left(X\right)=\frac{\sum_{j=1}^{N}\alpha_j\overline{\tau}_j^{tot}\left(\xi_{A_0}\right)}{\sum_{j=1}^{N}\alpha_j\overline{\tau}_j^{tot}\left(\xi_{S_0}\right)}, \tag{4.6}$$

where Eq. (4.6) guarantees minimization of A_0-mode with respect to S_0-mode. $\overline{\tau}_j^{tot}\left(\xi_{A_0}\right)$ and $\overline{\tau}_j^{tot}\left(\xi_{A_0}\right)$ are spatial Fourier transform of the extracted interfacial shear stresses when element j is active. However, with the objective function described by Eq. (4.6), it was observed the numerator of Eq. (4.6) can tend toward zero to reach the minimum value without reaching a global minimum (Yazdanpanah Moghadam et al., 2015). Thus, a regulation term is required to maximize the desired mode over the whole wavenumber spectrum, such that an improved objective function for S_0-mode excitation is considered:

$$J_{S_0}\left(X\right)=\frac{\sum_{j=1}^{N}\alpha_j\overline{\tau}_j^{tot}\left(\xi_{A_0}\right)}{\sum_{j=1}^{N}\alpha_j\overline{\tau}_j^{tot}\left(\xi_{S_0}\right)}+\frac{\sum_{j=1}^{N}\left|\overline{\tau}_j^{tot}\left(\xi_{S_0}\right)\right|}{\sum_{j=1}^{N}\alpha_j\overline{\tau}_j^{tot}\left(\xi_{S_0}\right)}, \tag{4.7}$$

where the numerator of the second term is the maximum possible value of excitation terms for S_0-mode, because all variables of optimization process are constrained to $\left|\alpha_1\right|=1$ and $0<\left|\alpha_i\right|<1,\ i=2,...,N$, so that the Fourier transform of all other optimized interfacial shear stress configurations are less than this upper bound. Similarly, the objective function for selective A_0-mode excitation is expressed as:

$$J_{A_0}(X) = \frac{\sum_{j=1}^{N} \alpha_j \overline{\tau}_j^{tot}\left(\xi_{S_0}\right)}{\sum_{j=1}^{N} \alpha_j \overline{\tau}_j^{tot}\left(\xi_{A_0}\right)} + \frac{\sum_{j=1}^{N} \left|\overline{\tau}_j^{tot}\left(\xi_{A_0}\right)\right|}{\sum_{j=1}^{N} \alpha_j \overline{\tau}_j^{tot}\left(\xi_{A_0}\right)}, \tag{4.8}$$

The objective function in Eq. (4.8) is highly nonlinear, discontinuous and has unreliable or undefined derivatives, such that a genetic algorithm (GA) is used as preferred optimization algorithm (Cantú-Paz & Goldberg, 1996; Haupt & Haupt, 2004; Yazdanpanah Moghadam et al., 2015). Table 4. 1 illustrates the options of the GA process for each evolutionary step.

Table 4. 1 Parameters and operators of the GA.

Number of populations	1500
Population function	Linearfeasible
Fitness Scaling	Rank
Selection	Roulette
Crossover	heuristic
Ratio	1.1
Mutation	Gaussian
Scale	0.01
Shrink	1
Migration	Neighborhood
Interval	10
Direction	Forward
Fraction	0.2
Stopping Criteria	
Generations	850
Stall Generation Limit	500

4.5 Design and Performance Validation

In this section, the presented approach is used to design the MEPT and then derive the optimal input signals to control the interfacial shear stress. The MEPT is manufactured and its performances are presented in the following.

Table 4. 2 Experimental driving frequencies, wavelengths and wavenumbers.

f_0 (kHz)	λ_s (mm)	λ_a (mm)	ξ_s (rad/m)	ξ_a (rad/m)
100	53.5	11.8	117.4	533.7
200	26.7	7.9	235.1	795.6
300	17.6	6.1	357.0	1030.0
400	13.3	5.1	472.5	1237.1
500	10.6	4.4	592.8	1443.9

The host structure is identical to the one used in the FEM (see section 4.4 for more details) and the material properties are determined precisely using tensile test (Czichos, Saito, & Smith, 2006) and the GW propagation approach (Chimenti, 1997). In the following, the validation of the MEPT and optimization process is performed for five excitation frequencies from 100 kHz to 500 kHz by steps of 100 kHz, where A_0 or S_0-modes are selectively excited. Table 4. 2 illustrates the wavelengths and wavenumbers at experimental driving frequency.

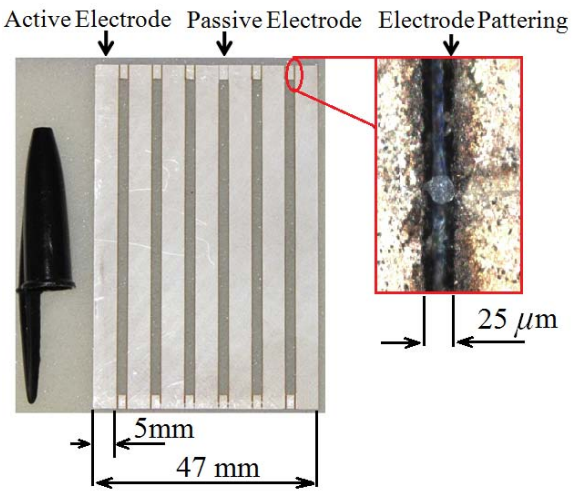

Figure 4. 3 Proposed concept for the Multi-Element Piezoelectric Transducer (MEPT) constituted of identical strip elements to induce optimized interfacial shear stress, and non-excited areas to keep parallelism between the elements.

4.5.1 Manufacturing constraints of the MEPT

Simplicity, manufacturing cost and limitations are main targets driving the design of the MEPT. Practically, design and fabrication of a patterned electrodes bulk piezoceramic transducer with specified interfacial shear stress is not straightforward because the boundary conditions vary from free to clamped when elements are contiguous, affecting the interfacial shear stress field (Yazdanpanah Moghadam, Tahani, et al., 2013). In order to minimize the effect of the boundaries on the interfacial shear stress, a gap between PZT elements has thus been integrated as for IDTs.

The first design constraint of the MEPT is keeping all elements parallel to each other precisely. The idea here is to define a constant gap between elements, but keeping a physical link between elements. For this purpose, the piezoceramic and top electrode of the MEPT are cut and patterned to disconnect active elements from passive elements using a LPKF laser micro-machining system (http://www.lpkf.com/index.htm) and the resulting MEPT is presented in Figure 4. 4.

4.5.2 Design parameters of the MEPT

The first design parameter is the thickness t_p. The thickness of MEPT is selected in order to reduce the interfacial normal stress with respect to the interfacial shear stress (N Quaegebeur et al., 2015), but not too small, since the fragility of the MEPT increases during laser micro-machining process. Based on available PZT thicknesses standards, the optimal thickness t_p = 0.25 mm was selected.

The second design parameter is the gap size g. Experimenting with fabrication it was concluded that for a 0.25 mm thick PZT, the minimum possible gap size between elements should be g = 2 mm to make dummy PZT removal process possible, without breaking the MEPT. The gap was selected as small as possible to limit the fragility of the transducer and minimize its footprint of the host structure.

The third design parameter is the width *a* of the elements. As the MEPT is designed and tested for a wide range of frequencies [100, 500] kHz, the first priority is the bandwidth. It is justified in (Yazdanpanah Moghadam et al., 2015) that a wider bandwidth is achieved when *a* (the continuous excitation area) is chosen below the smallest excited wavelength λ_{A0} that is 4.4 mm for the driving frequency band. However, fragility of the PZT in the micro-machining process limits the size selection to a = 5 mm.

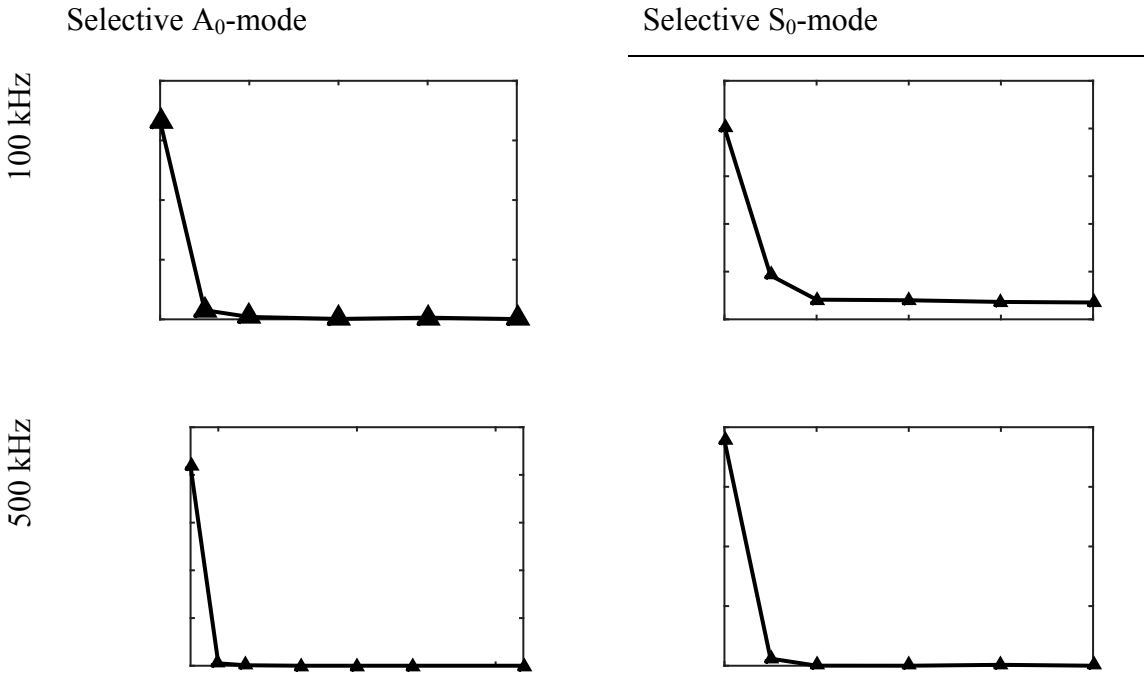

Figure 4. 4 Convergence study of objective function of desired mode with respect to the number of elements at 100 kHz and 500 kHz.

The fourth design parameter is the number of elements *N* and consequently the total size of the MEPT. In order to select the number of elements, a convergence study is conducted using the objective function of desired mode with respect to the number of elements. As 100 kHz and 500 kHz are the lower and upper frequencies of the desired transducer, the convergence study is performed and presented in Figure 4. 4 for those two frequencies in order to determine the minimum number of elements.

Figure 4. 4 demonstrates that with $N = 6$ elements at $f_0 = 100$ kHz, the A_0-mode can be excited over S_0-mode, while $N = 7$ elements are required to generated S_0-mode over A_0-mode due to its larger wavelength. On the other hand, convergence at 500 kHz happens from $N = 5$ elements for both A_0 and S_0-modes generation. Thus, it is concluded that the number of elements $N = 7$ should be determined using the lower frequency band when S_0-mode generation is desired.

Table 4. 3 Optimal amplitude A (V) and phase φ^0 of input harmonic excitation signal to each element of MEPT for mode-selective excitation in a 1.6 mm thick aluminum plate.

Frequency (kHz)	Selective Mode	Amplitude and phase delay	Element Number						
			1	2	3	4	5	6	7
100	A_0	A (V)	1	0.99	0.99	0.99	0.99	0.99	0.99
		φ^0	0	157	315	90	230	359	185
	S_0	A (V)	1	0.52	0.64	0.75	0.69	0.81	0.81
		φ^0	0	305	228	228	116	142	120
200	A_0	A (V)	1	0.99	0.98	0.98	0.89	0.97	0.78
		φ^0	0	124	234	270	34	76	197
	S_0	A (V)	1	0.89	0.45	0.65	0.45	0.23	0.45
		φ^0	0	234	321	178	56	34	234
300	A_0	A (V)	1	1	1	0.99	0.99	0.99	0.76
		φ^0	0	333	267	195	181	87	80
	S_0	A (V)	1	0.21	0.68	0.38	0.61	0.62	0.85
		φ^0	0	108	149	339	194	294	164
400	A_0	A (V)	1	0.98	0.93	0.40	0.84	0.99	0.90
		φ^0	0	273	146	72	220	72	309
	S_0	A (V)	1	0.99	0.96	0.94	0.63	0.99	0.57
		φ^0	0	166	333	138	316	142	285
500	A_0	A (V)	1	0.99	0.59	0.80	0.99	0.70	0.99
		φ^0	0	274	81	310	164	86	246
	S_0	A (V)	1	0.62	0.72	0.59	0.83	0.85	0.99
		φ^0	0	197	238	310	88	167	204

4.5.3 Optimal Interfacial Shear Stress

The optimization approach presented in section 4.4.1.2 is used here to determine the amplitude and phase to be applied to each element for mode-selective GW excitation. Table 4. 3 indicates the optimization results for each of the 7 elements in terms of phase and amplitude.

Table 4. 3 shows that the GA does not need to vary the amplitudes of input signals at lower frequencies, while only the phase is adjusted. At high frequencies both amplitude and phase are required to be varied by the GA in order to achieve selective mode generation. Thus, A_0-mode at lower frequencies can be achieved faster as less number of variables should be investigated by the GA. On the other hand, for S_0-mode generation, both amplitude and phase delay are varied at all driving frequencies. It proves that, as proposed to A_0-mode, selective S_0-mode generation is not straightforward even at low frequencies and objective function convergence is achieved slower in these cases.

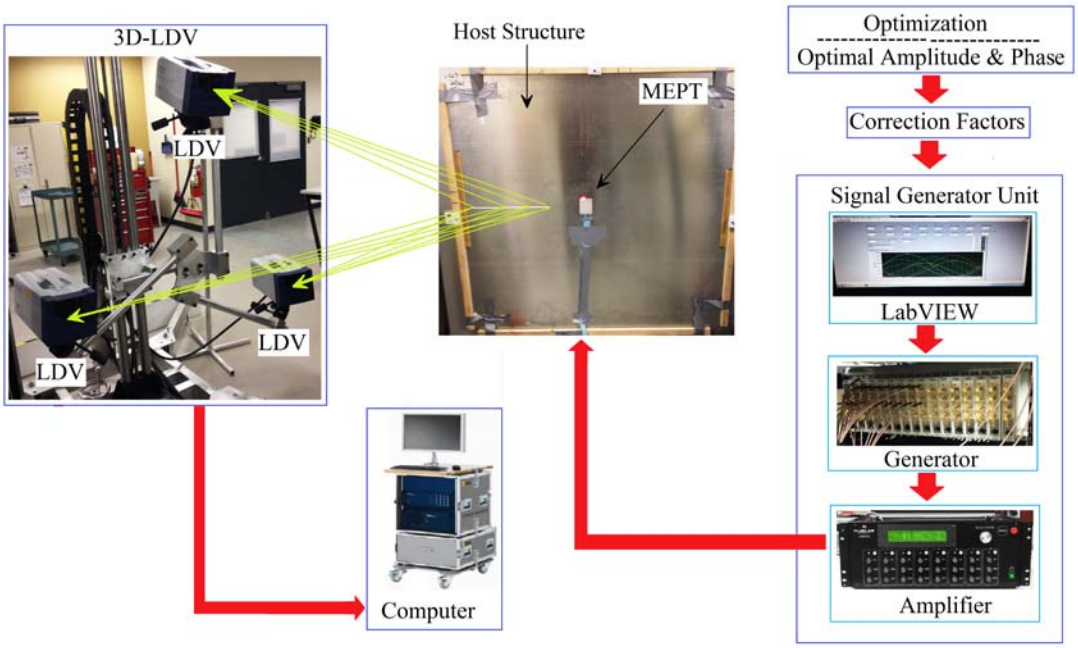

Figure 4. 5 Schematic of experimental set up to excite the MEPT's elements for mode-selective GW generation.

4.5.4 Experimental Setup

The MEPT is bonded on top surface of the plate using conductive epoxy with controlled thickness of 30 μm after using an installation template. As presented in Figure 4. 5, the presented approach provides optimized input signal of each element of the MEPT to generate mode-selective GW. These signals are used by LabVIEW software to excite seven channels of the multi-element single generator NI-FPGA 5781 front-end mounted on a PXIe-1075 chassis. The generated signals are then amplified by a seven channels of a high-frequency voltage amplifier (Produitson UA-8400). Then, the amplified signals are applied to elements of the MEPT by the amplifier.

Prior to the experiment, since the seven amplifier channels are not ideal, the drift between the amplification gain is measured using an oscilloscope and a correction factor is introduced to adjust the signals obtain by the GA. In the first step of the experiment, each element of the METP is excited individually to consider some parameters that were not taken into account in the proposed analytical method.

The in-plane and out-of plane velocities along a straight visual line perpendicular to the center of the active elements are measured using a 3D-LDV / Polytec PSV 400-3D. The transfer functions between the velocity components and the actuator voltage are measured using a harmonic single frequency excitation (N Quaegebeur et al., 2015). A schematic of experimental set up to excite the MEPT's for mode-selective GW generation is presented in Figure 4. 5.

4.5.5 Experimental correction factors

The individual contribution of each element of the MEPT is first derived in order to consider some parameters that were not taken into account in the presented analytical method such as material attenuation, possible non-uniformity of adhesive layers, and stiffness variation at bonding area of the MEPT. To handle this, each element of the MEPT is excited individually and the induced velocity field is analyzed using 3D-LDV. The Spatial Fourier transform of the in-plane and out-of -plane velocity fields for each element are computed and presented in Figure 4. 6.

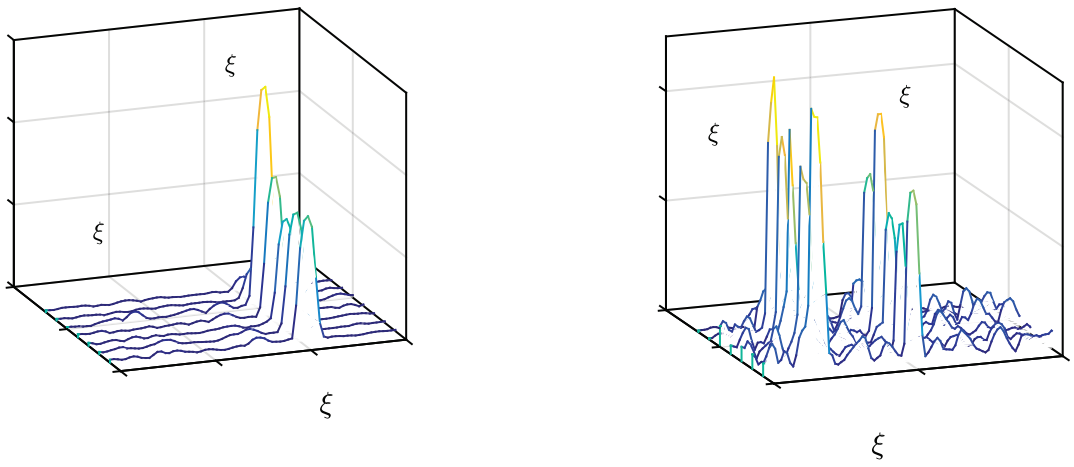

Figure 4. 6 In-plane and out-of-plane amplitude of the spatial Fourier transform of propagated GW by each element (E) of the MEPT as a function of wavenumber at 300 kHz.

It is clearly shown in Figure 4. 6 that the contribution of each mode varies between different elements and the amplitude generated by further elements decreases, due to the attenuation by all the other. In addition, the thickness of adhesive layer may not be constant for all the elements, which strongly affects the interfacial shear stress profile.

Table 4. 4 Contribution factor for each element for selective A_0 and S_0-mode generation at driving frequency.

Frequency (kHz)	Element Number / Selected Mode	1	2	3	4	5	6	7
100	S0	1	1.017	1.432	0.408	1.645	1	1.335
	A0	1	0.932	1.171	0.835	0.894	0.872	1.042
200	S0	1	1.350	1	0.718	2.415	0.332	1.783
	A0	1	1.119	1.101	0.659	1.074	1.143	1.099
300	S0	1	1.330	0.870	2.784	0.308	5.790	2.481
	A0	1	1.041	1.142	0.757	0.628	7.134	2.261
400	S0	1	0.890	1.347	1.170	0.271	0.822	1.117
	A0	1	0.911	0.887	0.524	1.450	0.896	1.466
500	S0	1	0.843	3.557	0.514	0.250	0.325	0.929
	A0	1	0.506	1.510	0.858	0.650	0.906	1.103

Using Figure 4. 6, a correction factor is defined for each element. S_0-mode carries out most of energy longitudinally. So, for selective S_0-mode generation, the correction factor for element *i* is defined as the ratio between its in-plane component amplitude at the wavenumber corresponding to the S_0-mode and the one of the first element. On the other hand, A_0-mode carries out most of its energy transversally. So, for selective A_0-mode generation, the correction factor for element *i* is defined as the ratio between its out-of-plane component amplitude at the wavenumber corresponding to the A_0-mode and the one of the first element. The correction factors are summarized in Table 4. 4.

4.5.6 Mode-selective GW excitation

In this section, the performances of the manufactured MEPT are tested experimentally by applying the optimized input excitation signals to each element. The Spatial Fourier Transform of the velocity fields (in-plane and out-of-plane components) are presented in Figure 4. 7 for element 1 only (dotted line) and using the 7 elements (solid line) with the optimal weighting as a function of desired mode and frequency.

Figure 4. 7 illustrates that the MEPT allows effective mode selective generation of the A_0-mode. Indeed, at 100, 200 and 300 kHz, the MEPT increases the out-of-plane component contribution for A_0-mode by a factor of 4.5, 6, and 7.5 times than using a single element as illustrated in Figure 4. 7 (b), (f), and (j). Moreover, in Figure 4. 7 (a), (e), (i), the in-plane component of A_0-mode is strengthen over S_0-mode considerably as the ratio of A_0-mode to S_0-mode varies respectively from 1.1, 0.5, and 0.67 to 10, 13, and 169 using the MEPT. Considering the S_0-mode selectivity, the ratio of in-plane component of S_0-mode to A_0-mode at these frequencies increases from 1, 0.5, and 1.5 to 10, 19, and 8, respectively. On the other hand, the out-of-plane component of A_0-mode, although not suppressed completely, is weakened considerably by a factor of 4, 2.5, and 5 times, compared to a single element.

In order to assess the performance of the MEPT at frequencies 400 kHz and 500 kHz, the tuning phenomena should be considered. Indeed, if the element width a is equal to a half-integer number of wavelengths (λ) of excited GW-mode as:

$$a = \lambda\left(n + \frac{1}{2}\right), \quad n = 0,1,2,... \tag{4.9}$$

then an optimal coupling can be reached and the transferred energy is maximized (EV Glushkov et al., 2010). Similarly, if the size of the transducer is equal to an integer number of a wavelengths as

$$a = \lambda n, \quad n = 0,1,2,... \tag{4.10}$$

minimal values of energy is then obtained.

Table 4. 2 presents that wavelength for A_0-mode is 5.1 mm at 400 kHz. On the other hand, the length of elements of MEPT is a = 5 mm. So, based on Eq. (4.10), as $a \approx \lambda_{A0}$, it is predicted that A_0-mode receives minimum energy and its maximization should not be easy even using the MEPT. Experimental tests in Figure 4. 7 illustrate that although the A_0-mode is not increased much longitudinally by the MEPT compared to the single PZT, the S_0-mode is at least minimized in x-component amplitude. So, in this case, although the first term of Eq. (4.7) cannot be used properly because of tuning phenomena, the MEPT can decrease longitudinal amplitude of the S_0-mode. As a result, in cases where the size of the elements is equal to an integer number of A_0-mode wavelength, that mode cannot be magnified by the MEPT, but the presented method can minimize unwanted mode considerably.

Figure 4. 7 (o) and (p) presents that the S_0-mode at 400 kHz is generated selectively using the MEPT, but not by maximizing the desired mode. As A_0-mode has minimum energy at this frequency, the first term of Eq. (4.7) minimizes the objective function individually and does not let the second term to play effectively. So, S_0-mode is not maximized as compare with using a single PZT, but A_0-mode is decreased considerably.

At 500 kHz, two phenomena co-exist: (1) the half-integer number of S_0-mode wavelengths almost reaches the elements length of the MEPT that satisfies the Eq. (4.9), (2) the size of the elements are very close to the integer of a number of a A_0-mode wavelength that satisfies Eq. (4.10). So, it affects mode-selective generation and suppression at this frequency. As all elements carry out the maximum energy for S_0-mode and minimum energy for A_0-mode, it is predicted that minimizing S_0-mode and maximizing A_0-mode should be difficult, while maximizing S_0-mode and minimizing A_0-mode should be very easy at this frequency. Figure 4. 7 (s) and (t) present that not only S_0-mode has an increased amplitude over A_0-mode longitudinally but the out-of-plane component is also large since suppressing S_0-mode on its tuned wavenumber is not straightforward. So, in this case, MEPT cannot suppress effectively the unwanted mode due to the tuning effect that naturally maximizes the S_0-mode.

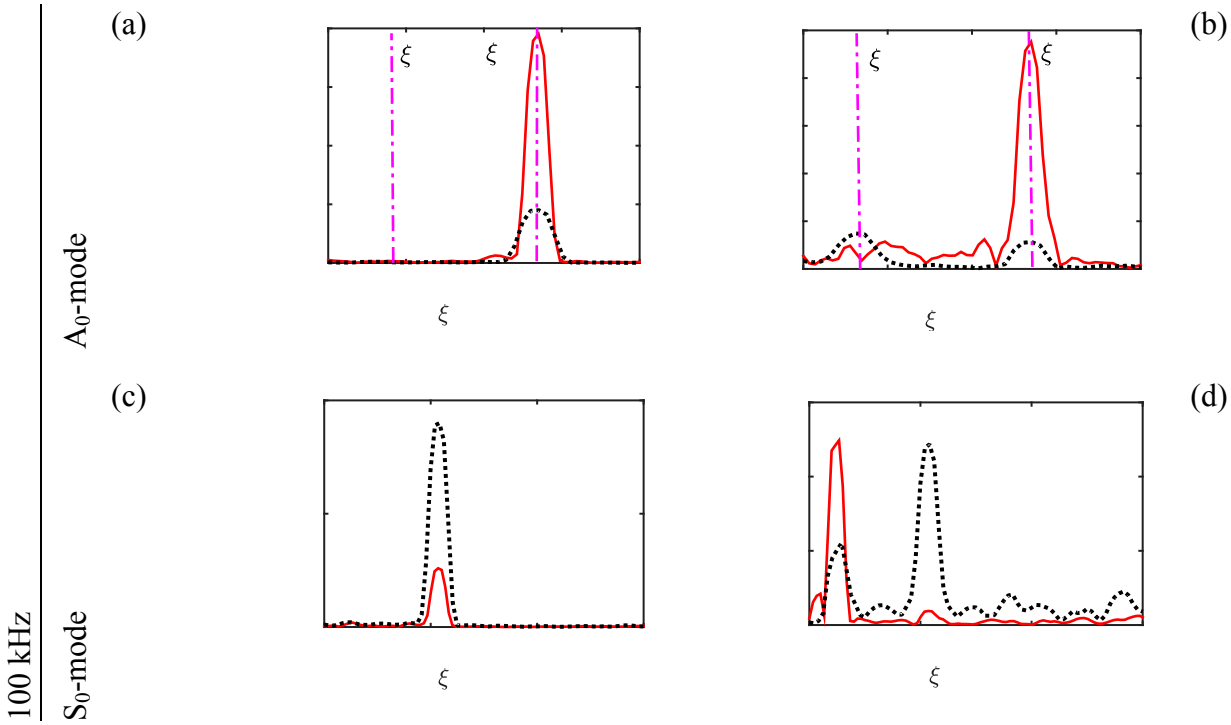

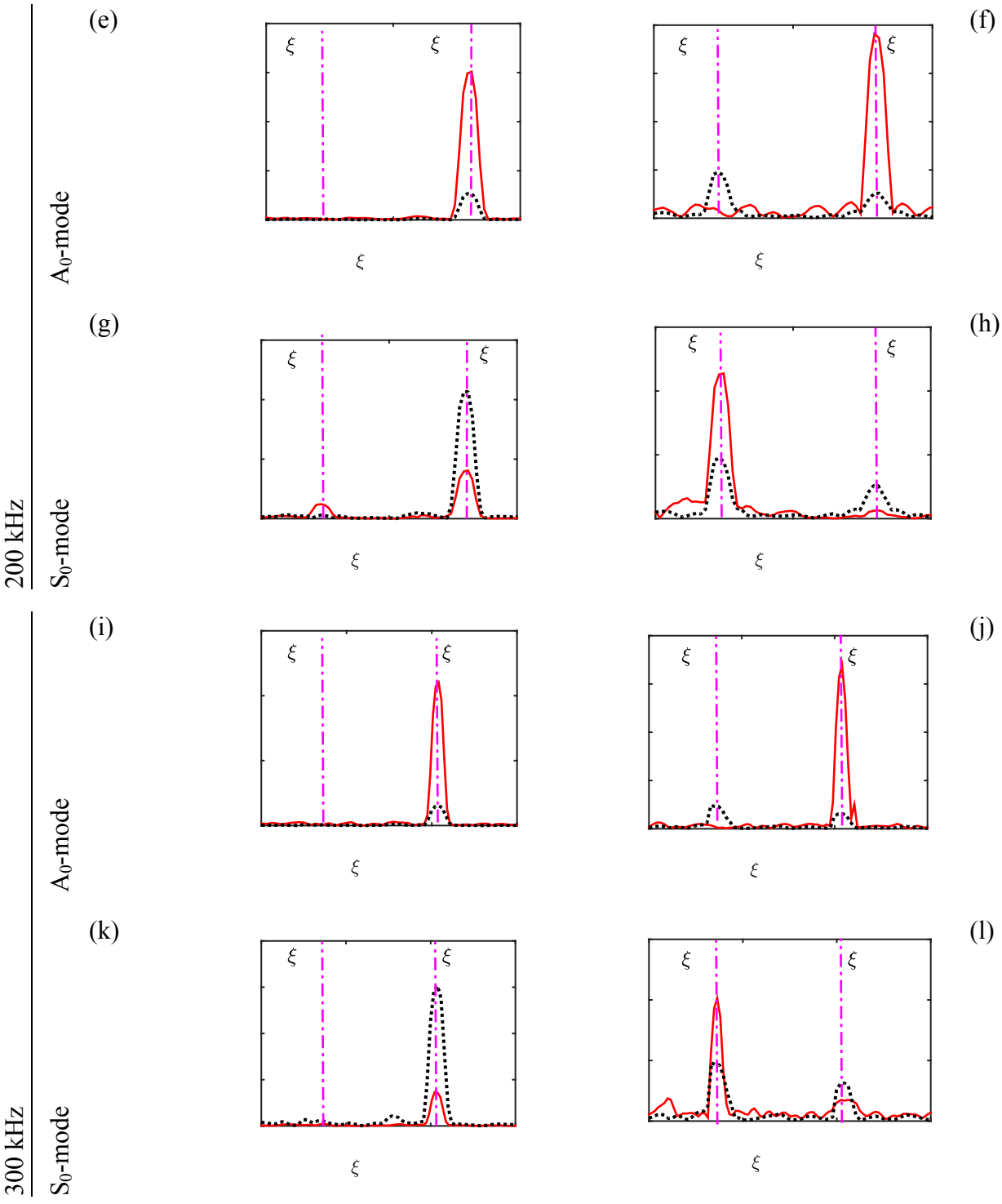
200 kHz
300 kHz
A0-mode
S0-mode
A0-mode
S0-mode
(e)
(f)
(g)
(h)
(i)
(j)
(k)
(l)
ξ

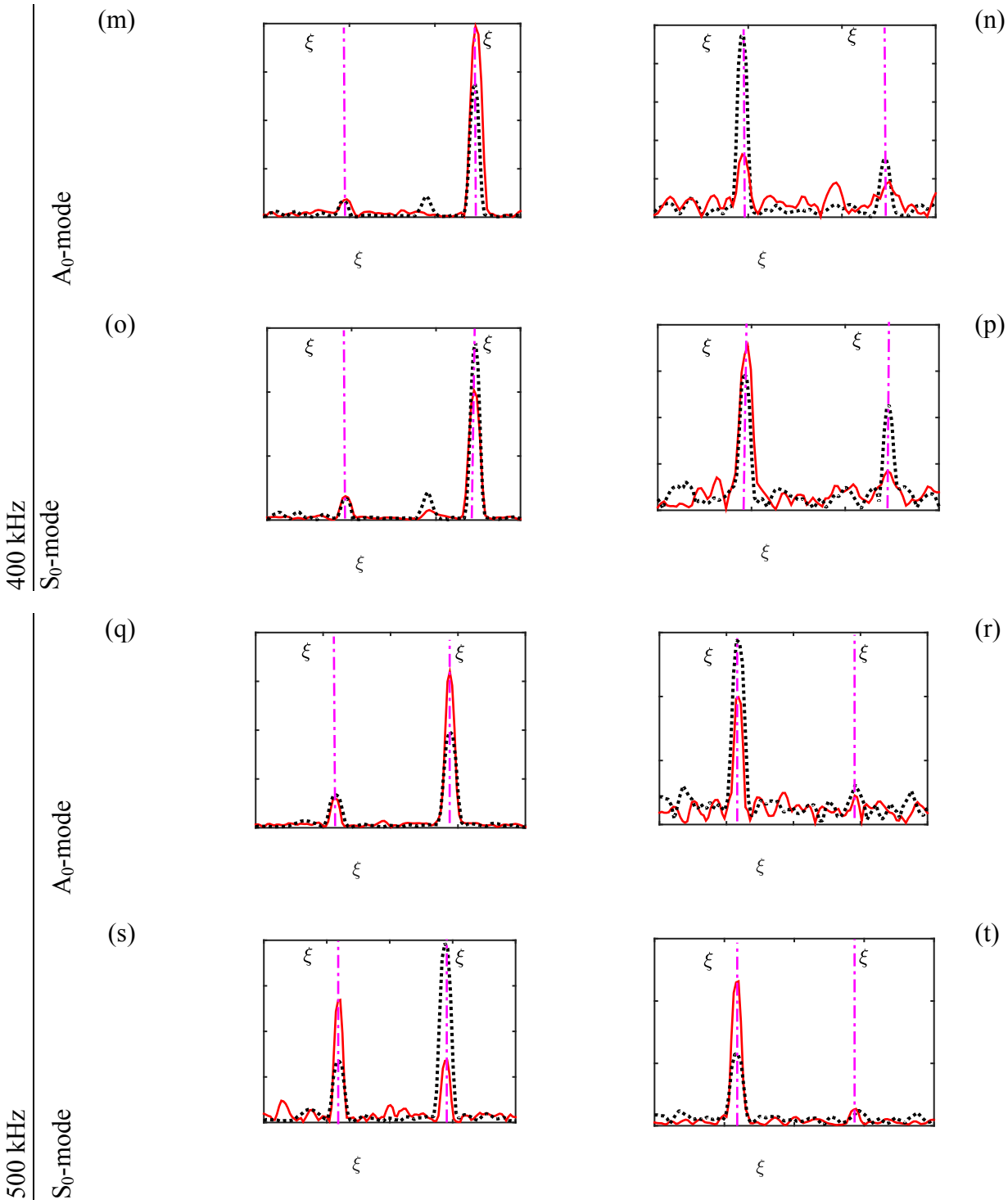

Figure 4. 7 Comparison of *x* and *z* components amplitude velocity of propagated GW from the MEPT (solid line) and a single element PZT (dotted line) for A_0 and S_0-modes at the driving frequency.

4.6 Conclusion

The design methodology of a novel Multi-Element Piezoelectric Transducer (MEPT) is presented for mode-selective GW generation. The idea is based on a systematic optimization process for controlling the interfacial shear stress induces by the MEPT on the host structure. An optimization approach is presented based on a hybrid numerical/analytical model for determining the optimal interfacial shear stress to be applied. Optimal geometry of the MEPT is investigated, manufactured using laser micro-machining and then validated experimentally. Experimental tests illustrate the A_0-mode can be generated dominantly over S_0-mode for both longitudinal and transverse components. In addition, S_0-mode can be generated selectively using the MEPT. Although in some cases transverse component of A_0-mode is not suppressed completely, it is weakened considerably using the MEPT. Experimental tests illustrate the high capability of the MEPT for mode-selective GW generation, as unwanted mode is suppressed by a factor up to 170 times compared with the results obtained with a single piezoceramics. Extension in the case of transient signals is ongoing.

4.7 Ackowledgement

This study has been conducted with the financial support from the Natural Sciences and Engineering Research Council of Canada (NSERC).

CHAPTER 5

CONCLUSION

5.1 Discussion

In this thesis, an investigation was performed for mode-selective GW generation with surface bonded piezoelectric transducers. In this thesis a comprehensive review of mode-selective transducer designs was presented and their limitations and advantages were mentioned.

In the second step of the thesis, an analytical approach was developed for modeling GW propagation through the thickness of the plate generated by an arbitrary uniform shear stress. In this method, the excitation zone is divided into a number of small elements which are all contributing to the GW generation. Using an objective function based on superposition of contributions from elementary uniform shear stresses and a Genetic Algorithm optimization, the global optimized mode-selective interfacial shear stresses profiles are computed. Optimal transducer size and element numbers for next step of this thesis are studied and it is demonstrated that a greater selectivity, extended bandwidth, fast convergence and limited complexity can be achieved.

In the next step of the thesis, a novel Multi-Element Piezoelectric Transducer (MEPT) was presented for mode-selective GW generation. The presented analytical method in the previous step is developed and adapted here for GW generation by a surface bonded PZT. An approach is developed based on a hybrid numerical/analytical model for modeling GW. The optimization method is then developed and two new objective functions are presented to investigate optimal interfacial shear stress. Optimal geometry of the MEPT is investigated, manufactured using laser micro-machining and then validated experimentally. Experimental tests illustrate the A_0-mode can be generated dominantly over S0-mode for both longitudinal and transverse components. In addition, S_0-mode can be generated selectively using the MEPT. Experimental tests illustrate the

high capability of the MEPT for mode-selective GW generation, as unwanted mode is suppressed by a factor up to 170 times compared with the results obtained with a single piezoceramic.

5.2 Originality of the Work

In this work, a novel approach is proposed to design mode-selective transducers. In addition to being simple and cost-effective, this approach brings the following originalities:

1) an analytical solution that not only models the GW propagation on the surface of the plate, but also models it through the thickness of the plate,

2) novel objective functions that are proposed, so that the shear stress can be explicitly optimized to both excite one mode and suppress other undesired modes,

3) the size of the excitation area that is not constrained, such that mode-selective excitation is still possible even if the excitation width is smaller than all excited wavelengths,

4) the mode selectivity that is increased and the bandwidth extended with respect to a single piezoceramic tuning approach,

5) a new manufacturing approach that is developed to create the designed transducer on a large, thin, and fragile substrate.

5.3 Limitations and future work

Mode-selective generation by MEPT has some limitations. At transducer tuning frequencies, the tuned mode cannot be suppressed completely, as presented in section 4.5.6. This method could be developed for high frequencies at which many modes are excited. The MEPT can be re-designed in 3D to scan a whole area of a plate. This 3D MEPT could have several segments similar to CLoVERs to have GW directivity in addition to the mode selectivity. GW modes are very sensitive to temperature, so that determination of correction factors and validation tests should be performed at the same temperature. The attenuation is an important parameter could be taken in to the account for analytical modeling of GW propagation. It is recommended to design and a mode-selective piezoelectric transducer for curve plates, composite plates, and do the

optimization for a specific case, for example a real wing of airplane applying SHM standards such as SAE ARP6461 Aerospace Recommended Practice.

APPENDIX A

MICRO-MACHINING WITH THE LPKF PROTOLASER U3

A.1 Minimal Requirements, High Performance

The LPKF ProtoLaser U3 requires only an electrical connection, dust extraction and compressed air - and then things can take off. It will go through any laboratory door and can be easily moved on its rollers. Figure A.1 illustrates the LPKF ProtoLaser U3.

A.2 Broad Range of Materials

Ceramic, LTCC (green tape), FR4, Rogers, protective sheets and metal foils or flexible and flex-rigid materials: the LPKF ProtoLaser U3 can process the most varied materials quickly, cleanly and precisely.

A.3 Advantages of Laser Processing

The LPKF ProtoLaser U3 opens up a host of new options for product development. If you are doing your own prototyping, it can process unusual materials, deal with a complex substrate structure and is ideal for multi-layer production.

The laser process itself stands out from competing processes due to its high flexibility and fast processing. The laser uses no environmentally hazardous chemicals, requires no masks and keeps outlay for tool production to a minimum. The laser works contact-free and therefore can also be used with sensitive materials.

The ProtoLaser U3 can make prototypes of a quality that meets or even exceeds that of industrial processing. It is also suitable for small series production and for production of individual components with high variance.

The laser process itself stands out from competing processes due to its high flexibility and fast processing. The laser uses no environmentally hazardous chemicals, requires no masks and keeps outlay for tool production to a minimum. The laser works contact-free and therefore can also be used with sensitive materials. The technical data of the LPKT ProtoLaser U3 is presented in Table A. 1.

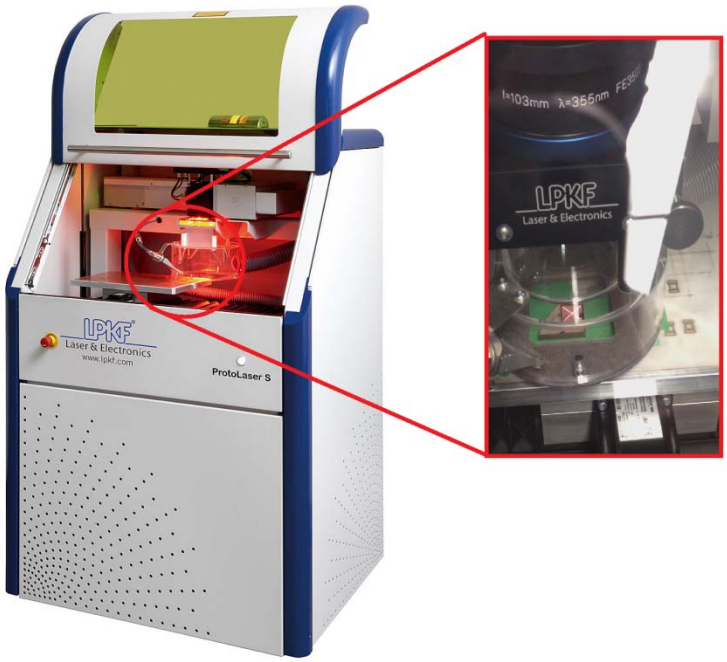

Figure A. 1 The LPKF ProtoLaser U3

A.4 Impressive Results with the LPKF ProtoLaser U3

Piezoelectric materials are used to generate GWs. Piezoelectric ceramics are so sensitive to impact, fragile to stress/strain, and are depolarized under thermal loading. Laser micro-machining on piezoelectric transducers using the LPKE ProtoLaser U3 prides is strongly recommended. Laser-structured printed boards trump etched printed boards on important criteria such as repeat accuracy, exact geometry and conformity with simulation results, especially in the ceramic range.

The first step of using the LPKF is drawing 2D sketches of the design using CircuitCAM software. These sketches are saved with *.CAD format. These files are then imported to the BoardMaster software. BoardMaster refers each line of the sketch to a tool process of the LPKF, which could be etching, cutting, and drilling. Tutorials of the both software are detailed in catalogs provided by the manufacturer company. The important track of working with the LPKF is defining the most optimal adjustments for each tool.

Table A. 1. The technical data of the LPKT ProtoLaser U3

Max. Material size and layout area (X/Y/Z)	229 × 305 × 10 mm (9" × 12" × 0.4")
Laser wavelength	355 nm
Diameter of focused laser beam	15 μm (0.6 mil)
Repeatability	± 2 μm (± 0.08 min)
Dimensions (W × H × D)	875 mm × 1.1430 mm × 750 mm (34.5" × 56.3" × 29.5")
Weight	260 kg (9573 pounds)
Operating conditions	
Power supply	110/230 V, 50 - 60 Hz, 1.4 kW
Compressed air supply	8 bar (116 pis), 1601/min (5.66 cfm)
Cooling	Air cooled (internal cooling cycle)
Ambient temperature	22±2 ^{0}C (68 ^{0}F+ ^{0}F)
Required accessories	Exhaust unit, PC, compressor
	Microsoft Windows 2000/XP/7, 7000 MHz processor resolution
Hardware and software requirements	Min. 512 MB RAM (1 BG recommended), screen resolution min. 1024 × 768 pixel, USB 2.0

As the MEPT is manufactured by electrode patterning (etching) and material cutting on a 0.25 mm piezoelectric ceramic, the most optimal adjustments for these two tools are presented in details in Table A. 2. Presented data for etching can be used for all thickness of PZT as the thickness as electrodes are removed easily. It should be noted that these data is obtained through many hours of experimental testing specifically of the case under study and for thickness of the PZT, cutting data should be updated though the same data can be used for electrode patterning. These values of power are defined as 6.45 and 4.25 for cutting and etching process, respectively, because more power is required for materials removal through the thickness of the piecework. Mark speed is the speed of the laser beam. So, it is defined as 1 for cutting process, so that the

laser has is focused on specific area for a longer time and removes material appropriately. The optimal mark speed for electrode pattering is defined as 100 to move the laser beam faster to prevent of cutting the material deeply and making the piecework fragile. The value of polygon delay represents a waiting time between the individual vectors of a vector sequence. The optimal polygon delay for cutting process is obtained as 100 as its too long value cause the mirrors move too slowly and having stop between the vectors, so that it lets the materials cools down, regarding to its high power value as high thermal gradient leads to thermal cracking in the piecework.

Table A. 2 Optimal adjustments for a micro-machining on a PZT-5A of thickness 0.25mm using LPKT ProtoLaser U3

	Cutting	Etching (Electrode Patterning)
Frequency [kHz]	70	70
Power [W]	6.45	4.65
Jump delay [µs]	2000	2000
Jump Speed [mm/s]	2000	2000
Laser off delay [µs]	100	100
Laser on delay [µs]	500	500
Mark speed [mm/s]	1	100
Polygon delay [µs]	100	0
Air pressure	No	No
Repetition	20	30
Tool delay [ms]	0	0
Tool *z*-offset [µs]	0	0

REFERENCES

Achenbach, J., & Xu, Y. (1999). Wave motion in an isotropic elastic layer generated by a time-harmonic point load of arbitrary direction. *J Acoust Soc Am, 106*(1), 83-90.

Alleyne, D. N., & Cawley, P. (1992). The interaction of Lamb waves with defects. *Ultrasonics, Ferroelectrics, and Frequency Control, IEEE Transactions on, 39*(3), 381-397.

Bader, B. W. (2009). Constrained and Unconstrained Optimization. In O. Elsevier (Ed.), *Constrained and Unconstrained Optimization*. Albuquerque, NM, USA: Sandia National Laboratories.

Balageas, D., Fritzen, C.-P., & Güemes, A. (2006). *Structural health monitoring* (Vol. 493): Wiley Online Library.

Baravelli, E., Senesi, M., Ruzzene, M., De Marchi, L., & Speciale, N. (2011). Double-channel, frequency-steered acoustic transducer with 2-D imaging capabilities. *Ultrasonics, Ferroelectrics, and Frequency Control, IEEE Transactions on, 58*(7), 1430-1441.

Bates, D., Smith, G., Lu, D., & Hewitt, J. (2000). Rapid thermal non-destructive testing of aircraft components. *Composites Part B: Engineering, 31*(3), 175-185.

Bausk, E. V. (1999). Optimization of broadband withdrawal weighted interdigital transducers for high selective SAW filters. *Ultrasonics, Ferroelectrics, and Frequency Control, IEEE Transactions on, 46*(5), 1276-1282.

Bellan, F., Bulletti, A., Capineri, L., Masotti, L., Yaralioglu, G. G., Degertekin, F. L., . . . Rosi, E. (2005). A new design and manufacturing process for embedded Lamb waves interdigital transducers based on piezopolymer film. *Sensors and Actuators A: Physical, 123*, 379-387.

Bent, A. A., Hagood, N. W., & Rodgers, J. P. (1995). Anisotropic actuation with piezoelectric fiber composites. *Journal of intelligent material systems and structures, 6*(3), 338-349.

Bermes, C., Kim, J.-Y., Qu, J., & Jacobs, L. J. (2007). Experimental characterization of material nonlinearity using Lamb waves. *Appl Phys Lett, 90*(2), 021901.

Bertsimas, D., & Tsitsiklis, J. N. (1997). *Introduction to linear optimization* (Vol. 6): Athena Scientific Belmont, MA.

Bland, S. M., & Kapania, R. K. (2006). *Sensor Placement Optimization for Lamb Wave Based Structural Health Monitoring.* Paper presented at the Collection of Technical Papers: 11th AIAA/ISSMO Multidisciplinary Analysis and Optimization Conference.

Brown, L. (2000). *Optimizing the design of piezoelectric polymer ultrasound transducers.* Paper presented at the Ultrasonics Symposium, 2000 IEEE.

Cantú-Paz, E., & Goldberg, D. E. (1996). *Modeling idealized bounding cases of parallel genetic algorithms.* Paper presented at the In.

Castaings, M., Le Clezio, E., & Hosten, B. (2002). Modal decomposition method for modeling the interaction of Lamb waves with cracks. *J Acoust Soc Am, 112*(6), 2567-2582.

Chee, C., Tong, L., & Steven, G. (2000). A mixed model for adaptive composite plates with piezoelectric for anisotropic actuation. *Computers & Structures, 77*(3), 253-268.

Chimenti, D. (1997). Guided waves in plates and their use in materials characterization. *Applied Mechanics Reviews, 50*(5), 247-284.

Crawley, E. F., & De Luis, J. (1987). Use of piezoelectric actuators as elements of intelligent structures. *AIAA journal, 25*(10), 1373-1385.

Czichos, H., Saito, T., & Smith, L. R. (2006). *Springer handbook of materials measurement methods*: Springer Science & Business Media.

Clark, T., Simonetti, F., Rohkin, S., & Cawely P. (2009). Development of a low-frequency high purity A0 mode transducer for SHM applications. *IEEE Trans Ultrason Ferroelectr Freq Control*, *56*(7), 1437.

Dennis Jr, J. E., & Schnabel, R. B. (1996). *Numerical methods for unconstrained optimization and nonlinear equations* (Vol. 16): Siam.

di Scalea, F. L., Matt, H., & Bartoli, I. (2007). The response of rectangular piezoelectric sensors to Rayleigh and Lamb ultrasonic waves. *J Acoust Soc Am, 121*(1), 175-187.

Ditri, J. J., & Rajana, K. M. (1995). Analysis of the wedge method of generating guided waves *Review of Progress in Quantitative Nondestructive Evaluation* (pp. 163-170): Springer.

Farrar, C. R., & Worden, K. (2007). An introduction to structural health monitoring. *Philosophical Transactions of the Royal Society of London A: Mathematical, Physical and Engineering Sciences, 365*(1851), 303-315.

Flynn, E., & Todd, M. (2009). Optimal placement of piezoelectric actuators and sensors for detecting damage in plate structures. *Journal of intelligent material systems and structures*.

Flynn, E. B., & Todd, M. D. (2010). A Bayesian approach to optimal sensor placement for structural health monitoring with application to active sensing. *Mechanical Systems and Signal Processing, 24*(4), 891-903.

Fortunko, C., King, R., & Tan, M. (1982). Nondestructive evaluation of planar defects in plates using low-frequency shear horizontal waves. *Journal of Applied Physics, 53*(5), 3450-3458.

Frost, H. (2012). Electromagnetic-ultrasound transducers: principles, practice, and applications. *Physical Acoustics Vol*, 179-275.

Giurgiutiu, V. (2003). *Lamb wave generation with piezoelectric wafer active sensors for structural health monitoring.* Paper presented at the Smart Structures and Materials.

Giurgiutiu, V. (2005). Tuned Lamb wave excitation and detection with piezoelectric wafer active sensors for structural health monitoring. *Journal of intelligent material systems and structures, 16*(4), 291-305.

Giurgiutiu, V. (2007). *Structural health monitoring: with piezoelectric wafer active sensors*: Academic Press.

Giurgiutiu, V., & Bottai-Santoni, G. (2009). Extension of the shear-lag solution for structurally attached ultrasonic active sensors. *AIAA journal, 47*(8), 1980-1983.

Glushkov, E., Glushkova, N., Kvasha, O., & Lammering, R. (2010). Selective Lamb mode excitation by piezoelectric coaxial ring actuators. *Smart Materials and Structures, 19*(3), 035018.

Glushkov, E., Glushkova, N., Kvasha, O., & Seemann, W. (2007). Integral equation based modeling of the interaction between piezoelectric patch actuators and an elastic substrate. *Smart Materials and Structures, 16*(3), 650.

Glushkov, E., Glushkova, N., Seemann, W., & Kvasha, O. (2006). Elastic wave excitation in a layer by piezoceramic patch actuators. *Acoustical Physics, 52*(4), 398-407.

Grondel, S., Delebarre, C., Assaad, J., Paget, C., & Levin, K. (2001). *Modelling of Lamb wave generation for application in health monitoring of composite plates.* Paper presented at the Ultrasonics Symposium, 2001 IEEE.

Grondel, S., Paget, C., Delebarre, C., Assaad, J., & Levin, K. (2002). Design of optimal configuration for generating A0 Lamb mode in a composite plate using piezoceramic transducers. *J Acoust Soc Am, 112*(1), 84-90.

Ha, S., & Chang, F.-K. (2010). Adhesive interface layer effects in PZT-induced Lamb wave propagation. *Smart Materials and Structures, 19*(2), 025006.

Haupt, R. L., & Haupt, S. E. (2004). *Practical genetic algorithms*: John Wiley & Sons.

Hayward, G., Hailu, B., Farlow, R., Gachagan, A., & McNab, A. (2001). *Design of embedded transducers for structural health monitoring applications.* Paper presented at the SPIE's 8th Annual International Symposium on Smart Structures and Materials.

http://www.lpkf.com/index.htm.

Huang, G., & Sun, C. (2006). The dynamic behaviour of a piezoelectric actuator bonded to an anisotropic elastic medium. *International journal of solids and structures, 43*(5), 1291-1307.

Huston, D. (2010). *Structural sensing, health monitoring, and performance evaluation*: CRC Press.

Imano, K. (2007). A tilted angle polarization type piezoelectric transducer for plate wave generation. *IEICE Electronics Express, 4*(10), 340-343.

Joo, Y.-S., Park, C.-G., Lee, J.-H., Kim, J.-B., & Lim, S.-H. (2011). Development of ultrasonic waveguide sensor for under-sodium inspection in a sodium-cooled fast reactor. *Ndt & E International, 44*(2), 239-246.

Kamal, A. M., Lin, B., & Giurgiutiu, V. (2014). Exact analytical modeling of power and energy for multimode lamb waves excited by piezoelectric wafer active sensors. *Journal of intelligent material systems and structures, 25*(4), 452-471.

Kannajosyula, H., Lissenden, C., & Rose, J. (2013). Analysis of annular phased array transducers for ultrasonic guided wave mode control. *Smart Materials and Structures, 22*(8), 085019.

Ke, W., Castaings, M., & Bacon, C. (2009). 3D finite element simulations of an air-coupled ultrasonic NDT system. *Ndt & E International, 42*(6), 524-533.

Kessler, S. S. (2002). *Piezoelectric-based in-situ damage detection of composite materials for structural health monitoring systems.* Massachusetts Institute of Technology.

Kessler, S. S., Spearing, S. M., & Soutis, C. (2001). Optimization of Lamb wave methods for damage detection in composite materials. *Technology Laboratory for Advanced Composites Department of Aeronautics and Astronautics Massachusetts Institute of Technology, SHM-2001*.

Koduru, J. P., & Rose, J. L. (2013). Mode controlled guided wave tomography using annular array transducers for SHM of water loaded plate like structures. *Smart Materials and Structures, 22*(12), 125021.

Lamb, H. (1917). On waves in an elastic plate. *Proceedings of the Royal Society of London. Series A, Containing papers of a mathematical and physical character*, 114-128.

Lemistre, M., & Balageas, D. (2001). Structural health monitoring system based on diffracted Lamb wave analysis by multiresolution processing. *Smart Materials and Structures, 10*(3), 504.

Li, J., & Rose, J. L. (2001). Implementing guided wave mode control by use of a phased transducer array. *Ultrasonics, Ferroelectrics, and Frequency Control, IEEE Transactions on, 48*(3), 761-768.

Li, S., & Cliff, J. (2011). *Health Monitoring of Structural and Biological Systems X*. Paper presented at the Health Monitoring of Structural and Biological Systems, San Diego.

Li, S., & Lissenden, C. J. (2010). *Modeling Ultrasonic Guided Wave Generation From Piezoelectric Fiber Composite Strip Actuators.* Paper presented at the ASME 2010 Conference on Smart Materials, Adaptive Structures and Intelligent Systems.

Liang, Y., & Hwu, C. (2001). On-line identification of holes/cracks in composite structures. *Smart Materials and Structures, 10*(4), 599.

Lin, C. M., Chen, Y. Y., Felmetsger, V. V., Senesky, D. G., & Pisano, A. P. (2012). AlN/3C–SiC Composite Plate Enabling High-Frequency and High-Q Micromechanical Resonators. *Adv Mater, 24*(20), 2722-2727.

Lin, M., & Rogers, C. A. (1993). Modeling of the actuation mechanism in a beam structure with induced strain actuators. *paper# AIAA-93-1715-CP*, 3608-3617.

Lissenden, C. J., Li, S., & Rose, J. L. (2010). *Continuous piezoelectric health monitoring systems based on ultrasonic guided waves.* Paper presented at the SPIE Smart Structures and Materials+ Nondestructive Evaluation and Health Monitoring.

Liu, T., Veidt, M., & Kitipornchai, S. (2002). Single mode Lamb waves in composite laminated plates generated by piezoelectric transducers. *Composite Structures, 58*(3), 381-396.

Luginbuhl, P., Collins, S. D., Racine, G.-A., Grétillat, M.-A., De Rooij, N. F., Brooks, K. G., & Setter, N. (1997). Microfabricated Lamb wave device based on PZT sol-gel thin film for mechanical transport of solid particles and liquids. *Microelectromechanical Systems, Journal of, 6*(4), 337-346.

Mahapatra, D. R., Singhal, A., & Gopalakrishnan, S. (2005). Numerical analysis of Lamb wave generation in piezoelectric composite IDT. *Ultrasonics, Ferroelectrics, and Frequency Control, IEEE Transactions on, 52*(10), 1851-1860.

Mańka, M., Rosiek, M., Martowicz, A., Uhl, T., & Stępiński, T. (2010). Design and simulations of interdigital transducers for Lamb-wave based SHM systems.

Marantidis, C., Van Way, C. B., & Kudva, J. N. (1994). *Acoustic-emission sensing in an on-board smart structural health monitoring system for military aircraft.* Paper presented at the 1994 North American Conference on Smart Structures and Materials.

Matt, H., & di Scalea, F. L. (2007). *Macro-fiber composite piezoelectric rosettes for acoustic source location in complex structures.* Paper presented at the The 14th International Symposium on: Smart Structures and Materials & Nondestructive Evaluation and Health Monitoring.

Mitchell, M. (1998). *An introduction to genetic algorithms*: MIT press.

Mohamed, R., Demers, D. L., & Masson, P. (2011). *A parametric study of piezoceramic thickness effect on the generation of fundamental Lamb modes.* Paper presented at the SPIE Smart Structures and Materials+ Nondestructive Evaluation and Health Monitoring.

Mohamed, R., & Masson, P. (2010). *A time domain spectral element model for piezoelectric excitation of lamb waves in isotropic plates.* Paper presented at the SPIE Smart Structures and Materials+ Nondestructive Evaluation and Health Monitoring.

Monkhouse, R., Wilcox, P., & Cawley, P. (1997). Flexible interdigital PVDF transducers for the generation of Lamb waves in structures. *Ultrasonics, 35*(7), 489-498.

Monkhouse, R., Wilcox, P., Lowe, M., Dalton, R., & Cawley, P. (2000). The rapid monitoring of structures using interdigital Lamb wave transducers. *Smart Materials and Structures, 9*(3), 304.

Moulin, E., Assaad, J., Delebarre, C., & Osmont, D. (2000). Modeling of Lamb waves generated by integrated transducers in composite plates using a coupled finite element–normal modes expansion method. *J Acoust Soc Am, 107*(1), 87-94.

Murayama, R., & Mizutani, K. (2002). Conventional electromagnetic acoustic transducer development for optimum Lamb wave modes. *Ultrasonics, 40*(1), 491-495.

Nocedal, J., & Wright, S. (2006). *Numerical optimization*: Springer Science & Business Media.

Papadimitriou, C. H., & Steiglitz, K. (1998). *Combinatorial optimization: algorithms and complexity*: Courier Corporation.

Park, G. (2000). Assessing structural integrity using mechatronic impedance transducers with applications in extreme environments.

Pasco, Y., & Masson, P. (2009). *Modelling of piezoelectric fiber composite material for unltasonic wave generation*. Paper presented at the Cansmart, Montreal.

Pierce, S. G., Culshaw, B., Manson, G., Worden, K., & Staszewski, W. J. (2000). *Application of ultrasonic Lamb wave techniques to the evaluation of advanced composite structures.* Paper presented at the SPIE's 7th Annual International Symposium on Smart Structures and Materials.

Pruell, C., Kim, J.-Y., Qu, J., & Jacobs, L. (2009). A nonlinear-guided wave technique for evaluating plasticity-driven material damage in a metal plate. *Ndt & E International, 42*(3), 199-203.

Qin, L., Chen, Q., Cheng, H., & Wang, Q.-M. (2010). Analytical study of dual-mode thin film bulk acoustic resonators (FBARs) based on ZnO and AlN films with tilted c-axis orientation. *Ultrasonics, Ferroelectrics, and Frequency Control, IEEE Transactions on, 57*(8), 1840-1853.

Quaegebeur, N., Micheau, P., Masson, P., & Maslouhi, A. (2011). *Structural health monitoring strategy for detection of interlaminar delamination in composite plates.* Paper presented at the SPIE Smart Structures and Materials+ Nondestructive Evaluation and Health Monitoring.

Quaegebeur, N., Ostiguy, P., & Masson, P. (2015). Hybrid empirical/analytical modeling of guided wave generation by circular piezoceramics. *Smart Materials and Structures, 24*(3), 035003.

Raghavan, A., & Cesnik, C. E. (2005). Finite-dimensional piezoelectric transducer modeling for guided wave based structural health monitoring. *Smart Materials and Structures, 14*(6), 1448.

Rogers, C. A. (1993). Intelligent material systems-the dawn of a new materials age. *Journal of Intelligent Material Systems and Structures;(United States), 4*(1).

Rosalie, S., Vaughan, M., Bremner, A., & Chiu, W. K. (2004). Variation in the group velocity of Lamb waves as a tool for the detection of delamination in GLARE aluminium plate-like structures. *Composite Structures, 66*(1), 77-86.

Rose, J., Pilarski, A., & Ditri, J. (1993). An approach to guided wave mode selection for inspection of laminated plate. *Journal of reinforced plastics and composites, 12*(5), 536-544.

Rose, J. L. (2004). *Ultrasonic waves in solid media*: Cambridge university press.

Salas, K., & Cesnik, C. (2010). Guided wave structural health monitoring using CLoVER transducers in composite materials. *Smart Materials and Structures, 19*(1), 015014.

Salas, K., & Cesnik, C. E. (2009). Guided wave excitation by a CLoVER transducer for structural health monitoring: theory and experiments. *Smart Materials and Structures, 18*(7), 075005.

Salas, K. I., & Cesnik, C. E. (2010). Design and characterization of a variable-length piezocomposite transducer for structural health monitoring. *Journal of intelligent material systems and structures, 21*(3), 349-360.

Santoni, G. B., Yu, L., Xu, B., & Giurgiutiu, V. (2007). Lamb wave-mode tuning of piezoelectric wafer active sensors for structural health monitoring. *Journal of Vibration and Acoustics, 129*(6), 752-762.

Schmidt, D., Sinapius, M., & Wierach, P. (2013). Design of mode selective actuators for Lamb wave excitation in composite plates. *CEAS Aeronautical Journal, 4*(1), 105-112.

Schulz, M. J., Sundaresan, M. J., Ghoshal, A., & Pai, P. F. (2000). *Active fiber composites for structural health monitoring.* Paper presented at the SPIE's 7th Annual International Symposium on Smart Structures and Materials.

Sheikh, A., Topdar, P., & Halder, S. (2001). An appropriate FE model for through-thickness variation of displacement and potential in thin/moderately thick smart laminates. *Composite Structures, 51*(4), 401-409.

Shelke, A., Kundu, T., Amjad, U., Hahn, K., & Grill, W. (2011). Mode-selective excitation and detection of ultrasonic guided waves for delamination detection in laminated aluminum plates. *Ultrasonics, Ferroelectrics, and Frequency Control, IEEE Transactions on, 58*(3), 567-577.

Sohn, H., & Lee, S. J. (2010). Lamb wave tuning curve calibration for surface-bonded piezoelectric transducers. *Smart Materials and Structures, 19*(1), 015007.

Su, Z., & Ye, L. (2004). Selective generation of Lamb wave modes and their propagation characteristics in defective composite laminates. *Proceedings of the Institution of Mechanical Engineers, Part L: Journal of Materials Design and Applications, 218*(2), 95-110.

Su, Z., Ye, L., & Lu, Y. (2006). Guided Lamb waves for identification of damage in composite structures: A review. *Journal of sound and vibration, 295*(3), 753-780.

Sze, K., & Yao, L. (2000). A hybrid stress ANS solid-shell element and its generalization for smart structure modelling. Part I—solid-shell element formulation. *International Journal for Numerical Methods in Engineering, 48*(4), 545-564.

Trilaksono, A., Watanabe, N., Hoshi, H., Kondo, A., Iwahori, Y., & Takeda, S.-I. (2013). Continuous Damage Monitoring of a Thin Composite Structural with Mismatched Stiffener in a Combined Joint Using Fiber Bragg Grating under Tension and Three-Point Loading.

Veidt, M., Liu, T., & Kitipornchai, S. (2001). Flexural waves transmitted by rectangular piezoceramic transducers. *Smart Materials and Structures, 10*(4), 681.

Viktorov, I. (1967). *Rayleigh and lamb waves: Physical Theory and Applications*. New York: Plenum Press.

Viktorov, L. A., Zubova, O. M., & Kaekina, T. M. (1965). Investigation of Lamb Wave Excitation by the "Wedge" Method. *Soviet Physics-Acoustics, 10*, 354-359.

Von Ende, S., & Lammering, R. (2007). Investigation on piezoelectrically induced Lamb wave generation and propagation. *Smart Materials and Structures, 16*(5), 1802.

Von Ende, S., Schäfer, I., & Lammering, R. (2007). Lamb wave excitation with piezoelectric wafers–an analytical approach. *Acta Mechanica, 193*(3-4), 141-150.

Vose, M. D. (1999). *The simple genetic algorithm: foundations and theory* (Vol. 12): MIT press.

Wan, X., Zhang, Q., Xu, G., & Tse, P. W. (2014). Numerical Simulation of Nonlinear Lamb Waves Used in a Thin Plate for Detecting Buried Micro-Cracks. *Sensors (Basel), 14*(5), 8528-8546.

Wang, G., Wan, Z., Wang, X., & Lv, Y. (2008). Genetic algorithm based on simplex method for solving linear-quadratic bilevel programming problem. *Computers & Mathematics with Applications, 56*(10), 2550-2555.

Wang, X.-M., & Ying, C. (2001). Scattering of Lamb waves by a circular cylinder. *J Acoust Soc Am, 110*(4), 1752-1763.

Wang, X., & Huang, G. (2001). Wave propagation in electromechanical structures: induced by surface-bonded piezoelectric actuators. *Journal of intelligent material systems and structures, 12*(2), 105-115.

Wang, X., & Huang, G. (2003). On the elastic wave propagation induced by a network of piezoelectric actuators. *Acta Mechanica, 160*(1-2), 1-18.

Wang, X., & Huang, G. (2006). Wave propagation generated by piezoelectric actuators attached to elastic substrates. *Acta Mechanica, 183*(3-4), 155-176.

Wilcox, P., Lowe, M., & Cawley, P. (2001). Mode and transducer selection for long range Lamb wave inspection. *Journal of intelligent material systems and structures, 12*(8), 553-565.

Wilkie, W., High, J., & Bockman, J. (2002). *Reliability testing of NASA piezocomposite actuators.* Paper presented at the Proceedings of the 8th International Conference on New Actuators.

Williams, R. B., Park, G., Inman, D. J., & Wilkie, W. K. (2002). An overview of composite actuators with piezoceramic fibers. *Proceeding of IMAC XX*, 4-7.

Wooh, S.-C., & Shi, Y. (2001). Synthetic phase tuning of guided waves. *Ultrasonics, Ferroelectrics, and Frequency Control, IEEE Transactions on, 48*(1), 209-223.

Yan, F., Borigo, C., Liang, Y., Koduru, J. P., & Rose, J. L. (2011). *Phased annular array transducers for ultrasonic guided wave applications.* Paper presented at the SPIE Smart Structures and Materials+ Nondestructive Evaluation and Health Monitoring.

Yazdanpanah Moghadam, P., Quaegebeur, N., & Masson, P. (2013). *Piecewise semi-analytical modeling of guided wave generation by piezoelectric transducers*, International Workshop on Smart Materils, Strucutres NDT in Canada 2013 Conference & NDT for the Energy Industry, Calgary.

Yazdanpanah Moghadam, P., Quaegebeur, N., & Masson, P. (2015). Mode selective generation of guided waves by systematic optimization of the interfacial shear stress profile. *Smart Materials and Structures, 24*(1), 015003.

Yazdanpanah Moghadam, P., Tahani, M., & Naserian-Nik, A. M. (2013). Analytical solution of piezolaminated rectangular plates with arbitrary clamped/simply-supported boundary conditions under thermo-electro-mechanical loadings. *Applied Mathematical Modelling, 37*(5), 3228-3241.

Yazdanpanah Moghadam, P., Quaegebeur, N., & Masson, P. (2015). *Optimal excitation of interfacial shear stress array for mode selective Guided wave generation*, International Workshop on Smart Materils, Strucutres NDT in Canada 2015 Conference & NDT for the Energy Industry, Vancouer.

Yeum, C. M., Sohn, H., & Ihn, J. B. (2011). Lamb wave mode decomposition using concentric ring and circular piezoelectric transducers. *Wave motion, 48*(4), 358-370.

Yi, T., Li, H., & Gu, M. (2011). *An integrated MATLAB toolbox for optimal sensor placement based on multiple optimization strategies*. Paper presented at the 8th International Workshop on Structural Health Monitoring 2011: Condition-Based Maintenance and Intelligent Structures.

Yu, L., Bottai-Santoni, G., & Giurgiutiu, V. (2010). Shear lag solution for tuning ultrasonic piezoelectric wafer active sensors with applications to Lamb wave array imaging. *International Journal of Engineering Science, 48*(10), 848-861.